IN VIVO NEAR-INFRARED FLUORESCENCE IMAGING OF SKIN AND CUTANEOUS MELANIN

by

XIAO HAN

B.Sc., Tsinghua University, 1999

A THESIS SUBMITTED IN PARTIAL FULLFILMENT OF
THE REQUIREMENTS FOR THE DEGREE OF

Master of Science

in

The Faculty of Gradua te Studies

(Physics)

The University of British Columbia

October, 2006

Abstract

In this Medical Physics M.Sc. project, a near-infrared (NIR) fluorescence imaging system was built for *in-vivo* diagnosis and evaluation of pigmented skin abnormalities and diseases. Light coming from a 785 nm diode laser is coupled into a ring light guide to uniformly illuminate the skin surface with a field-of-view (FOV) of 25 mm diameter. The diffuse reflectance and emitted fluorescence photons are collected by an NIR-sensitive CCD camera, with computer-controlled filter switch to select between reflectance mode and fluorescence mode. Both reflectance and fluorescence images of skin disorders were obtained with an exposure time of 2 seconds. The results show that cutaneous melanin in pigmented skin disorders emits higher NIR autofluorescence (AF) than surrounding normal tissue. This finding challanged the conventional concept that melanin is a non-fluorescence substance. The developed NIR autofluorescence imaging method also provided a new and direct way to characterize cutaneous melanin and can potentially be used for evaluation and diagnosis of pigmented skin diseases and skin cancers, such as melanoma.

TABLE OF CONTENTS

LIST OF FIGURES

ACKNOWLEDGEMENTS

I would like to thank my primary supervisor, Dr. Haishan Zeng, who introduced to me this interesting research field. His daily patient yet strict supervision and always optimistic encouragements made all my progress possible. From him I could always learn about the most up-to-date frontier of biomedical optics.

I would also like to thank my clinical advisor, Dr. Harvey Lui, for teaching me so much about dermatology and offered me the opportunity to do clinical pilot study with the imaging system. He always let me know what the clinical demands are, and what technical improvements could change clinical dermatology.

Special thanks go to Dr. David I. McLean, who helped me arrange patients and brought up a huge number of interesting and insightful ideas during group meetings. His challenging questions and jokes made my research life serious but always enjoyable.

Other members of the Lamp Group also gave me generous help during instrument design and pilot clinical study. It was a great pleasure to work in this group together with Drs Jianhua Zhao, Doug Thiessen, Wei Zhang, Ahmad Al Robaee, Hana Alkhayat, Michael Chen, and Michael Short.

I shall also thank my friends and fellow students at British Columbia Cancer Research Center and the Department of Physics and Astronomy at UBC. You made my two years' experience in Canada a life-long cheerful memory.

Finally, my deepest gratefulness goes to my Father and Mother. Thank you for your encouragements and support from the other side of the ocean.

1. Introduction

1.1 Background

In this paper we discuss the application of *in-vivo* NIR fluorescence imaging technique in skin diagnosis, describe a prototype NIR imaging system, and show the preliminary result of a clinical pilot study on pigmented skin diseases and skin cancers using the system.

There are revolutionary progress in medical imaging technologies and techniques in the last 20 years. With imaging modalities such as X-ray and X-ray Computed Tomography (CT) scan, Magnetic Resonance Imaging (MRI), Positron Emission Tomography (PET), and Ultra-sound, we can see the inside of the human body with minimal invasion and maximum clarification. Yet, these clinical routinely-used techniques mostly produce image contrast between disease and normal tissue by the different physical properties of mass lesions or tumors, and usually can't effectively detect the subtle molecular alterations at the early stage of those diseases and cancers. In contrast, optical techniques (imaging and spectroscopy) offer excellent sensitivity in detecting these early biophysical and biochemical changes at the molecular level.

From the view of physics, the above disadvantage of conventional medical imaging techniques is that we are probing the tissue molecules with radiation of inappropriate energy level. When a tissue molecule starts a biochemical change, the molecular energy level shift ranges from 1 ~ 10 eV, which spectrally correspond to ultra-violet (UV) to infrared (IR) photons. Therefore, using optical methods within this energy range is directly targeting those molecular changes; while X-ray or gamma photons with energy above 100 eV cannot 'see' those tiny molecular energy level shift and thus only produce projections, or simple anatomic shadow images of the tumors. Even so, if we have the capability to focus X-ray or gamma photons as we focus a beam of light, we can still produce an image of human body with ultra-high resolution due to their extremely short wavelength. Unfortunately, researchers have so far been unable to focus higher energy photons due to the lack of a satisfactory material for making such a lens. As a result, complex mathematical methods are employed to reconstruct an image based on multiple

projections from a lot of angles, which limits the image resolution and significantly increase the signal acquisition and processing time.

Despite the above argument, high energy photons still dominate current clinical diagnoses because of their ability of penetrating tissue. Compared to X-ray and gamma photons, strong scattering and absorption limit the propagation range of light photons to within only the surface and sub-surface layers of human body.

From the view of dermatology, the limited propagation range is not a problem because most of the skin abnormalities occur within several millimeters below the skin surface. Using NIR light in the range of 700 ~ 1100 nm, a penetration depth of 1~2 centimeters into skin can be easily achieved with moderate power density level. Therefore, optical techniques within NIR wavelength range provide an excellent tool kit to detect the early stage biochemical changes of skin diseases at the molecular level.

In reality, however, not much success has been achieved in NIR optical diagnosis. The major reason is that none of the native skin tissue components seem to offer strong contrast under NIR light, and NIR autofluorescence (see chapter 4) is relatively weak compared to that in UV or visible light spectral range. In order to obtain molecular vibrational information by Raman scattering, researchers develop complicated techniques just to get rid of this NIR autofluorescence background. This situation began to change in the last few years.

Demos and co-workers carefully compared far-red and NIR autofluorescence emission from cancerous and normal tissue and found that they have distinct features, which is probably due to porphyrin retention in cancer cells. (Demos et al, 2004) More recently, Huang *et al* in our laboratory observed strong autofluorescence signal from cutaneous melanin under 785 nm NIR laser excitation, which is in sharp contradiction to melanin's very poor fluorescence under UV and visible light excitation. (Huang *et al*, 2006; Han *et al* 2006)

Since skin cancers are very common in North America, and the diagnosis of melanin-involved skin lesions and skin cancers address an important clinical task for dermatologists, those recent findings make NIR fluorescence imaging/spectroscopy techniques a promising tool to study those skin abnormalities, and potentially a diagnostic modality for clinical decision-making process.

1.2 Objectives

The objectives of this project are:

1. To build an NIR optical imaging system for reflectance and fluorescence imaging of skin;
2. To verify our previous findings on autofluorescence from cutaneous melanin; and
3. To accumulate data from both non-pigmented and pigmented skin diseases and skin cancers for a complete understanding of cutaneous melanin and skin pigmentation and to demonstrate the potential of NIR autofluorescence imaging for skin diagnosis.

1.3 Scope and outline

This thesis focuses on *in-vivo* NIR autofluorescence imaging. The first chapter introduces the background and objectives of this project. Chapter 2 provides an overview of the existing medical imaging modalities with their working principles, strengths and limitations. Chapter 3 briefly describes skin anatomy, physiology, and commonly seen disorders of skin pigmentary system. Basic tissue-light interaction processes are covered in Chapter 4 and the current stage of NIR tissue imaging is reviewed in chapter 5. Chapter 6 describes the experimental work of this project, and the results and discussions are presented in chapter 7. In chapter 8 we draw conclusions based on the findings and discuss future directions.

2. Basic anatomy, physiology, and common pigmentary disorders of skin

This chapter provides a brief overview of basic anatomy and physiology of skin, as well as commonly seen skin disorders, particularly those associated with pigmentary system.

2.1 Basic skin anatomy

Human skin consists of two main layers, epidermis and dermis. Epidermis is a layer of epithelial tissue which itself has multiple sub-layers. Below the epidermis is dermis, which is a layer of dense connective tissue connecting epidermis with subcutaneous tissue beneath the skin, which is mainly fat and muscle. (Gawkrodger, Dermatology)

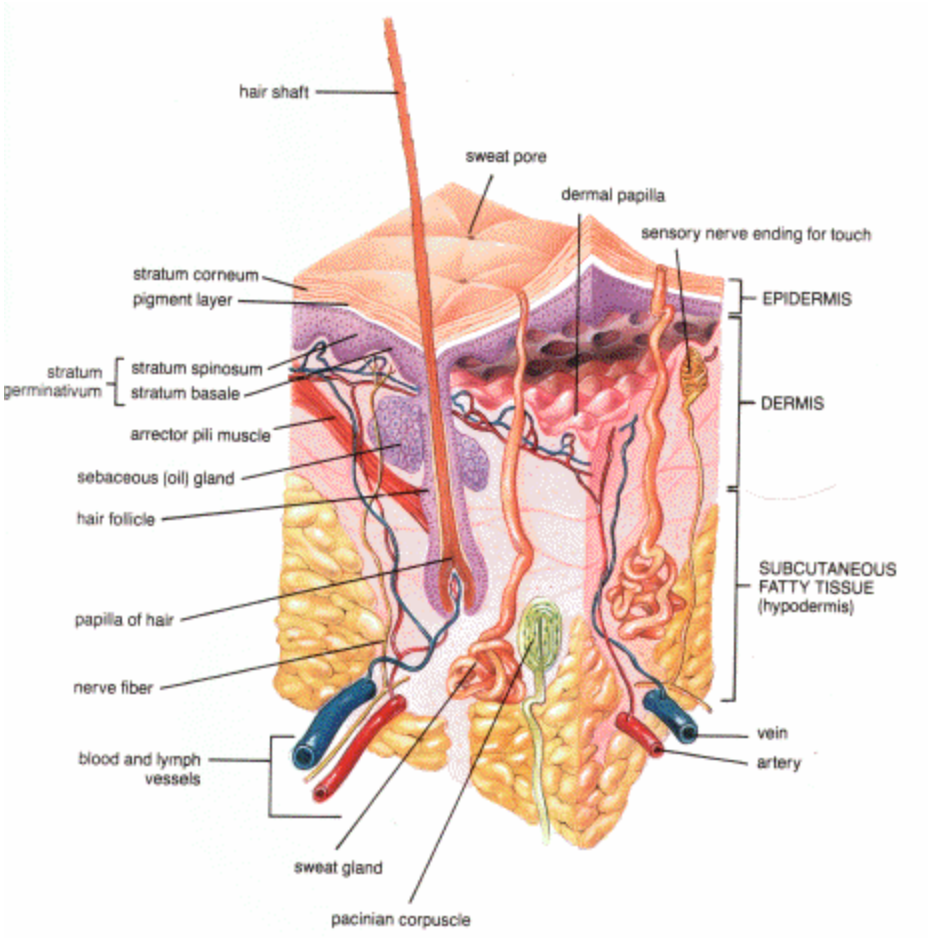

Figure 2-1. Illustration of skin anatomy.

The epidermis is about 100 micron thick and mainly constitutes of keratinocyte cells, which produce the protein keratin. New keratinocyte cells generated from the bottom layer of epidermis are pushed upward and gradually keratinized. As a result, the layers in epidermis represent the stages of the keratinization process. The basal cell layer is mostly comprised of keratinocytes which are able to divide through mitosis. Melanocytes are the cells synthesizing melanin and make up 5 – 10% of the basal cell population. Divided basal cells then migrate upwards to form three layers with different appearance and varying degrees of keratinization, namely, stratum spinosum, stratum granulosum, and stratum corneum. Stratum corneum is the outmost layer of skin and represents the end result of keratinization. Only dead cells exist in this layer and the previous cytoplasm is completely replaced by keratin.

Dermis is about 1 – 3 mm thick on most part of human body. The thin upper layer, papillary dermis, is composed of loosely interwoven collagen. The thicker and deeper reticular dermis layer is where coarser and horizontally running bundles of collagen can be found. In dermis, toughness and strength are provided by collagen fibers, while elasticity provided by elastin fibers. Blood vessels, nerves, lymph vessels, smooth muscles, sweat glands, hair follicles, and sebaceous glands are all embedded in the dermis.

2.2 Basic skin physiology

The skin and its appendages work together to provide important functions for human body. Those functions can be categorized into the following four aspects: sensation, protection, thermal regulation, and secretion.

Sensation

Receptor sites in the skin can detect changes in the external environment, such as temperature and pressure. Sensory neurons are in contact with receptor sites and transmit the impulse signal to the brain and spinal cord for interpretation and reaction. Thus the

receptor sites allow us to recognize stimuli from the outside world and react to them accordingly.

Protection

Skin provides protection for human body from external environment. Stratum corneum and skin appendages such as nails and hairs provide a tough barrier for sensitive internal organs. Also most of the harmful physical and chemical agents are prevented from penetrating into human body by this barrier.

Thermal regulation

The blood vessels in dermis can dilate or constrict to control the blood flow rate according to environmental temperature change. Dilated blood vessels bring more warm blood from internal body and increase the body surface temperature, while constricted blood vessels do the reverse. Also sweat gland helps adjust body temperature by excreting sweat which dissipates heat through evaporation.

Secretion

Important skin secretions include sebum and sweat. Sebum helps provide moisturization, prevent infection, and maintain skin texture and integrity. Sweat is essential in thermal regulation as well as in excreting waste from metabolism.

2.3 Skin pigmentary system

As previously mentioned in section 3.1, melanocytes are found in the basal cell layer of epidermis and are responsible for producing pigment melanin in elongated, membrane-bound organelles called melanosomes. Melanosomes are transferred to adjacent keratinocytes in granular packages and eventually reach the stratum corneum. Melanosomes are uniformly distributed in stratum corneum and as such, give a certain darkness level of skin and also provide a UV-absorbing blanket due to melanin's optical property (see chapter 4).

Skin color, which is largely determined by melanin concentration, varies from person to person. However, the amount of melanocytes does not depend on race, i.e. all races have the same number of melanocytes. In fact, it is the activity of an individual's melanocytes that determine how dark he or she looks. Racial variation in melanocyte activity is by and large determined by the specific genes. Also, exposure to sun light, in particular, 290 – 320 nm (UV-B) light, can significantly stimulate the activity of melanocytes, which results in elevated melanin concentration and eventually, darkened skin color known as suntan.

2.4 Common disorders of human pigmentary system

2.4.1 Vitiligo and albinism

When melanin is absent from a certain area of skin, that area appears completely white, instead of normal skin color. This is seen in vitiligo and albinism.

Vitiligo is an acquired skin disease which causes skin patches of various sizes deplete of pigmentation. The depigmented white patches often locate on exposed skin areas. From histology one can see that melanocytes are absent from the lesion. The cause of vitiligo is so far unknown.

Albanism, on the contrary, is an uncommon disease caused by gene mutation and as such, affects the whole body, i.e. including the skin and skin appendages. In albinos' bodies, melanocyte numbers are normal, however, the recessive gene resulted from mutation prevents the melanocytes from producing melanin. As a result, their hair is white, their eyes pink, and their skin appears very fair.

2.4.2 Seborrheic kerotoses

Seborrheic kerotosis is the presence of benign wart-like growths on the surface of the skin. (NIH website: www.nlm.nih.gov/medlineplus/ency/article/000884.htm) Seborrheic

kerotoses are hyperpigemented lesions having a visual color of yellow, brown, or black, and have a slightly elevated, waxy, and flat surface. The shape is mostly round to oval. There are usually multiple growths.

2.4.3. Melanocytic nevi

Malanocytic nevi, or moles, are commonly seen skin pigmentary disorders, especially in caucasoids. For some unknown reason which seems to relate to inherited trait, melanocytes migrate to the epidermis from the neural crest during embryonic development and form cells containing melanin known as nevus cells. The depth distribution of these nevus cells determines the type of a nevus. A junctional nevus is formed when nevus cells cluster at the dermo-epidermal junction area; an intradermal nevus is formed by nests of nevus cells in the dermis. And a compound nevus shows both components. When nevus cells go deep in the dermis, the tissue scattering effect gives the lesion a blue color, as in a blue nevus. (Anderson, 1981)

The clinical presentations of each type of melanocytic nevi are different:

- Junctional nevi: they are flat macules with various sizes from 2 to 10 mm, and with color from light to dark brown. They are usually oval or round in shape and commonly found on palms, soles, or genitalia.

- Compound nevi: they are usually smaller than 10 mm in diameter, smooth at surface, and have varying degree of pigmentation. Some large compound nevi have a warty or cerebriform appearance.

- Intradermal nevi: They are dome-shaped papule or nodule, may or may not be pigmented, and mostly seen on the face or neck.

- Blue nevi: they look steely blue, are usually solitary, and mostly found on the extremities.

2.4.4. Skin cancer

2.4.4.1 Malignant Melanoma

Malignant melanoma is a malignant tumor of melanocytes, mostly arising in the epidermis. It is the most lethal skin tumor and the incidence rate has increased over the past few years. Malignant melanomas usually progress through two stages, horizontal and vertical. First the malignant melanocyte cells grow within the epidermis, then evolve into a stage when tumor cells grow vertically into dermis.

In clinical presentation, there are four main variants: superficial spreading melanoma, lentigo malignant melanoma, acral lentiginous malignant melanoma, and nodular malignant melanoma. The following 'ABCD Rule' summarizes the signs to look for when diagnosing malignant melanomas:
(www.cancer.org/docroot/SPC/content/SPC_1_ABCD_Mole_Check_Tips.asp)
A: Asymmetry – the tumor appears asymmetric;
B: Border – the edges are irregular, ragged, notched, or blurred;
C: Color – the color usually have differing shades of brown or black;
D: Diameter – the area is larger than 6 mm or is growing larger.

The exact cause of malignant melanoma is still unknown. However, it is believed that repeated short but intensive exposure to ultraviolet radiation may be involved.

2.4.4.2. Non-melanoma skin cancers

Besides malignant melanoma, basal cell carcinoma (BCC) and squamous cell carcinoma (SCC) are also commonly seen skin cancers. They are less lethal and don't directly involve skin pigmentary system.

Basal cell carcinomas are the most commonly seen skin cancer and typically found on the face in elderly or middle-aged subjects. These tumors arise from the basal keratinocytes

of the epidermis. Although locally invasive, they very rarely metastasize. The pathology shows that BCC is composed of uniform basophilic cells, in well-defined islands, that invade the dermis from the epidermis as buds, lobules, or stands.

Squamous cell carcinoma is a malignant tumor which is derived from keratinocytes and usually arises in a damaged skin area. It is mostly found in people over 55 years old and is more common in males than in females, and may metastasize. The malignant keratinocytes which keep the ability of keratin production destroy the dermo-epidermal junction and invade the dermis in an irregular manner.

3. Basic tissue optics

3.1 Light-tissue interaction

When a beam of light shines onto the surface of skin, the incident photons start to interact with the tissue molecules, by exchanging energy with the orbital electrons or with the molecules as a whole. On one hand, photons change the state of tissue molecules, which is used for therapeutic applications, such as in photothermolysis, photodynamic therapy (PDT), tissue welding, and so on. On the other hand, tissue molecules change the state of photons, and some of which can escape from tissue and be detected. These detected photons contain information of those tissue molecules, and extraction of this information leads to diagnostic applications, such as in diffuse reflectance imaging and spectroscopy, Raman spectroscopy, and so forth.

This paper focuses on diagnostic uses of light-tissue interaction. Suppose there is a large amount of photons striking on the tissue, major interaction types are listed as follows:

- Specular reflectance

When the incident light reaches the skin surface, a certain amount of light is directly reflected back to the air. This is because the refractive index of tissue is different from that of air and as such, part of the light energy cannot be coupled into tissue. Reflectance R, or the ratio of reflected light intensity to total incident light intensity, is given by Frenel Equations:

$$R = \left| \frac{n_t \cos q_i - n_i \cos q_t}{n_t \cos q_i + n_i \cos q_t} \right|^2$$

where n_i and n_t are the refractive indices of the incident medium (usually air) and the tissue, respectively. $?_i$ and $?_t$ denote the incident angle and the refraction angle, which is determined by Snell's Law:

$$n_i \sin q_i = n_t \sin q_t$$

- Diffuse reflectance

When photons travel through tissue, they are constantly being absorbed and scattered. When a photon is absorbed, it gives its energy to the interacting molecule (the absorbing molecule is called a chromophore) and vanishes. When a photon is scattered, it changes its momentum and/or energy. In most cases, the scattering process is elastic, in which it excites a molecule to a higher energy state and, when the molecule returns to the ground state, a new photon with the same energy is emitted, with isotropic angular distribution. Statistically this causes deflections of light propagation tracks. There is a small chance for a photon to experience inelastic scattering. This will be introduced in the section of Raman scattering later.

If a photon experiences single or multiple elastic scatterings, while avoided from being absorbed along its track and successfully escapes outside of tissue, it can be detected as diffuse reflectance light. Together with specular reflectance light, they give the appearance of skin tissue by our visual inspection.

- Fluorescence

When a photon interacts with a molecule, there is a possibility that the molecule will produce fluorescence light. In this case, the molecule first absorbs the photon and is excited to a higher energy level. Instead of directly returning to the ground level, the molecule comes to an intermediate level without generating radiation. Then from that intermediate energy level, the molecule returns back to the original ground state and emits a photon with longer wavelength to conserve the total energy. These re-emitted red-shifted photons constitute fluorescence light.

- Raman scattering

During an inelastic scattering, or Raman scattering, the scattered photon passes some energy to the interacting molecule, which excites vibrations or rotations of the molecule.

Since each molecule has its characteristic modes of vibration and rotation, the amount of energy shift in the Raman scattered photon contains information of the molecular bond. This can be recognized as a fingerprint of that particular molecular bond.

3.2 Tissue optical properties

3.2.1 Definitions

3.2.1.1 Absorption

When a collimated beam of light with intensity of I propagates through a homogeneous medium, the effect of absorption is quantified by the absorption coefficient:

$$dI = -m_a I dx$$

where dI denotes the intensity of absorbed light when traveling through a distance of dx. Here we assume that the only attenuating interaction is absorption (no scattering). Therefore, the physical meaning of μ_a is the probability of absorption across a unit travel length.

From the microscopic point of view, the absorption coefficient can be expressed as:

$$m_a = r s_a$$

where ? is the density of absorber which each has absorption cross-section of s_a. And the reciprocal, $1/\mu_a$, is the mean free path a photon travels between consecutive absorption events.

The optical density (O.D.) characterizes the absorbing ability of a medium and is defined as:

$$O.D. = -\log\left(\frac{I_t}{I}\right)$$

where I_t is the transmitted light intensity. Thus a medium of O.D. 5 means that after propagating through the medium, the light intensity is attenuated to 10^{-5} of its original value.

3.2.1.2. Scattering

Following the same way in last section, if we replace the interaction of absorption with scattering, we can define the scattering coefficient:

$$dI = -m_s I dx$$

where we assume there is no absorption occurring along the photon's track. From the microscopic view, the scattering coefficient can be defined as the multiplication of the scatterer density and the individual scattering cross-section:

$$m_s = r s_s$$

And $1/\mu_s$ is the mean free path between two consecutive scattering events.

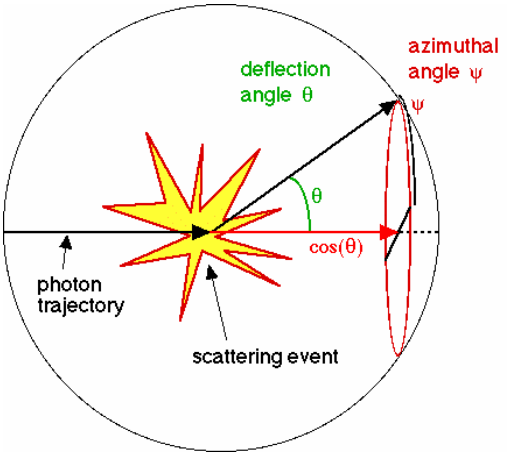

Figure 3-1. Illustration of anisotropy.

(http://omlc.ogi.edu/classroom/ece532/class3)

The scattered light can be deflected to 4p solid angle range. The statistical angular distribution is characterized by anisotropy g:

$$g = \langle \cos q \rangle = \int_0^p p(q) 2p \sin q dq$$

where p(?) is the scattering function which gives the angular dependence of deflected light. From the above expression, we can see that anisotropy is the average scattering angle, with g=0 as perfect isotropic scattering, and g=1 as purely forward scattering.

Combining scattering coefficient and anisotropy, we can have an equivalent isotropic scattering coefficient, or reduced scattering coefficient:

$$m_s' = m_s(1-g)$$

The physical meaning of reduced scattering coefficient is the total scattering cross-section when every scattering event is reduced to a perfect isotropic scattering event. Accordingly, reduced mean free path is the equivalent mean free path when every scattering event is isotropic.

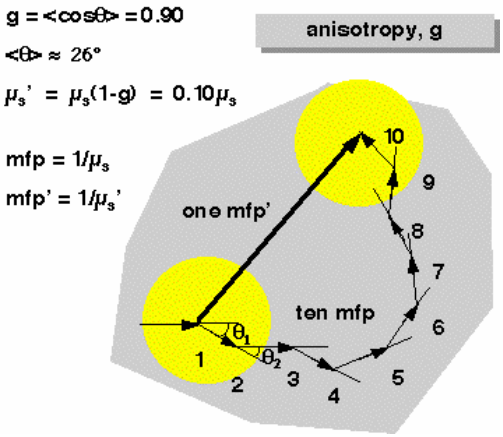

Figure 3-2. Illustration of reduced scattering coefficient. When g=0.90, statistically it takes 10 mean free paths to reach the next equivalent isotropic scattering event.

3.2.2. Skin optical properties

Figure 3-3 shows wavelength-dependent absorption of various tissue chromophores. It is clearly seen that between 600 – 1400 nm, there is minimal absorption. Therefore this wavelength range (far-red to NIR) is called therapeutic window, and is used to probe deeper tissue layers.

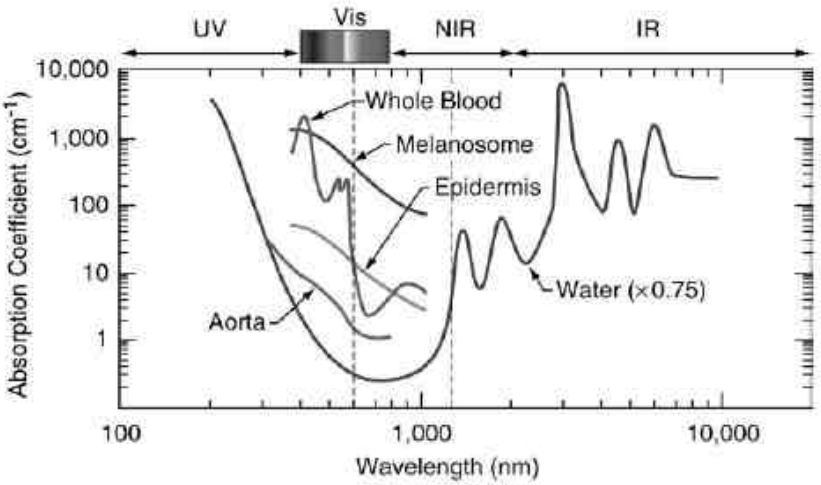

Figure 3-3. Absorption coefficients of human skin and its major components. (Vo-Dinh, T., 2003)

3.2.3. Melanin optical properties

Melanin is a complex tissue chromophore. There are two types of melanin from natural sources:

- Eumelanin. A black to brown insoluble material found in human black hair and retina.
- Pheomelanin. A yellow to brown, alkali soluble material found in red hair and red feathers.

Both types of melanin are important tissue chromophores, with their absorption curves shown below. However, neither of them shows strong fluorescence emission in previous studies. Although oxidation can enhance the fluorescence efficiency, it is still a relatively poor fluorophore. (Nordlund et al, 2006)

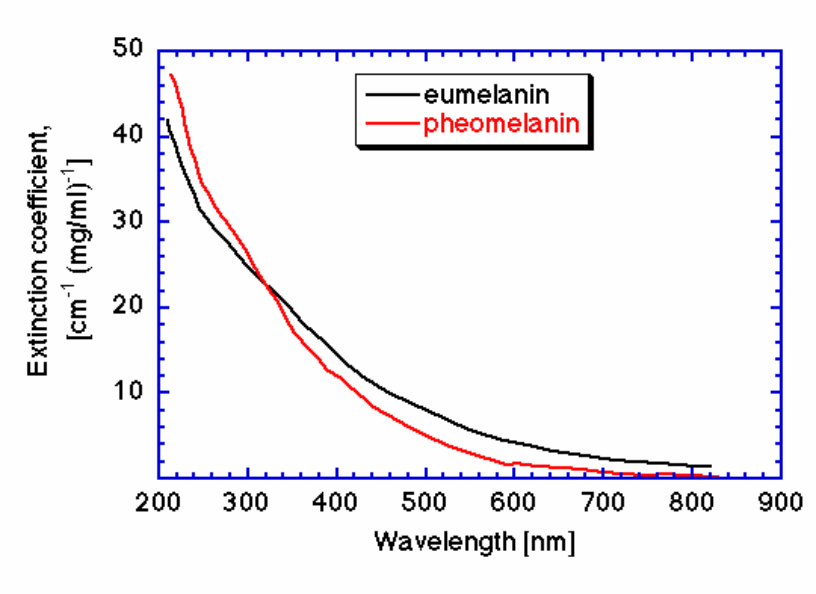

Figure 3-4 Extinction coefficients of eumelanin and pheomelanin.

(http://omlc.ogi.edu/classroom/ece532/class3)

4. *In-vivo* NIR fluorescence imaging of human tissue: fluorophores and techniques

The scope of this review is to update the progress that has been made on fluorescence imaging using near-infrared wavelengths in recent years, with an emphasis on *in vivo* studies. Near-infrared fluorescence imaging is becoming a popular technique for both studying basic tissue optical properties and investigating medical diagnostic applications. Comparing to fluorescence imaging in other wavelength ranges, NIR has the advantage of deeper penetration and less harmfulness to living tissue. NIR light can also target some fluorophores that cannot be excited by UV or shorter wavelength visible light.

When using NIR fluorescence imaging, there are two essential aspects to take into consideration: (1) what fluorophore(s) to look at, and (2) how to acquire the image.

4.1 Fluorophores

A fluorophore by definition means a molecule which fluoresces upon external light excitation, as compared to chromophore which is defined as a molecule absorbing incident light. It is actually a functional group in biomolecules which absorb the incident light in a specific wavelength range and re-emit light (fluorescence) in another specific wavelength range. The fluorescence intensity and absorption/emission wavelength range are determined by the intrinsic optical properties of the fluorophore as well as its micro-scale biochemical environment.

In tissue, there are some native molecules which emit fluoresce upon excitation of specific wavelengths. These molecules are called endogenous fluorophores and the emission is called autofluorescence. In comparison, exogenous fluorophores are bio-compatible fluorescent substances introduced into tissue, which are used to produce fluorescence in a desired condition.

4.1.1. Endogenous fluorophores

Most tissue endogenous fluorophores are excited by UV (< 400 nm) or visible light (400 – 700 nm). Proteins and nucleic acids are found to fluoresce under shorter UV light excitation (250 – 280 nm) and the dominant fluorophores in this case are tryptophan, tyrosin, and phenylalanine, with emission maxima between 280 nm and 350 nm. In longer UV and shorter visible wavelength range, collagen and elastin are major fluorophores with excitation band within 300 – 450 nm (blue light) and emission band between 400 and 600 nm. Other native fluorophores include the reduced form of coenzyme nicotinamide adenine dinucleotide (NADH), flavin mononucleotide (FMN) and dinucleotide (FAD). However, in far-red and near-infrared, only porphyrin has been reported to have fluorescence emission in the literature prior to our laboratory's work. (Tuan Vo-Dinh, Biomedical Photonics Handbook)

Melanin is an important tissue chromophore which absorbs strongly in UV and visible wavelength range, which gives it characteristic dark color in nevi and other pigmented skin disorders. However, melanin has always been considered a poor fluorophore. Only recently, it was first discovered by our group that under 785 nm excitation, cutaneous melanin exhibits strong fluorescence (Huang et al 2006, Han et al 2006). Since fluorescence is very closely related to a molecule's biochemical activity as well as its micro-environment changes, a thorough study of melanin's fluorescence property under NIR light excitation can largely expand our understanding of this important molecule, and is potentially useful in clinical diagnosis of pigmented skin diseases and skin cancers, such as melanoma.

4.1.2. Exogenous fluorophores

There are a number of synthesized molecules which can be used as exogenous fluorophores for NIR tissue fluorescence imaging. The most important and frequently used exogenous fluorophores are organic fluorescent dyes designed for NIR wavelength range. Besides desired excitation and emission bands in NIR range, an ideal fluorescent

dye used for tissue labeling should also have high absorption efficiency and high quantum yield, low photobleaching effects and low toxicity.

Based on the labeling mechanism, there are three types of fluorescent dyes: (1) non-specific label, (2) molecular-specific label, and (3) activatable label.

4.1.2.1. Non-specific fluorophores

These molecules don't attach to a specific target, in contrast, they randomly diffuse once introduced into tissue. Since a lot of disorders alter their nearby environment and make it favorable for those non-specific fluorophores to accumulate (in case of tumor, the nearby vasculature is significantly altered so that molecules have a high chance to leak out of blood vessel and stay with the tumor), those flourophores can effectively be used to light up under selected wavelength excitation, thus showing distribution of the target with pathological interest. A good example of these fluorophores is cyanine dye, which has all the desired optical properties as a contrast agent. In particular, Indocyanine Green (ICG), which absorbs strongly at 800 nm with an emission peak at 830 nm (in blood), has been approved by FDA and used widely in clinic for tumor detection. (Benson, 1978; http://omlc.ogi.edu/index.html)

It is also worth to note that *in vitro* study has shown a significant increase of fluorescence signal when ICG is put on roughened metal surface (Malicka, 2003), which has promising potential to greatly improve sensitivity of *in vivo* fluorescence imaging in the future. (Lacowicz, 2004)

4.1.2.2. Molecular-specific label

A strategy for probing specific molecules is to conjugate a fluorescent dye with specially designed ligands, which make the fluorophore selectively attach to the pathogen overexpressing particular receptors. Examples of the approach can be found in [Servick-Muraca, 2002; and Licha, 2002]. However, the problem of high background noise limits

the sensitivity of this technique, because all non-bound probe molecules also fluoresce under excitation and contribute to the background.

4.1.2.3. Activatable fluorophores

Another different type of fluorophore has been conceptualized and synthesized by R. Weissleder's group. The original fluorophores don't fluoresce because they are in a quenched state in normal condition. When the fluorophores reach those targeted tissue enzyme, they are immediately activated and start to fluoresce. More descriptions of this type of fluorophores can be found in [Licha 2002, and Ntziachristos 2003]. The advantage of this technique is that the signal to background ratio is higher, due to the low fluorescence from quenched fluorophores apart from targeted enzymes.

4.1.2.4 A new class of exogenous fluorophore: Quantum Dots

Quantum dots, or QDs, are specially engineered nanometer-sized semiconductor particles with typical sizes in nanometer range. Compared to organic fluorescent dyes, they have the following advantages:

- Ttunable optical properties by changing particle size
- Broad excitation band and narrow emission peak, which enables multi-color fluorescence labeling using single wavelength excitation
- No observable photobleaching effect
- Easy surface modification to acquire additional functions, e.g. water solubility
- Can attach ligands to target specific molecules by antibody/antigen reaction, peptides, etc.

An encouraging example of using NIR quantum dots for *in vivo* imaging has been demonstated by Kim *et al*. They tuned core/shell structured quantum dots (CdTe/CdSe) to emit at 850 nm to successfully obtained images of lymph nodes as deep as 1 cm in tissue. (Kim, 2004). Since the minimal autofluorescence from background as well as the

high extinction coefficient and quantum yield from QDs, an amount as small as 400 pico-mole was sufficient to produce fluorescence images almost free from background noise.

With fast progress in using quantum dots as biomarkers for tissue imaging, there are a number of excellent review articles on the topic in recent years (Pinaud 2006; Gao, 2004; Smith 2004). Despite the encouraging results, we should not overlook the potential health risks of these particles, since Cadmium is a strongly toxic substance and researches have yet been able to find an effective way of excreting Cadmium from human body. Instead, they can accumulate in the liver and kidney and distribute to other tissues with a half-life of about 20 years. (Pinaud, 2006; Hoet 2004).

4.2 Techniques

Various imaging techniques have been developed to produce fluorescence images with both endogenous and exogenous fluorophores in the NIR wavelength range. Three important types of NIR fluorescence imaging techniques are summarized here: surface imaging, tomographic imaging, and multi-photon imaging.

4.2.1. Surface imaging

Surface imaging is the most straightforward way in which the fluorescence image is formed directly by emitted fluorescence photons from skin surface. This method has in principle no difference from taking an image with a digital camera. In order to achieve satisfactory SNR (signal-to-noise ratio), especially when performing autofluorescence imaging where the signal from native tissue fluorophores is relatively weak, one needs to block the specularly and diffusely reflected incident light (without wavelength shift) as much as possible. A representative illustration of such an NIR fluorescence imaging system is shown in figure 4-1

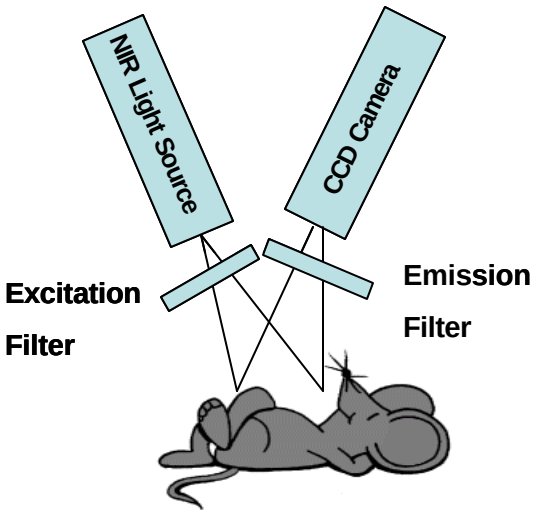

Figure 4-1. Illustration of a basic NIR fluorescence imaging system.

Demos and co-workers have studied the far-red and NIR autofluorescence emission from excised tissues. By combining NIR fluorescence and polarization imaging techniques, they developed methods for detecting cancer from *in-vitro* tissue samples. Their results show that the NIR images have the capability of detecting small cancers <= 1 mm surrounded by normal tissue. However, the relative difference of fluorescence intensity between tumor and normal tissue depends on the cancer types. (Figure 5-2, 5-3) For example, tumors in kidney have lower fluorescence signal than normal tissue, while for tumors in liver, fluorescence is higher than normal. (Demos 2004). They proposed that either elevated or reduced fluorescence signal intensity in cancer is due to the different activity of porphyrin production. However, there has not been rigorous microscopic biochemical study to support this hypothesis.

Figure 4-2. Images of a human liver tissue sample with hepatoblastoma. (a) Cross-polarized light-scattering image at 700 nm. NIR fluorescence images under (b) 532-nm and (c) 632.8-nm excitation. Cancer (CA) has higher fluorescence than normal tissue. (Demos, 2004)

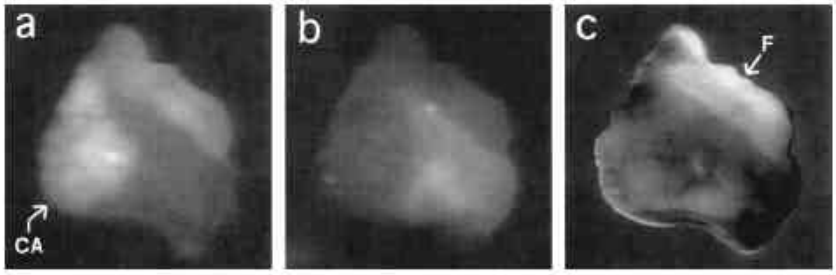

Figure 4-3. Images of a human kidney tissue with renal cell carcinoma. (a) Cross-polarized image at 700 nm. (b) NIR fluorescence images under 632.8 nm laser excitation. (c) Ratio of NIR autofluorescence image under 532-nm excitation over that under 632 nm excitation. CA, cancer; F, fat. Cancer has lower fluorescence than normal tissue. (Demos 2004)

Due to the lack of high yield endogenous fluorophores in NIR wavelength range, no *in vivo* autofluorescence imaging on human subjects has been reported prior to our work. Based on a recent discovery of strong autofluorescence from human cutaneous melanin from spectroscopic study [Huang et al, 2006], our group has built an NIR fluorescence imaging system which can acquire fluorescence images from melanin-involved human pigmentation and carried out a clinical pilot study. The imaging system will be described in Chapter 5, and results shown in chapter 6.

4.2.2. Tomographic imaging

On the other hand, 3-D tomographic imaging technique utilizing NIR light can be used with exogenous fluorophores to better quantify the spatial distribution of targeted molecules. In parallel to the idea of emission tomography in nuclear medicine, a fluorescent probe is injected into animal body and, by measuring multiple projections of fluorescence signal surrounding the animal, one can reconstruct the image and quantify the 3-D distribution of the fluorophore. An illustration of the imaging system is shown in figure 4-4. And figure 5-6 shows the comparison of Gd (Gadolinium)-labeled MR image and ICG-labeled Diffuse Optical Tomography (DOT) image of the same ductal carcinoma.

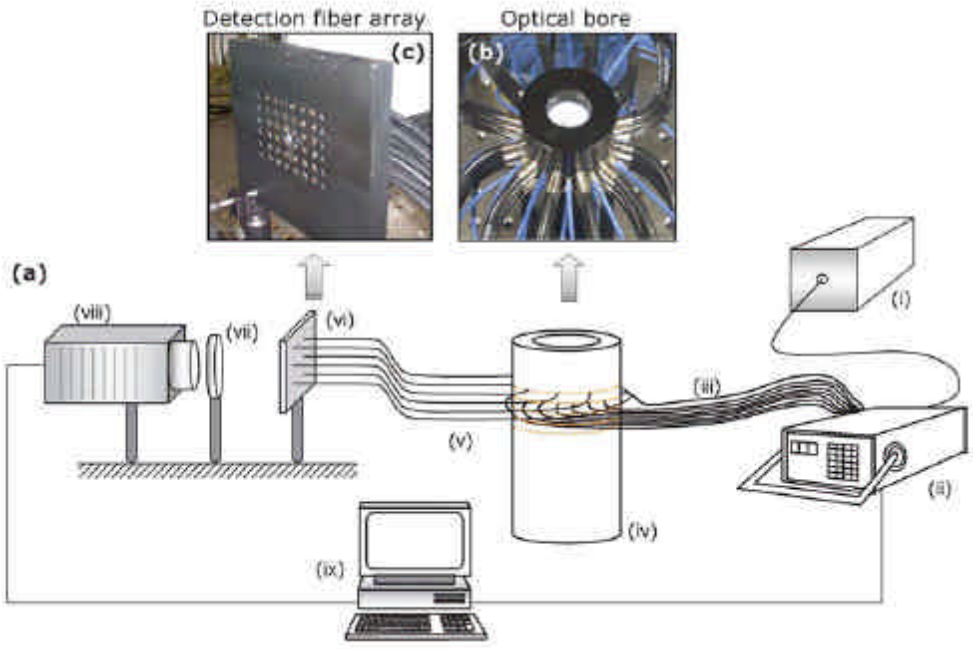

Figure 4-4. Example of an Fluorescence-mediated Molecular Tomography (FMT) scanner. (a) The scanner uses multiple sources and detectors to effectively collect light measurement at multiple projections around the animal's body. For details see text. (b) Photograph of the optical bore used for animal investigations. The source fibers (blue) and detection fiber bundles (black) are shown installed. (c) Photograph of the fiber bundle array arranged for imaging by the CCD camera. (from reference Ntziachchristos 2003)

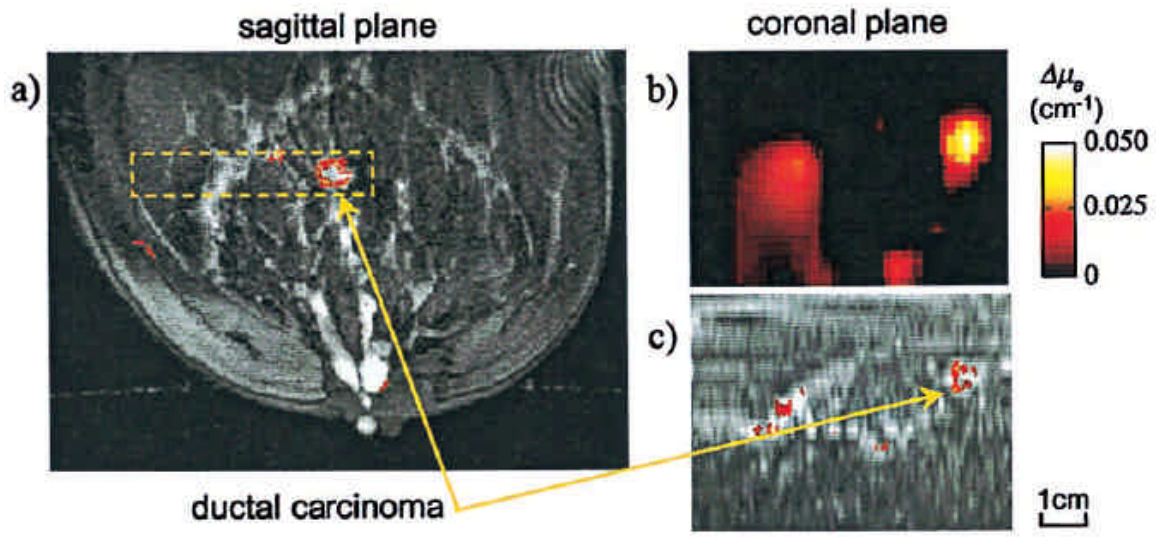

Figure 4-5. Ductal carcinoma. (a) Functional sagittal MR image after Gd contrast enhancement passing through the center of the cancerous lesion. (b) Coronal DOT image, perpendicular to the plane of the MRI image in (a), for the VOI indicated on (a) with the interrupted line box. (c) Functional MR coronal reslicing of the VOI with the same dimensions as (b). (from reference Ntziachchristos 2000)

4.2.3. Multi-photon fluorescence imaging

By using a specially designed gradient index (GRIN) lens and injecting an appropriate contrast agent, Levene and co-workers have shown that two-photon microscope is capable of taking fluorescence images of live animal brain. (Levene, 2004). For microangiography they imaged Quantum Dots as deep as ~800 microns below the surface of cortex by 830 nm excitation. And for brain imaging they detected yellow fluorescent protein (YFP) ~1 mm below the surface or cortex by 920 nm excitation. (figure 4-6, 4-7, 4-8)

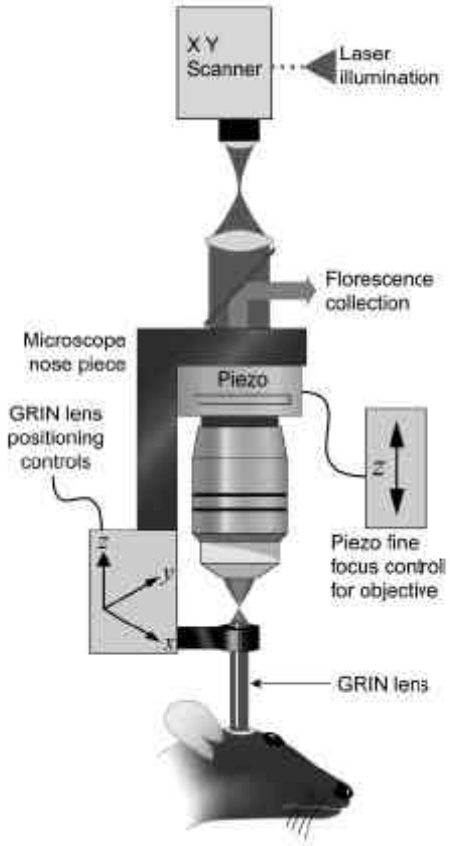

Figure 4-6 Experimental arrangement for using gradient index (GRIN) lenses in conjunction with multiphoton microscopy. A hydraulic micropositioning system locates the GRIN lens relative to the objective lens. A piezoelectric focus control performs fine focusing without moving the GRIN lens inside the animal. (from reference Levene 2004)

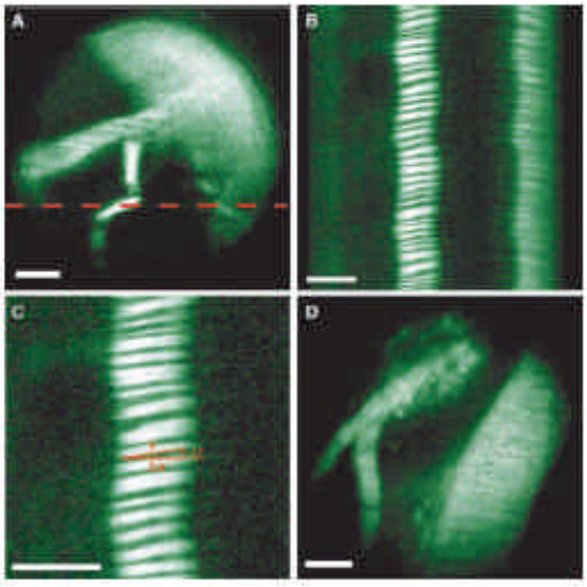

Figure 4-7 *In vivo* microangiography in wild-type mouse. A: blood vessels containing fluorescent quantum dots 800 micron below the surface of cortex. B: line scan of small capillary in A as indicated by dotted red line. C: zoom of section in B; **Δ** x is the spatial dimension of the line scan, **Δ** t is the time dimension, and the hypotenuse is the velocity. D: capillaries containing fluorescein-dextran more than 2 mm below the surface of cortex. Scale bars are 10 micron. (from reference Levene 2004)

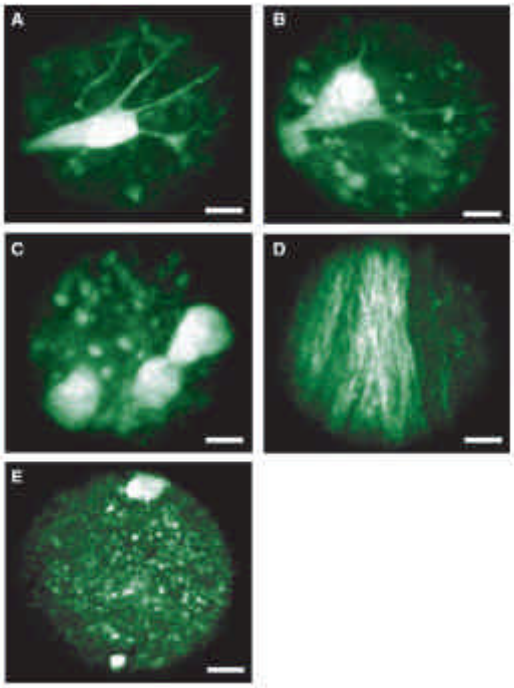

Figure 4-8. In vivo images of brain in anesthetized THY1-YFP line H mice. A–C: images of yellow fluorescent protein (YFP)-containing cell bodies of layer V neurons 700–800 micron below the surface of cortex. D: image of axon bundles in the external capsule ~1 mm below the surface of cortex. E: image of neuropil in hippocampal region CA1, ~1.5 mm below the surface of cortex. Scale bars are 10 micron. (from reference Levene 2004)

5. Instrument design and performance evaluation

5.1 Experiment setup

In the imaging system, light coming from a 785 nm diode laser is coupled to a ring light guide, which directs the excitation light to uniformly illuminate the interested skin area. Reflectance and fluorescence light are then collected by an NIR-sensitive CCD camera to form images. The system is designed to perform both reflectance and fluorescence imaging within a clinically affordable time. Switching between the two imaging modes is achieved by placing appropriate filters into the optical path. This is controlled by computer and as such, the resultant reflectance and fluorescence images are very well co-registered. The block diagram of the system is shown in the following figure 5-1 and a picture of the actual system is shown in figure 5-2.

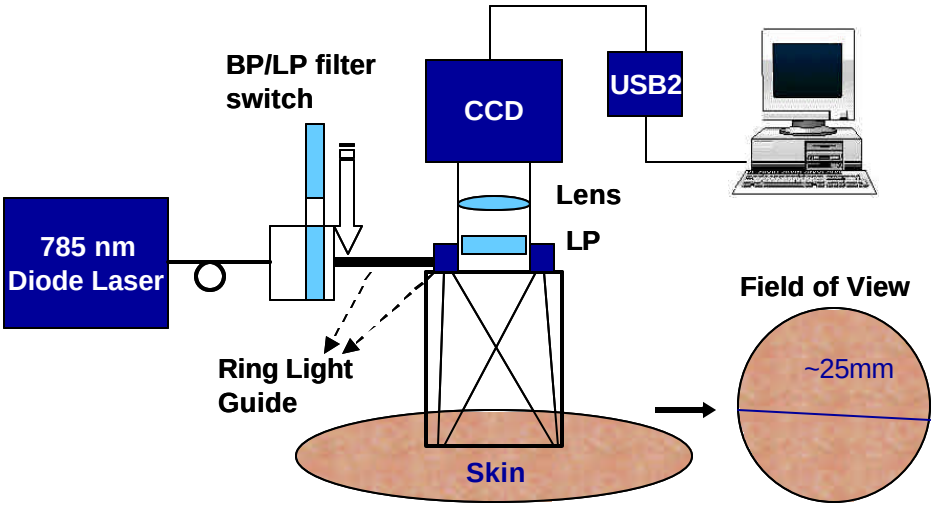

Figure 5-1. Block diagram illustration of the imaging system. BP: band-pass filter. LP: long-pass filter.

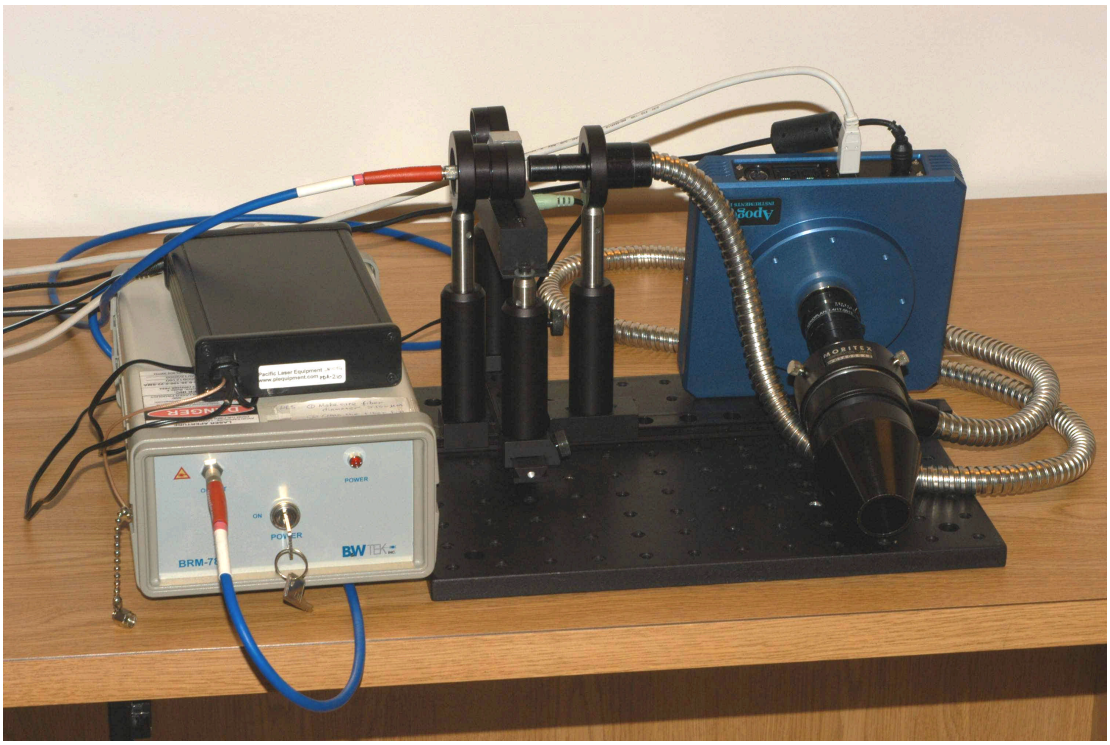

Figure 5-2. Photograph of the imaging system.

5.2 Components

5.2.1 Light source

The light source used in this system is a fiber-coupled, multimode diode laser with central wavelength at 785.113 nm (Model number: BRM-785-0.35-100-0.22-SMA, B&W TEK Inc., Newark, Delaware). The full-width-half-maximum (FWHM) is 0.176 nm and total power output is approximately 350 mW. An optical fiber (P200-2-VIS/NIR, Ocean Optics Inc., Dunedin, FL) is used to couple the laser with external optical path.

5.2.2 Excitation filter

For fluorescence mode, a band-pass filter (MaxLine™ Laser-line Filter LL01-785-25, Semrock, Rochester, NY) is inserted right after the laser light to block the broad laser tail outside of the central wavelength at 785 nm. This filter is indispensable for producing

autofluorescence images and more detailed discussions can be found in the 'pitfalls' section below.

For reflectance mode, a computer-controlled actuator (PLB-50, Pacific Laser Equipment, Santa Ana, CA, see figure 5-3) is used to switch the excitation filter to a colored glass long-pass filter (RG-830, Edmund Optics Inc., Barrington, NJ, see figure 5-4 for transmittance curve), which has the same cut-on wavelength as the emission filters (described below). This configuration is actually utilizing the laser tail (>830 nm) as illumination light and the reflected light is captured in the wavelength range of 830 ~ 1000 nm, with the upper end limited by the sensitivity range of the CCD camera. Usually the design for this dual mode system needs an additional dedicated illumination light source and/or involves filter change before the light collection. In contrast, the current design used for this system minimizes complications when switching between reflectance mode and fluorescence mode, because no additional light source is needed, and no mechanical filter movement on the camera side is involved. The resultant illumination light is shown in figure 5-5.

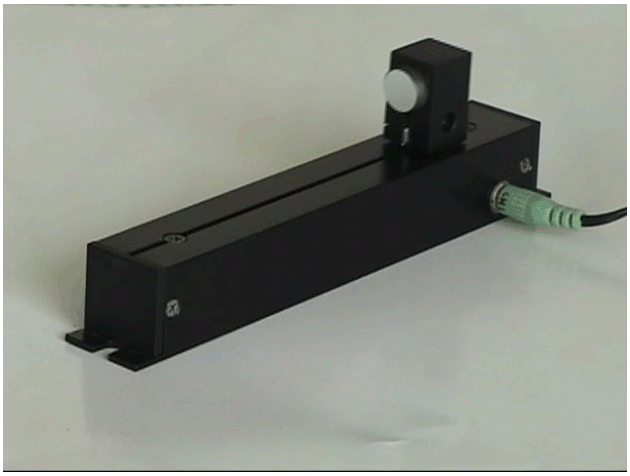

Figure 5-3. PLB-50 actuator used for a computer-controlled filter switch. (controller not shown)

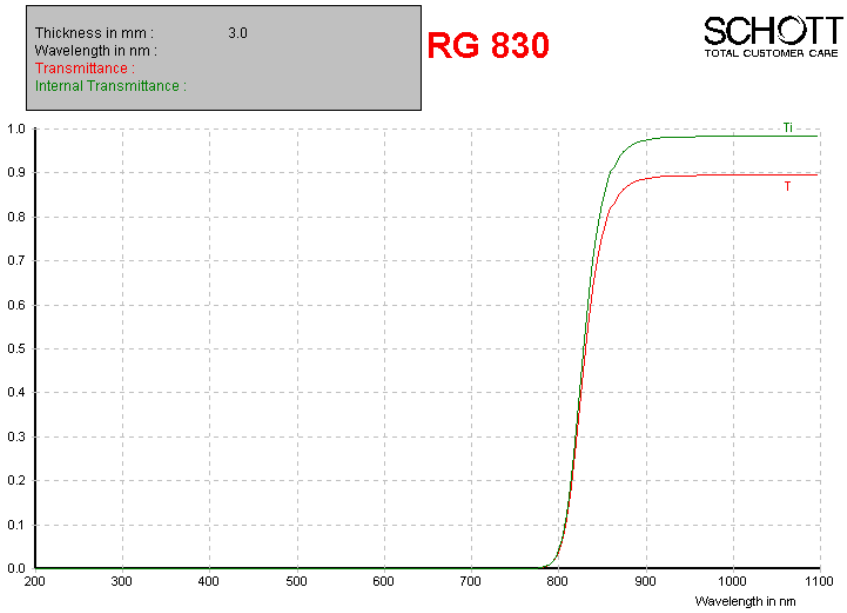

Figure 5-4. Schott glass filter RG-830.

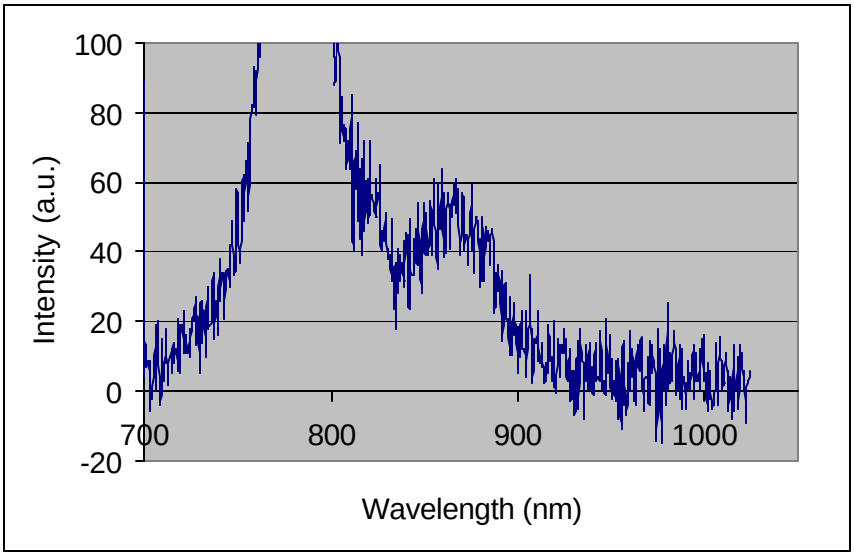

Figure 5-5. Actual illumination light measured for reflectance imaging mode. Notice there is a peak at ~870 nm produced by 830 nm LP filter. The reflected light with peak at 785 nm (main peak) will be blocked by emission filters cutting on at 830 nm, while the reflected light with smaller peak at 870 nm will go through emission filters and forms the reflectance image. In the reflectance image, the fluorescence generated by the main peak is negligible because this peak has already been reduced by about 4 orders by the LP filter as compared to original laser output.

5.2.3 Ring light guide and probe

After passing the band-pass filter, the light is coupled into a fiber-bundled ring light guide (Model number: MRG31-1500S, MORITEX USA INC., San Jose, CA). Multi-component glass optical fibers (core diameter: 45 microns) are bundled together at the entrance end and are randomly distributed on a ring-shaped area at the exit end. The heat resistance of the light guide is 200 ℃ which is well above the heat generation when the filtered laser light is transmitting inside the light guide. The transmittance rate of this light guide is above 60 percent at 785 nm. (figure 5-6)

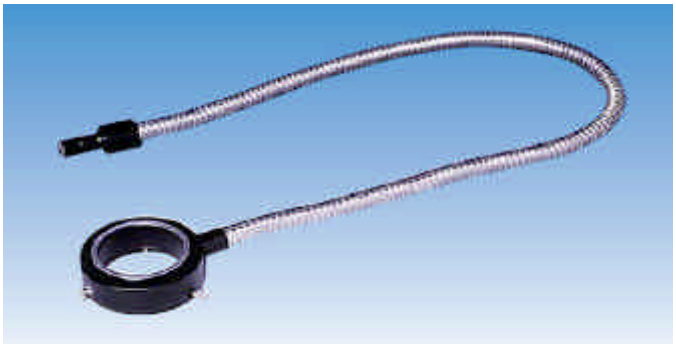

Figure 5-6. Ring light guide.

The transmitted light through the ring light guide gives a nearly uniform illumination at a specific distance, which is ensured by a customized probe. One end of the probe is connected to the ring light guide, and the other end is place gently on the skin surface to deliver the illumination light to skin. The probe also collects the reflectance and fluorescence light from the skin, while blocking ambient light from entering the optical path.

5.2.4 Lens

The reflected and fluorescence light from skin are collected by the probe and transmit through the hole of the ring light guide. Then a compact lens optimized for 400 – 1000 nm wavelength range (Xenoplan 1.4/17mm, Schneider Optics Inc., Hauppauge, NY) further collect the light and project it to the CCD camera. The focal length and iris of the

lens are fixed for most clinic measurements. But both of them are adjustable for special cases, such as an elevated skin lesion, which needs re-focusing as well as increasing the depth of field by reducing the iris size.

5.2.5 Emission filters

For fluorescence mode, the reflected excitation light needs to be blocked to show only the re-emitted fluorescence photons from skin tissue. Therefore, a long-pass filter set illustrated in figure 5-7 is inserted before the lens and the CCD camera. Ideally a single filter should suffice this purpose. For technical reasons, however, a filter combination of two colored glass LP filters (RG-830, Edmund Optics Inc., Barrington, NJ)) and an interference filter (RazorEdge Long Wave Pass Edge Filter LP02-785RU-25, Semrock, Rochester, NY) is necessary to completely remove the reflectance light. Detailed reasons are provided in section 5.3.2.

For reflectance mode, it is not necessary to place any filters before the detector. However, the design of the filter housing doesn't allow quick removal of the long-pass filters used for fluorescence mode. As a result, those long-pass filters stay for both fluorescence mode and reflectance mode, while the switching of imaging modes is accomplished by changing excitation filter (see section 5.2.2).

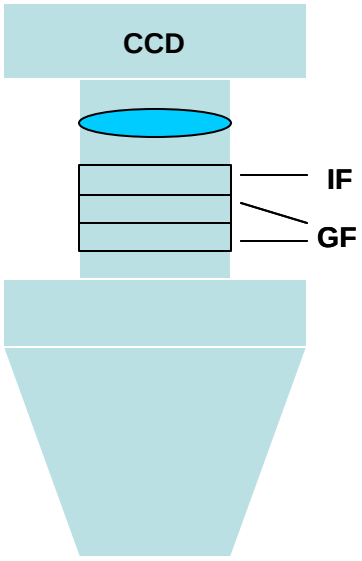

Figure 5-7. The emission filter set is placed after the probe and before the lens. GF: colored glass filter; IF: interference filter.

5.2.6 CCD camera with computer control

An NIR-optimized CCD camera (Alta® U1, Apogee Instruments Inc., Roseville, CA) is used as detector for the fluorescence signal. The sensitivity spectrum provided by the manufacturer is shown in figure 5-8. This camera is connected to a Pentium-4 computer by a USB2 port and a bundled software, MaxIm Plus (Version 4.51, Diffraction Limited, Ottawa, Ontario) which is used for CCD camera control in image acquisition as well as image viewing, processing, and analysis. (figure 5-9)

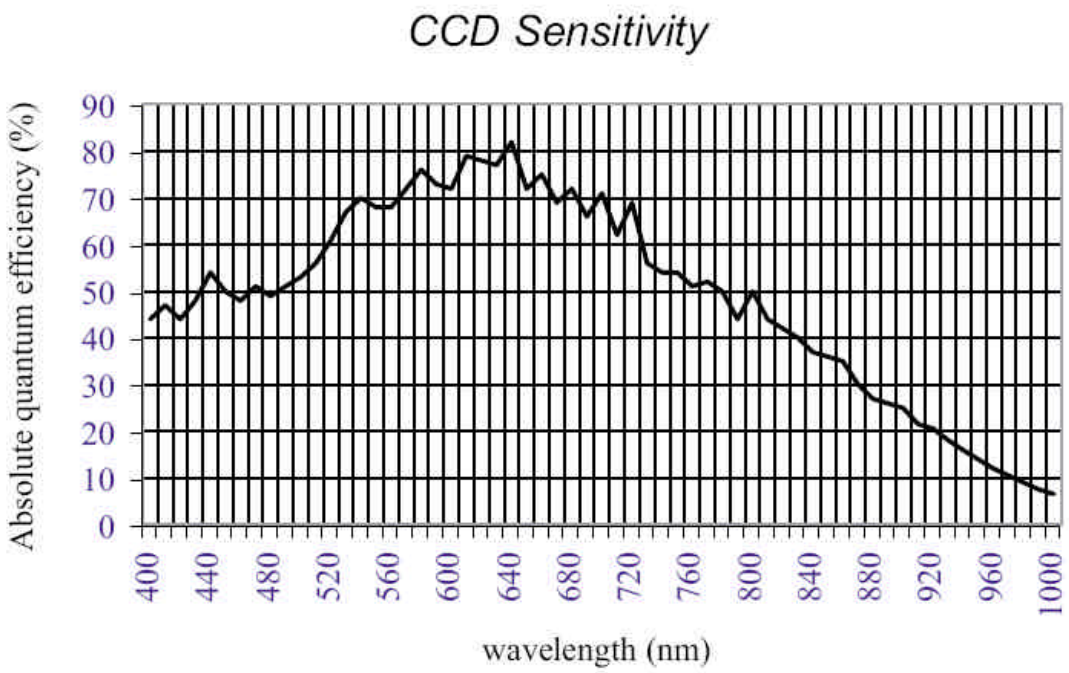

Figure 5-8. Absolute sensitivity spectrum of Alta U1 CCD camera

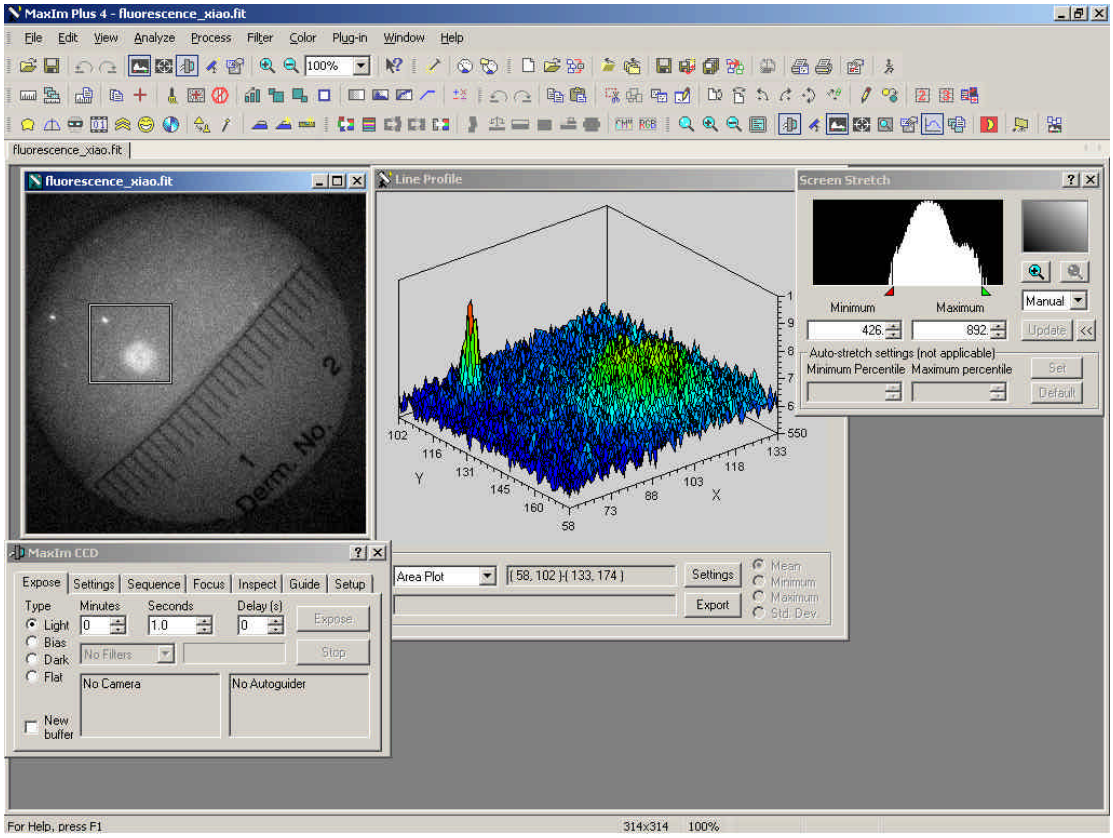

Figure 5-9. The imaging software, MaxIm Plus 4.

The components described above constitute the core of the imaging system. There are also some optional components could be added into the system to carry out additional functions or allow more flexibilities.

- Accessory 1: polarizers with rotational holder

A pair of glass polarizers (colorPol VIS 690 BC4, Codixx AG, Germany) customized for this project can be inserted into the optical path to produce polarized images. (Figure 5-10)

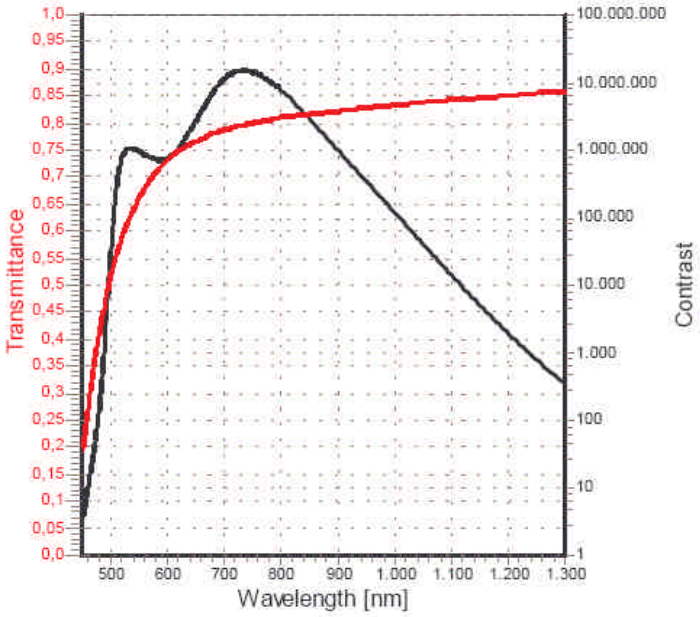

Figure 5-10. Spectral properties of colorPol VIS 690 BC4 glass polarizers.

- Accessory 2: alternative light source (Xe Lamp)

A xenon lamp was also tested as the light source for this imaging system. It has been discovered that, when using xenon lamp, the fluorescence generated by the Schott glass substrate of filters play a non-negligible role and as such, substantially decreased the image quality. As a result, before replacing the Schott glass filters with new filters with low autofluorescence substrate, xenon lamp is not a good choice as the light source.

- Accessory 3: focusing rail

For clinical applications, the camera is usually held by a physician or a technician during measurements. However, for animal or tissue sample studies, hand-held imaging is not stable and the images become blurry with extended exposure time. Therefore, a focusing rail is used to mount the camera and keep a constant distance between the camera and the sample to ensure good focus.

5.3 Pitfalls in system design

An important issue of *in-vivo* NIR fluorescence imaging is to achieve satisfactory signal-to-background ratio (SBR). This is not trivial because tissue autofluorescence in NIR is much weaker compared to that in visible light. The tail part of excitation light outside of main peak, reflected excitation light, and contaminant light from other ambient environment can easily beat the less intense NIR autofluorescence signal. Therefore, several pitfalls are listed as follows, with solutions suggested to avoid each of them.

5.3.1 Impurity of excitation laser line

Beyond the central wavelength at 785 nm, the laser tail extends to wavelengths above 830 nm. This extended laser tail, as a result, will produce its own reflectance from tissue and go through the emission long-pass filters with cutting-on wavelength at 830 nm. This reflectance acts as background noise and can be comparable or stronger than tissue autofluorescence. Figure 5-11 shows an example of imaging a nevus where this background noise presents a serious problem. When excited by 785 nm laser light, melanin in nevi exhibits higher NIR autofluorescence than normal tissue (Huang *et al* 2006)**.** Therefore, a nevus is expected to be brighter than surrounding normal skin in NIR AF images. However, without a BP filter to purify excitation laser light, the nevus becomes invisible in the NIR AF image. This is because the laser tail photons are absorbed by the nevus, which causes it look darker than normal skin. Summing up fluorescence and reflectance, which roughly cancels each other, the nevus can't be seen.

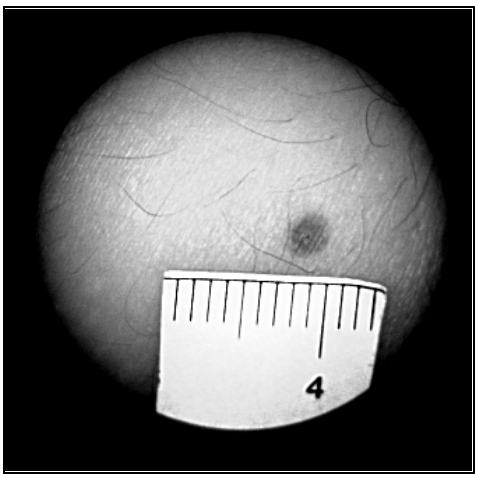

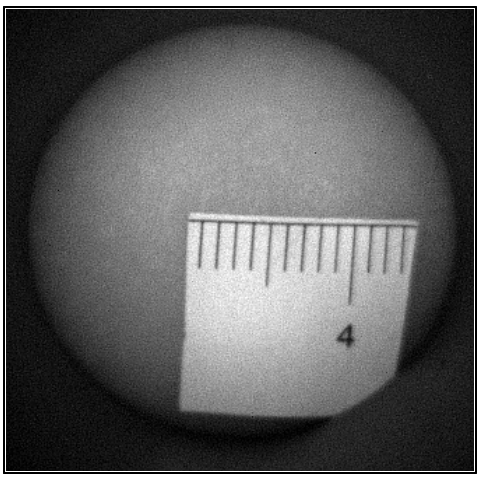

NIR reflectance image NIR fluorescence image

Figure 5-11. The effect of impure excitation light on imaging a junctional nevus. Left: reflectance image of the nevus; Right: fluorescence mixed with reflectance of the same nevus resulted from impure excitation light. The higher emission from fluorescence and the higher absorption from reflectance cancel each other and make the nevus invisible.

To solve this problem, a band-pass filter transmitting light at 785 nm is inserted right after the laser to block the laser tail. To evaluate how well the band-pass filter purifies the excitation light, spectral data are compared for with and without the band-pass filter after the laser. The experiment set-up is shown in figure 5-12, and the result is shown in figure 5-13. The purpose of the integrating sphere in this experiment is to collect reflected light from all directions.

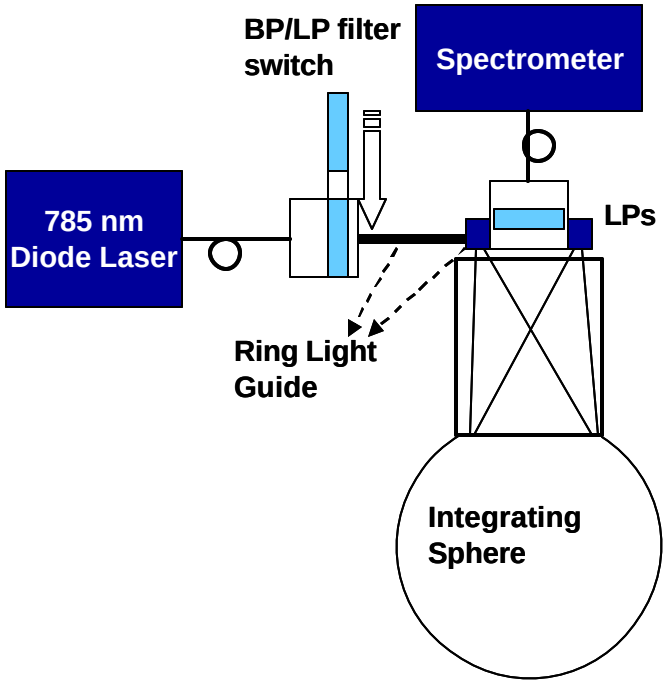

Figure 5-12. Experiment for test the effect of the BP785 filter. BP: band-pass filter at 785 nm. LPs: long-pass filters with effective cut-on wavelength at 830 nm. IF: interference long-pass filter with cut-on wavelength at 785 nm.

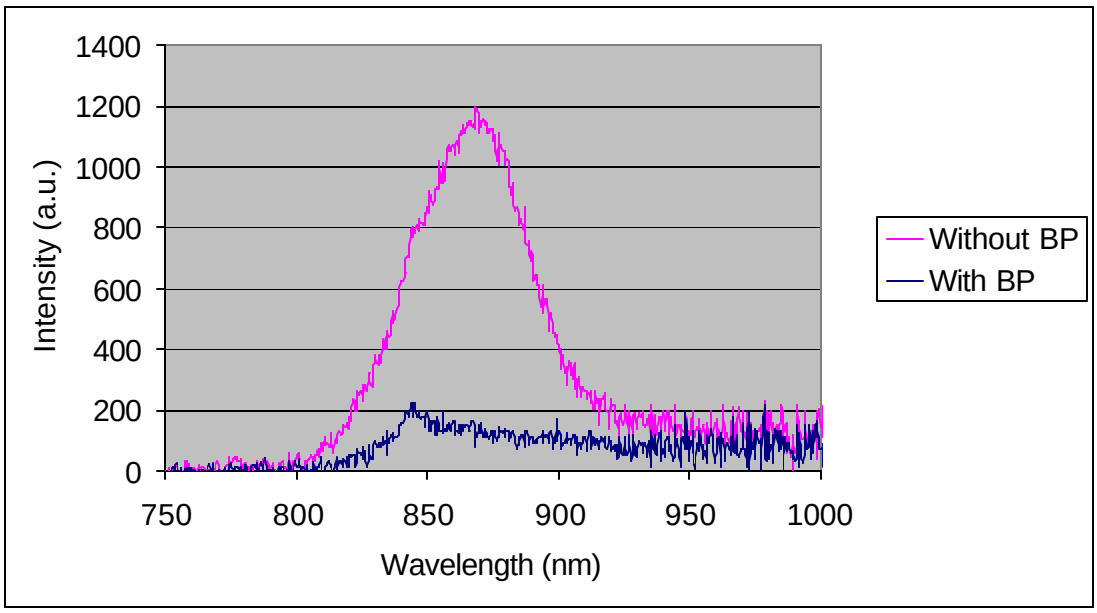

Figure 5-13. Comparison of the detected light spectrum with and without band-pass filter after the laser.

In figure 5-13, we can see that in both cases, the excitation light has been completely removed. In addition, if we assume the integrating sphere has no fluorescence at all, any light detected above 830 nm is background noise. From the graph it is clearly seen that the noise is reduced by 6-fold after we insert the band-pass filter. This is crucial in improving the contrast in fluorescence images. It is also noticed that the residual noise has a different spectrum shape than the original one, which suggests the noise comes from different sources in the two cases. Without the BP filter the noise is the reflected laser tail in the detection range of 830 ~ 1000 nm. The BP filter has an optical density value of 5, which completely removes the laser tail. However, the glass substrate of the BP filter also generates fluorescence, which also goes into the detection range. This means we cannot further reduce the background by removing more laser tail. In stead, we need to find a better filter substrate with lower autofluorescence.

5.3.2 Necessity of multiple emission filters

There are two types of filters extensively used in optical imaging, namely, interference type and absorption type (or colored glass), which can both produce the filtering effect but by different mechanisms. Interference filters use multi-layered coatings on the surface of a glass substrate to produce constructive interference for passing wavelengths and destructive interference for blocking (reflecting) wavelengths. Colored glass filters use a particular material dispersed inside the glass substrate to absorb unwanted light, while passing light in other wavelength range.

For this imaging system, neither single interference filter nor single colored glass filter gives satisfactory effect because each of them has its limitations and is complementary to each other for this imaging purpose. The advantage of interference filters is they have a very sharp cut-on edge at a particular wavelength and offer excellent contrast between passing and blocking spectral regions (usually > O.D. 5). But they are very sensitive to incident angle and as a result, require collimated beam incident at 0 degree for claimed performance. This is not easily achievable for the collected light in this imaging system configuration. In fact, the diffusely reflected light and scattered fluorescence light will

come from the whole spot of FOV and goes through the long-pass filter in different angles, and then be collected by the lens. Therefore, the collected light is neither collimated, nor incident at normal direction. As a result, the light going through the central region of the filter has higher contrast, i.e. less excitation light is leaked through the filter and enters the detector. But the light going through the peripheral region can't be filtered accurately, for the cutting-on edge has been slightly shifted to shorter wavelength range which overlaps with the excitation light wavelength due to non-zero entrance angle and as such, results in mixed reflectance and fluorescence photons reaching the CCD camera. The result is an image with darker center (almost pure fluorescence) and a brighter edge (fluorescence and laser reflectance, with the latter easily dominating). This is shown in figure 5-13, in which the detected light from a nevus is filtered by only one interference long-pass filter with cut-on wavelength of 791 nm (Semrock, LP02-785RU-25, Rochester, NY).

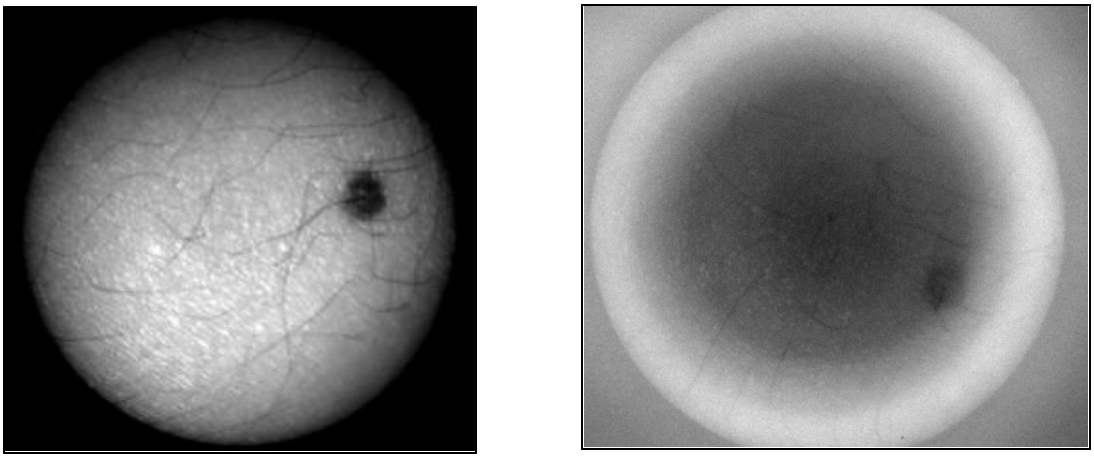

NIR reflectance image NIR fluorescence image

Figure 5-14. Example of using a single interference type long-pass filter as emission filter.

On the other hand, a single piece of colored glass filter doesn't give enough contrast either, i.e. excitation light will not be absorbed completely and part of it can enter the detector. About 4 or 5 pieces of colored glass filters need to be stacked together to provide an optical path long enough to completely absorb the excitation light. But in that

case, the fluorescence signal will be attenuated substantially too, which results in a very poor SBR.

The hints from the above argument are as follows:

- Interference type LP filters work better at the central area but has leakage at the peripheral part of the image.
- The colored glass LP filters work better at the peripheral part of the image due to longer optical path for absorption derived from the larger light incidence angle, but don't have complete absorption at the central area.

Based on this analysis, the solution is simply to use a combination of both types of filters, as described in section 5.2.5. Resultant clear images with good SBR can be found in chapter 6.

5.4 System evaluation for clinical applications

In order to use this imaging system in a clinical environment, there are several aspects worth of considerations, including: safety, easy of use, rapid data acquisition, and cost.

- Safety

The power density delivered to skin is measured to be 0.029 W/cm^2. This is well below the ANSI laser safety protocol.

- Cost

The total hardware cost of the whole imaging system, together with a dedicated computer and control software is estimated to be about 12,000 US Dollars. This is reasonable as a prototype system.

- Ergonomics (Ease of operation) (both operator and patient friendly)

For the person operating this imaging system to take images, it doesn't involve complicated procedures and is fairly easy to learn. In this study, a laboratory technician without optics background spent about 1 hour to learn the whole measurement procedures. Technical support is occasionally needed for system maintenance and troubleshooting.

For patients or volunteers, this system is very friendly. The entire procedure only involves gentle contact of the probe with the measuring skin surface and takes about 2 minutes for each lesion. Cleaning the measuring skin surface with an alcohol swab is needed prior to measurement.

- Rapid data acquisition

For each lesion, the current imaging system takes 2 seconds to acquire a fluorescence image and 1 second for a reflectance image. For most skin surface where the probe can stay steadily, this time is short enough to exclude the motion effect from the patient and the technician. However, for some special skin regions, such as nose, it is more difficult to keep the camera steady for 2 seconds and thus posing a limitation to obtaining a high quality image from those regions. The solution to this limitation is to replace the light source by another one with higher power output, which can shorten the exposure time needed for each image accordingly.

6. Results and discussions

6.1 Method

Using the NIR fluorescence imaging system described in the last chapter, a pilot study has been carried out at the Skin Care Center in Vancouver General Hospital as approved by the University of British Columbia Clinical Research Ethics Board (CREB Certification #: C05-0569). The main goal of the study is to verify the cutaneous melanin fluorescence from an imaging perspective. For this purpose, we measured patients and volunteers with pigmented skin lesions. Some of the lesions involve melanin and some have other chromophores accounting for the pigmentation. We expect to detect NIR fluorescence from those pigmented skin lesions caused by cutaneous melanin, while skin pigmentation caused by other substances serves as the control. For each lesion, we take a reflectance image and a fluorescence image using the NIR imaging system, and take a clinical picture using a Nikon digital camera as a reference.

In total we imaged 77 lesions on 54 volunteers and the results are shown below. For each type of lesion, one or two representative examples are chosen, with all other images listed in the appendix. Images of benign skin disorders, including normal and blue nevi, seborrheic keratoses, and vitiligo are provided first. Then we present the images of melanoma. Also a fluorescence image of melanin particles in wet and dry conditions is shown to provide comparison with *in vivo* cutaneous melanin. Finally a section of discussion summarizes the study results.

6.2. Results

6.2.1. Benign skin disorders

6.2.1.1. Nevi

Figures 6-1 to 6-4 show a junctional nevus, two compound nevi, and an intradermal nevus, respectively, from four different subjects. The junctional nevus is on the arm of a 24-year-old Asian male. The first compound nevus is on the arm of a 42-year-old Asian male, and the second is from a 17-year-old female's back. The intradermal nevus is from a 78-year-old male. It can be seen that the fluorescence signal is roughly uniform over the lesion and corresponds to darkness level in color image and NIR reflectance image. The low contrast in the reflectance image is mainly due to the reduced absorption of light by melanin in NIR wavelength range as compared to the visible wavelengths.

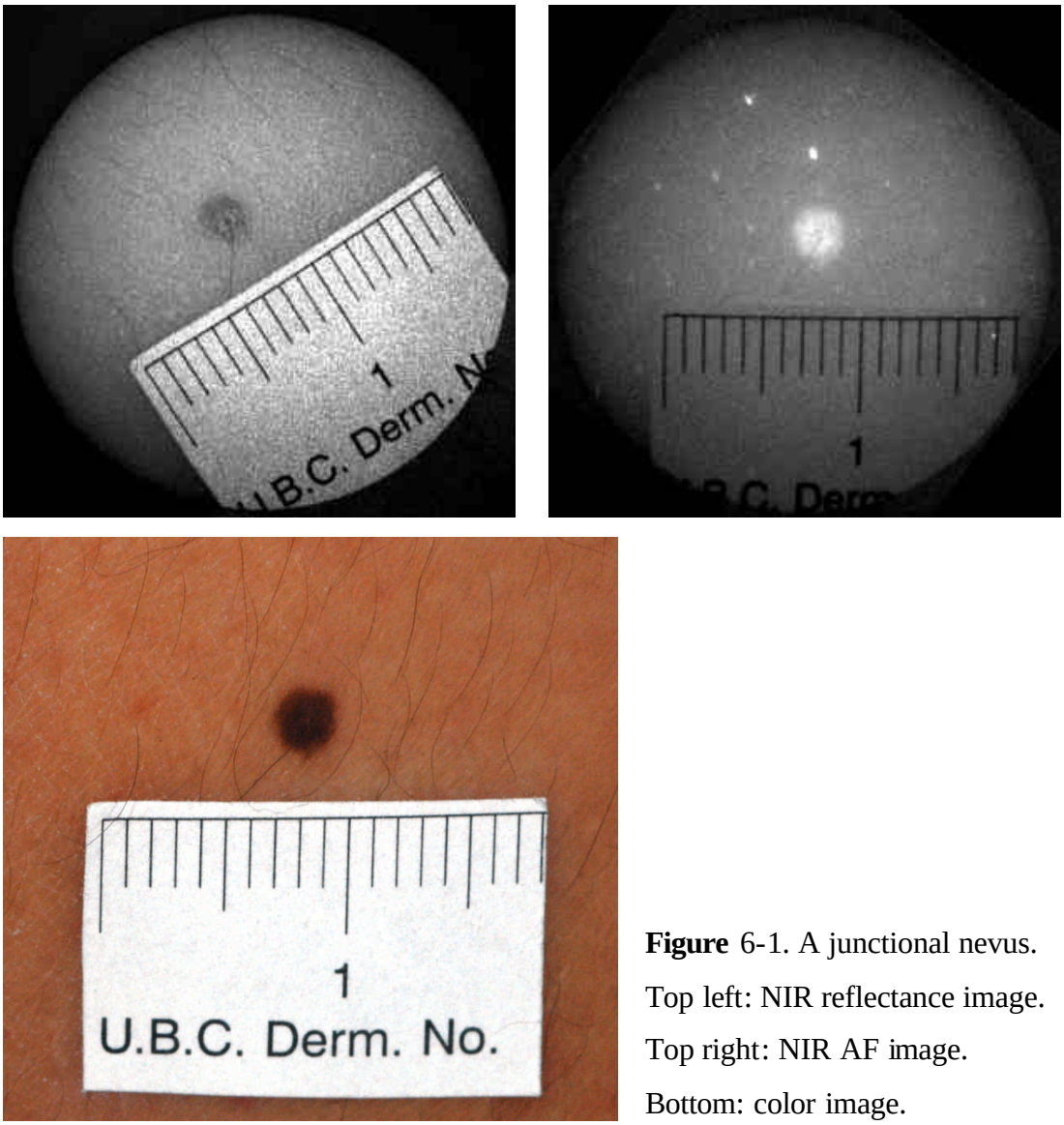

Figure 6-1. A junctional nevus.
Top left: NIR reflectance image.
Top right: NIR AF image.
Bottom: color image.

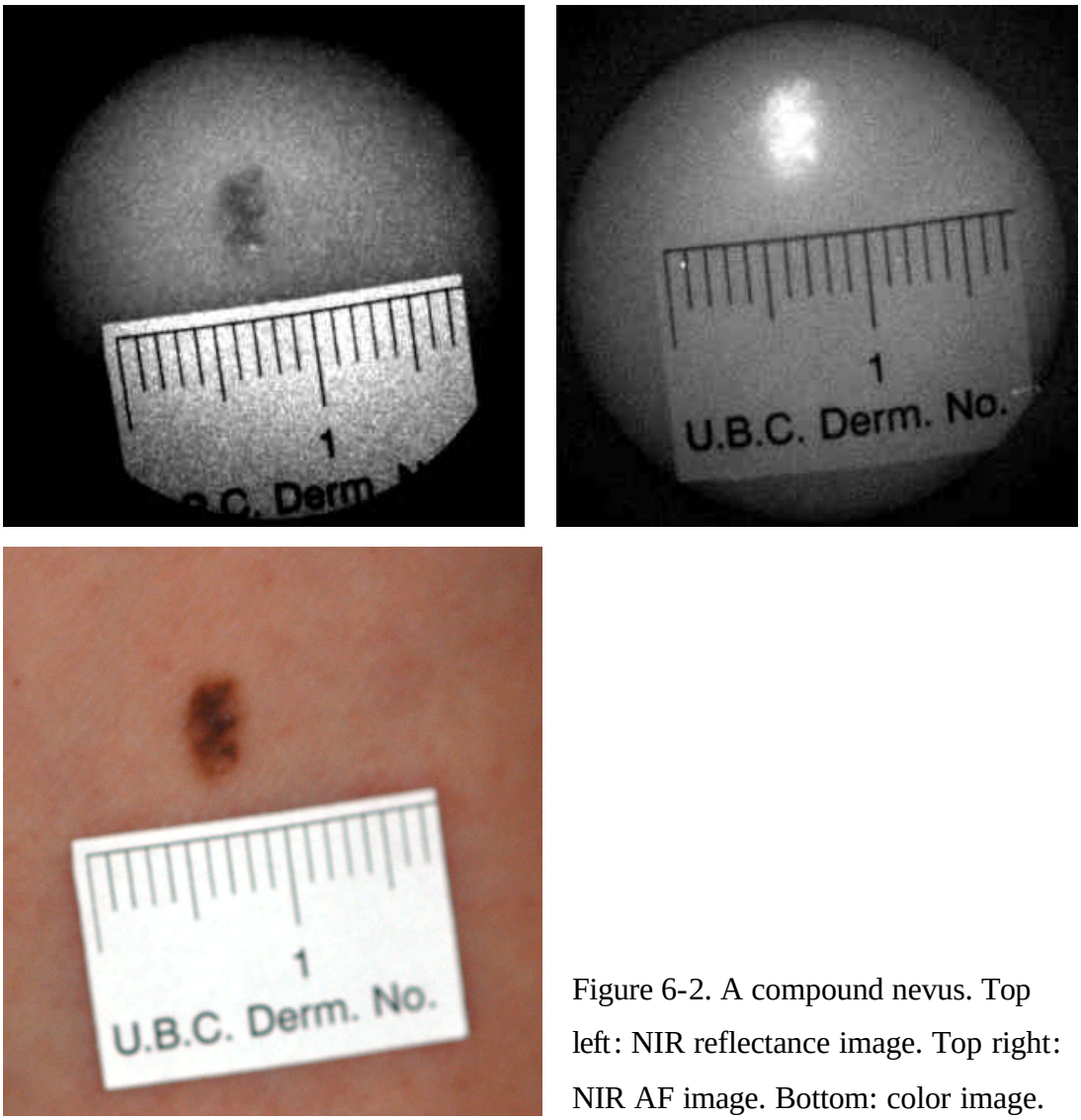

Figure 6-2. A compound nevus. Top left: NIR reflectance image. Top right: NIR AF image. Bottom: color image.

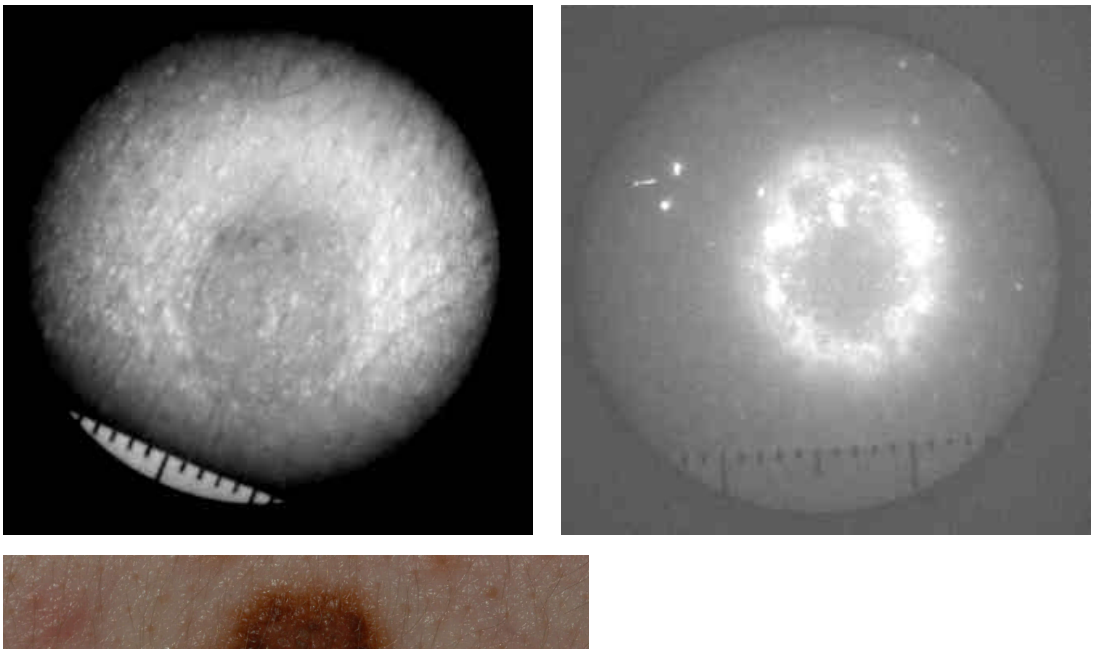

Figure 6-3. Another compound nevus. Top left: NIR reflectance image. Top right: NIR AF image. Bottom: color image. Notice the ring area in fluorescence image which reflects melanin concentration level.

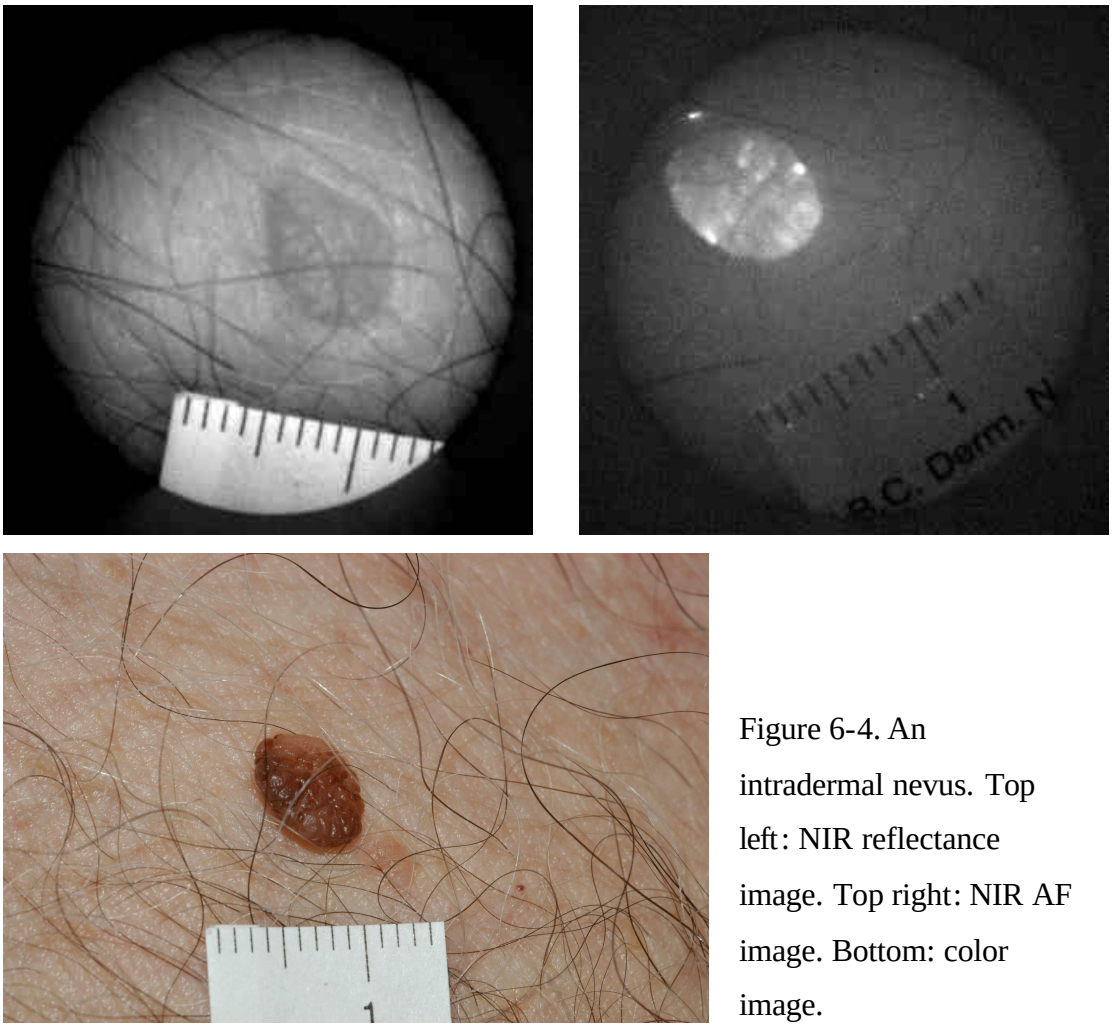

Figure 6-4. An intradermal nevus. Top left: NIR reflectance image. Top right: NIR AF image. Bottom: color image.

6.2.1.2. Blue nevi

Figure 6-2 shows the NIR AF image of a typical blue nevus, which is from the hand of a male volunteer. Contradicting to normal nevus, the fluoresecence distribution doesn't exactly correspond to visual darkness in reflectance image (central area appears darker), while the whole lesion appears very dark in NIR reflectance image.

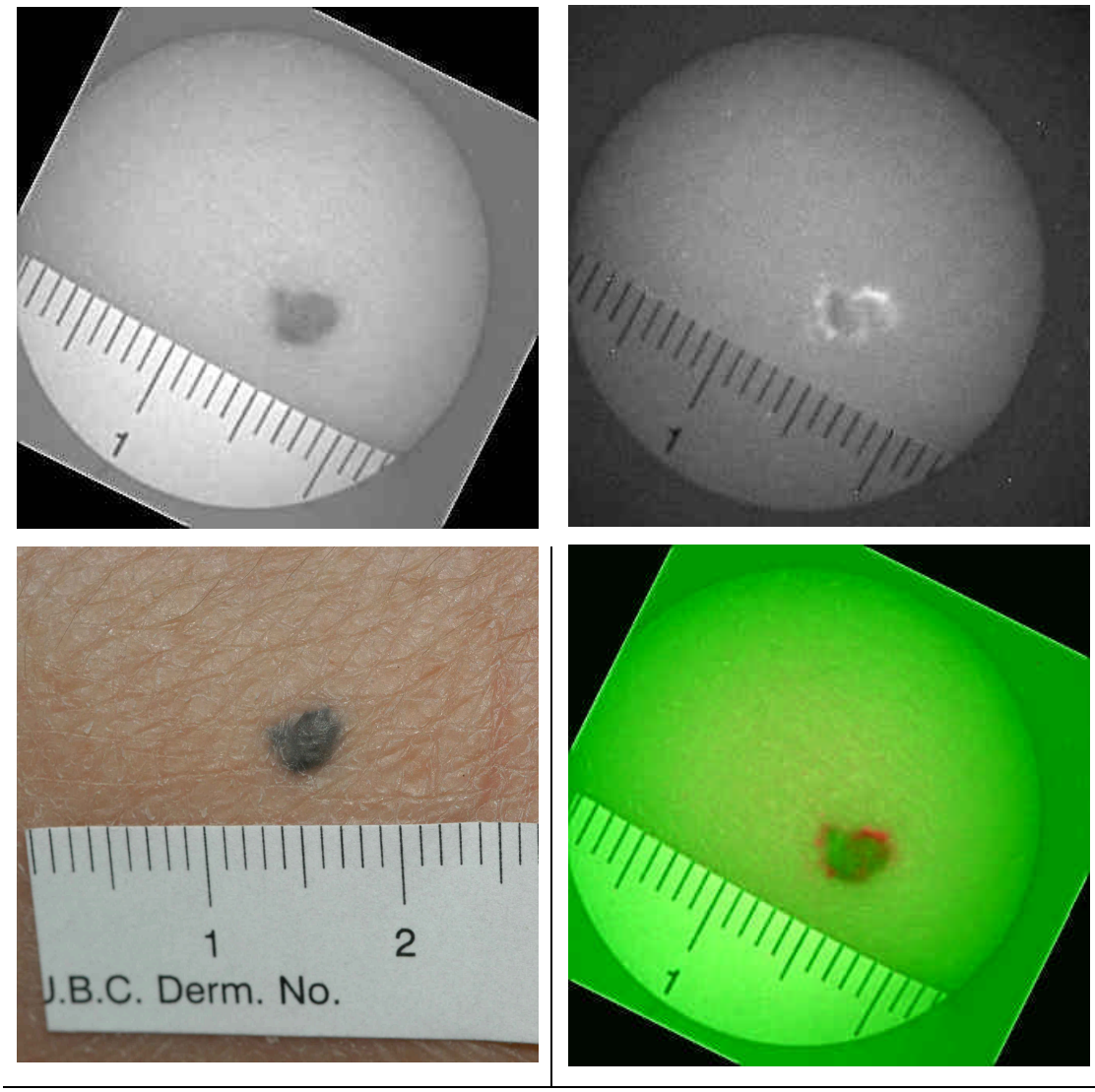

Figure 6-5. A blue nevus. Top left: NIR reflectance image. Top right: NIR AF image. Bottom left: color image. Bottom right: hybrid image of NIR reflectance and autofluorescence images. (Green represents reflectance and red represents fluorescence).

Other imaged melanin-involved lesions, including atypical nevi, nevi of ota, nevi of ita, freckles etc. are listed in the appendix. All the results of these lesions agree with the normal nevi, where fluorescence signal correspond to melanin distribution.

6.2.1.3. Seborrheic keratosis (SK)

Figure 6-6 shows a set of images of a typical SK from the back of a 60-year-old female. The NIR AF image looks similar to a normal nevus, with fluorescence roughly corresponding to melanin distribution. However, since SKs can be brown or yellow, sometimes there is not much, or even no melanin in an SK. Therefore, some other SKs don't show any NIR AF signals (see Appendix).

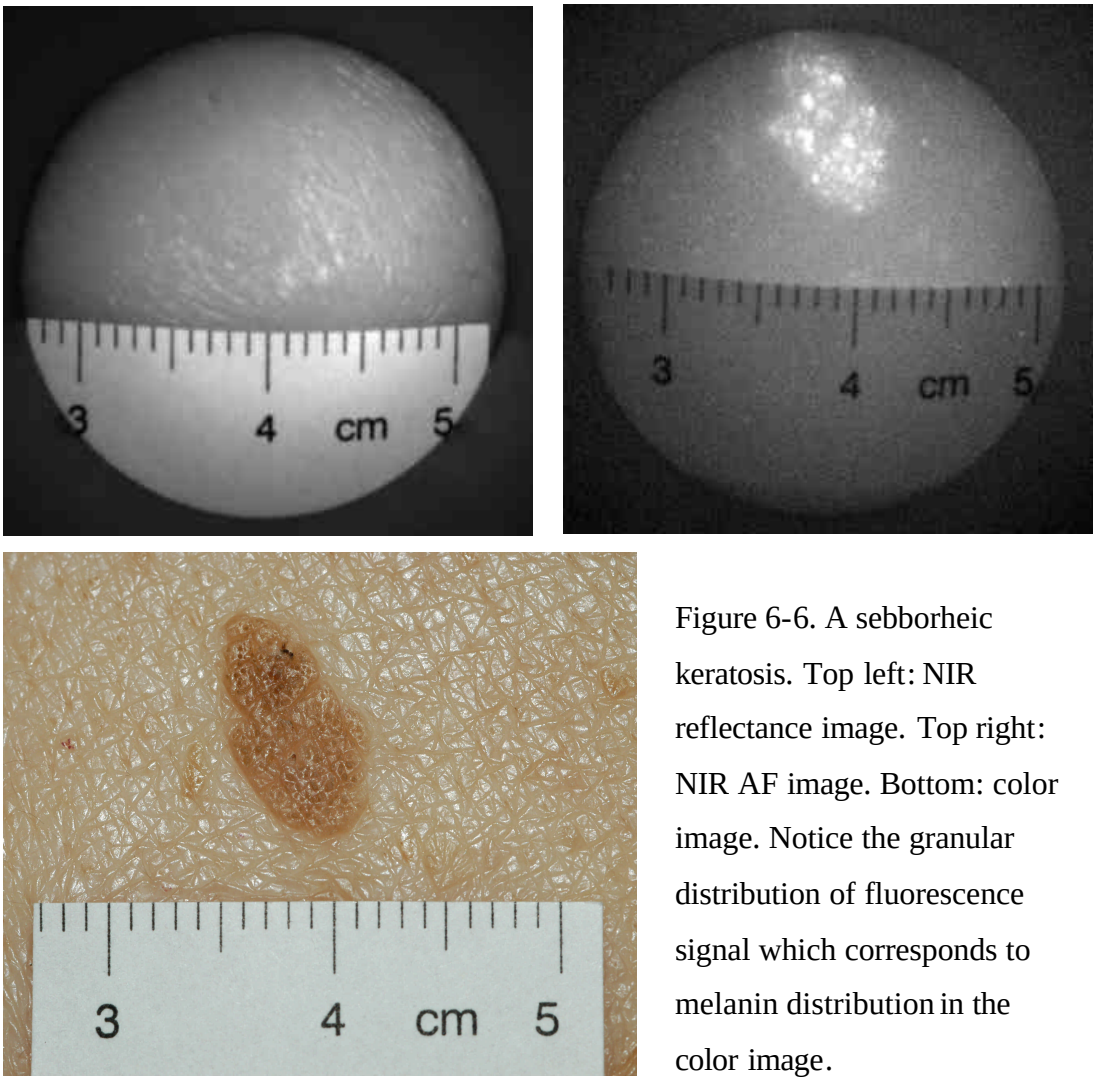

Figure 6-6. A sebborheic keratosis. Top left: NIR reflectance image. Top right: NIR AF image. Bottom: color image. Notice the granular distribution of fluorescence signal which corresponds to melanin distribution in the color image.

6.2.1.4. Vitiligo

It was expected to see contrast in the NIR AF images between vitiligo and its surrounding normal skin, due to the different level of melanin concentration. However, this is not seen in the example shown below (see figure 6-7, where the lesion is from a 34-year-old male patient). The most likely reason is that with the current system, the difference of melanin concentration between vitiligo and normal skin is not high enough to show differentiable fluorescence signal level. Improving the sensitivity and SBR of the imaging system will probably solve this problem.

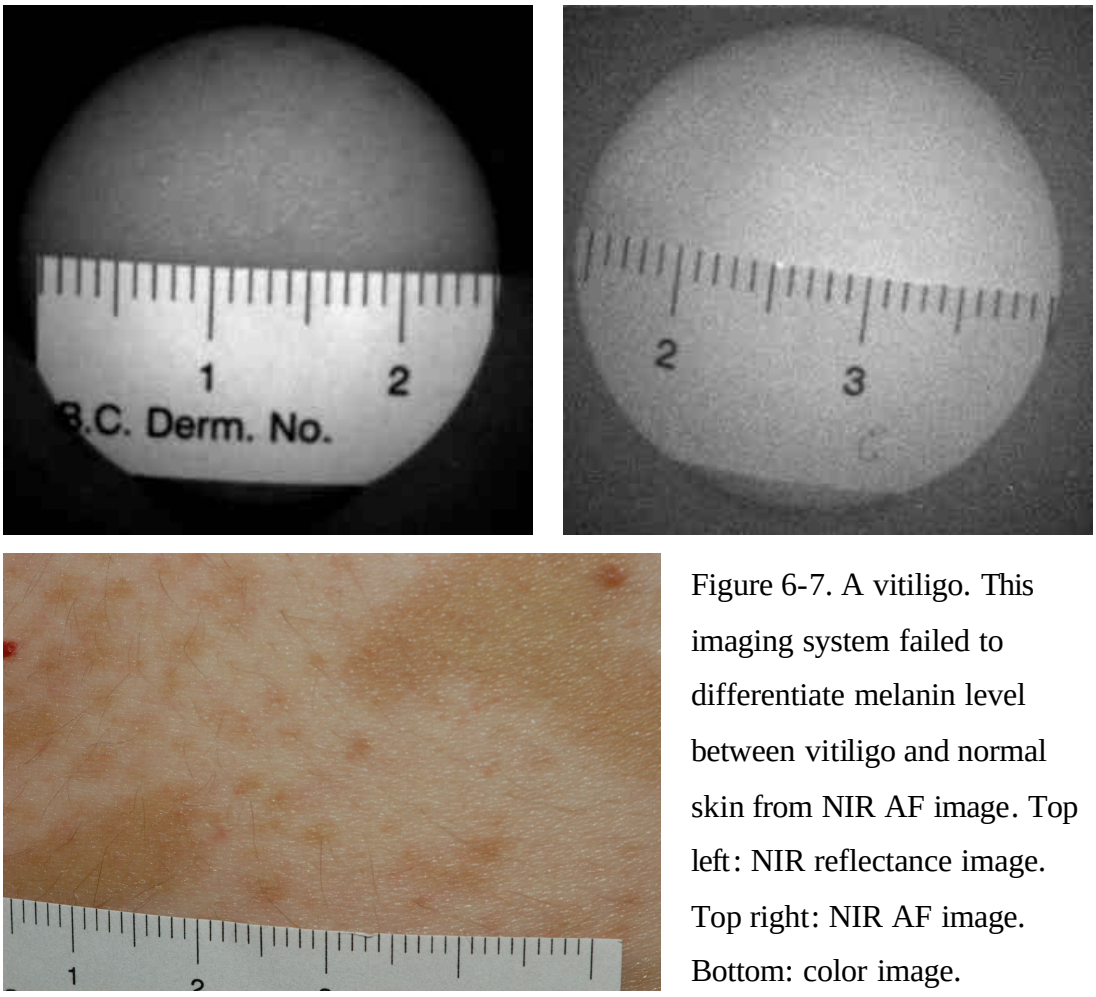

Figure 6-7. A vitiligo. This imaging system failed to differentiate melanin level between vitiligo and normal skin from NIR AF image. Top left: NIR reflectance image. Top right: NIR AF image. Bottom: color image.

6.2.1.5. Non-melanin involved skin disorders

Besides melanin, other tissue chromophores, such as oxy-hemoglobin in blood, also cause skin pigmentation. However, those chromophores don't fluoresce under NIR excitation. This section provides result of pigmented skin lesions without involvement of melanin, which are compared with those melanin-involved lesions as control.

Figure 6-8 shows psoriasis patches on a 62-year-old male patient. As expected, there is no significant fluorescence from the lesion in the NIR AF image.

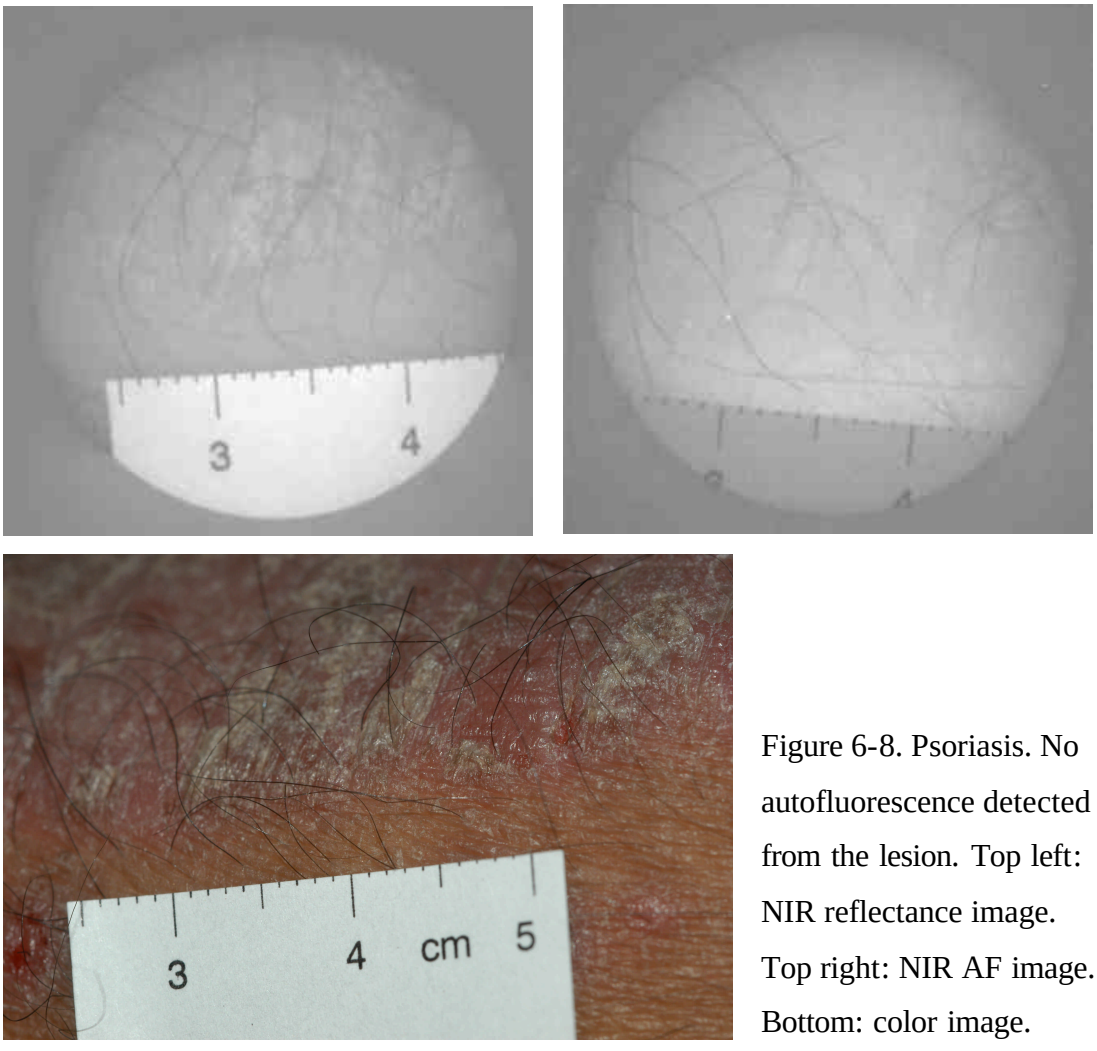

Figure 6-8. Psoriasis. No autofluorescence detected from the lesion. Top left: NIR reflectance image. Top right: NIR AF image. Bottom: color image.

Figure 6-9 shows a port wine stain (PWS) on a 34-year-old male patient's face. The lesion doesn't fluoresce. The pigmentation in PWS is mainly blood and it actually absorbs the fluorescence from the sebaceous gland (bright dots).

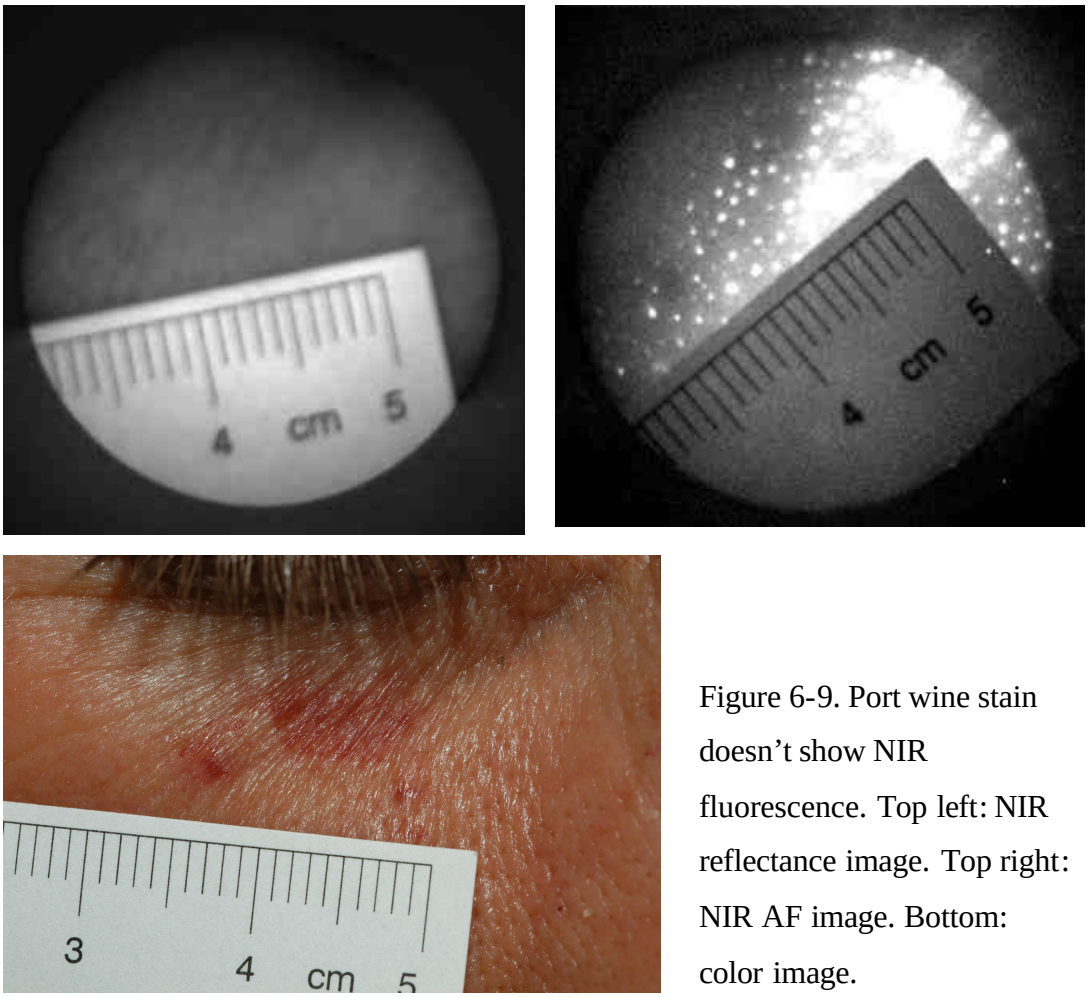

Figure 6-9. Port wine stain doesn't show NIR fluorescence. Top left: NIR reflectance image. Top right: NIR AF image. Bottom: color image.

More examples are provided below in figure 6-10 to 6-13, including a tattoo (from a 62-year-old male), a cherry angioma (from a 63-year-old male), a bruise (from a 60-year-old female), and a lentigo (from a 61-year-old female). Since none of the lesions involve melanin, they don't exhibit fluorescence under NIR excitation.

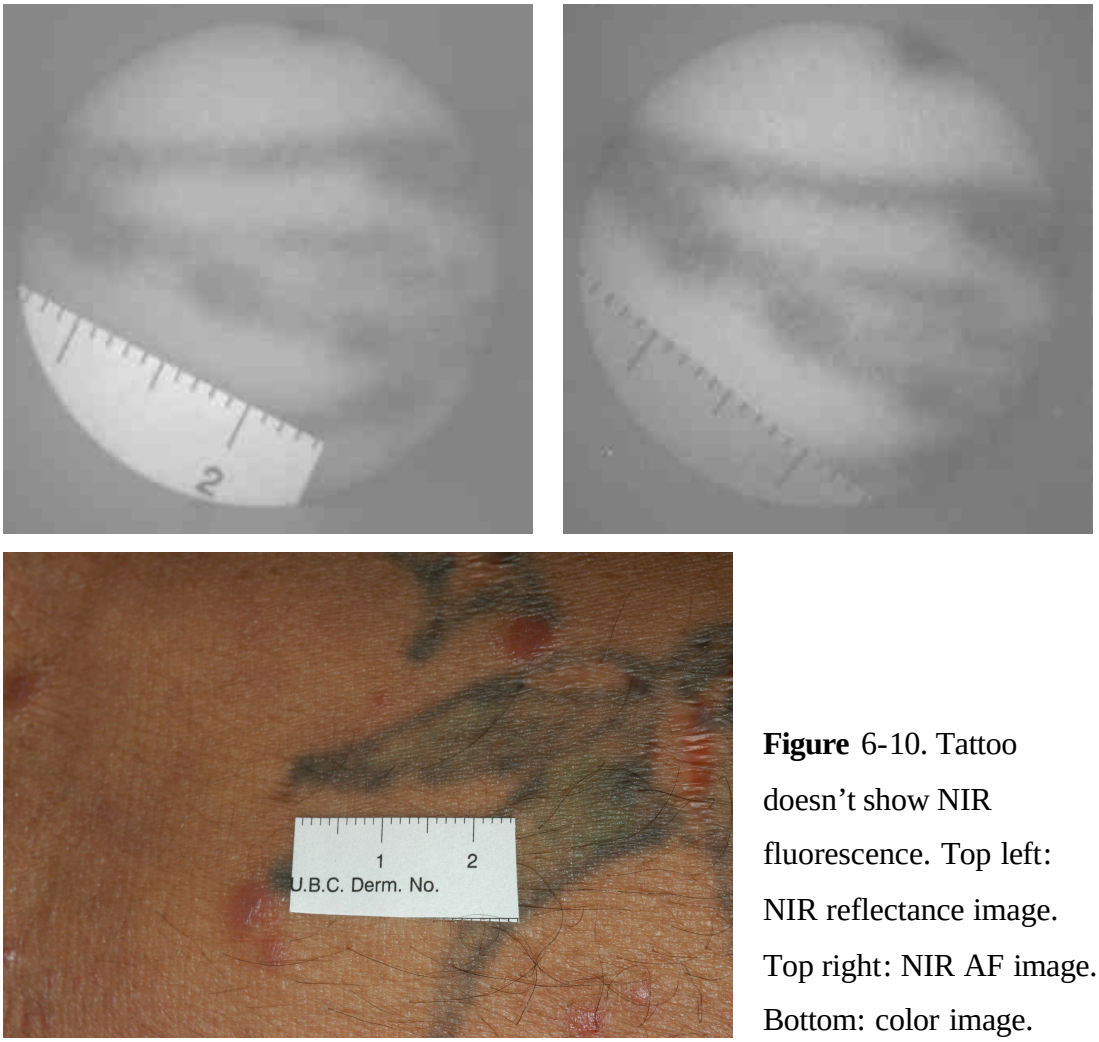

Figure 6-10. Tattoo doesn't show NIR fluorescence. Top left: NIR reflectance image. Top right: NIR AF image. Bottom: color image.

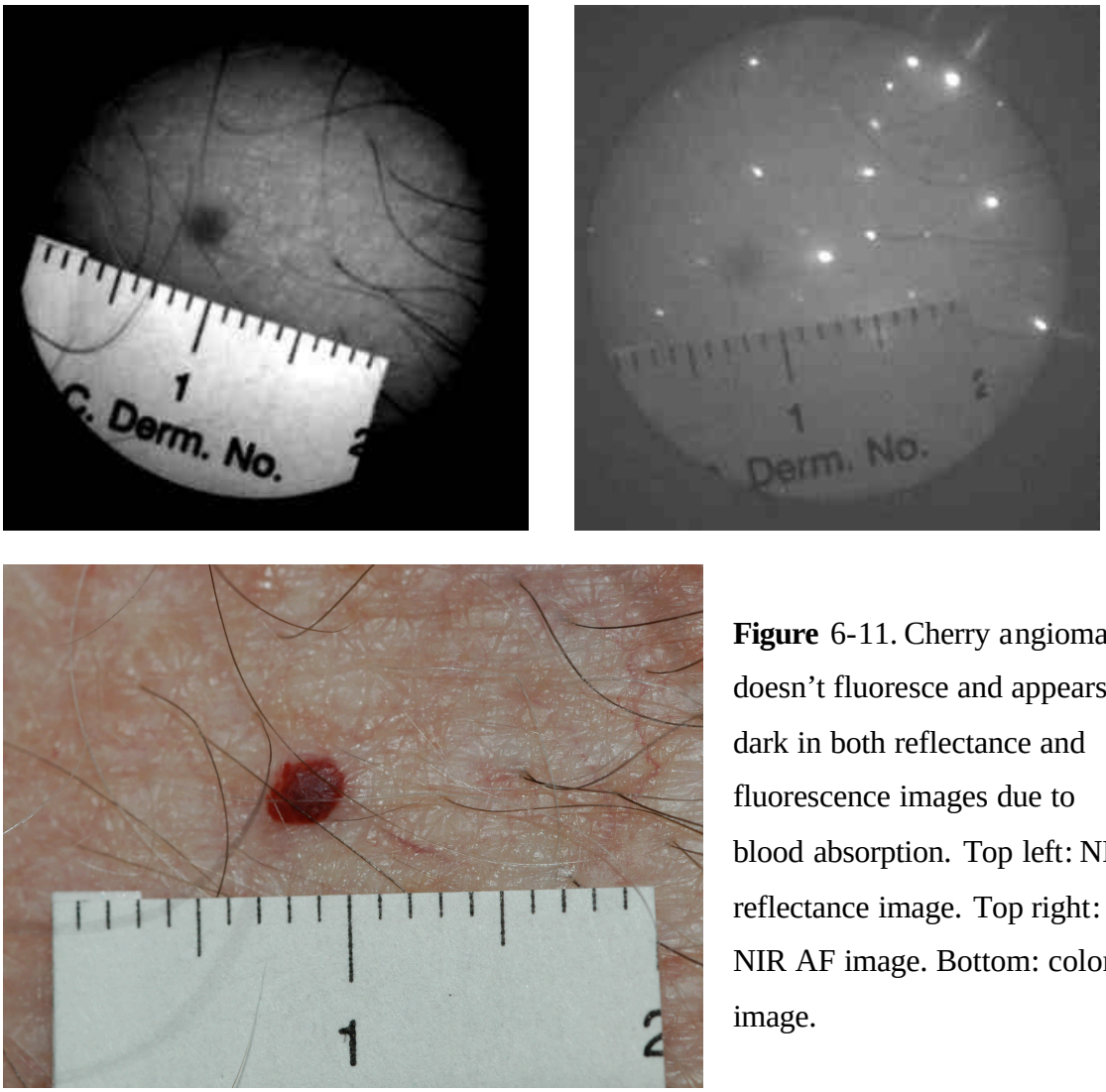

Figure 6-11. Cherry angioma. It doesn't fluoresce and appears dark in both reflectance and fluorescence images due to blood absorption. Top left: NIR reflectance image. Top right: NIR AF image. Bottom: color image.

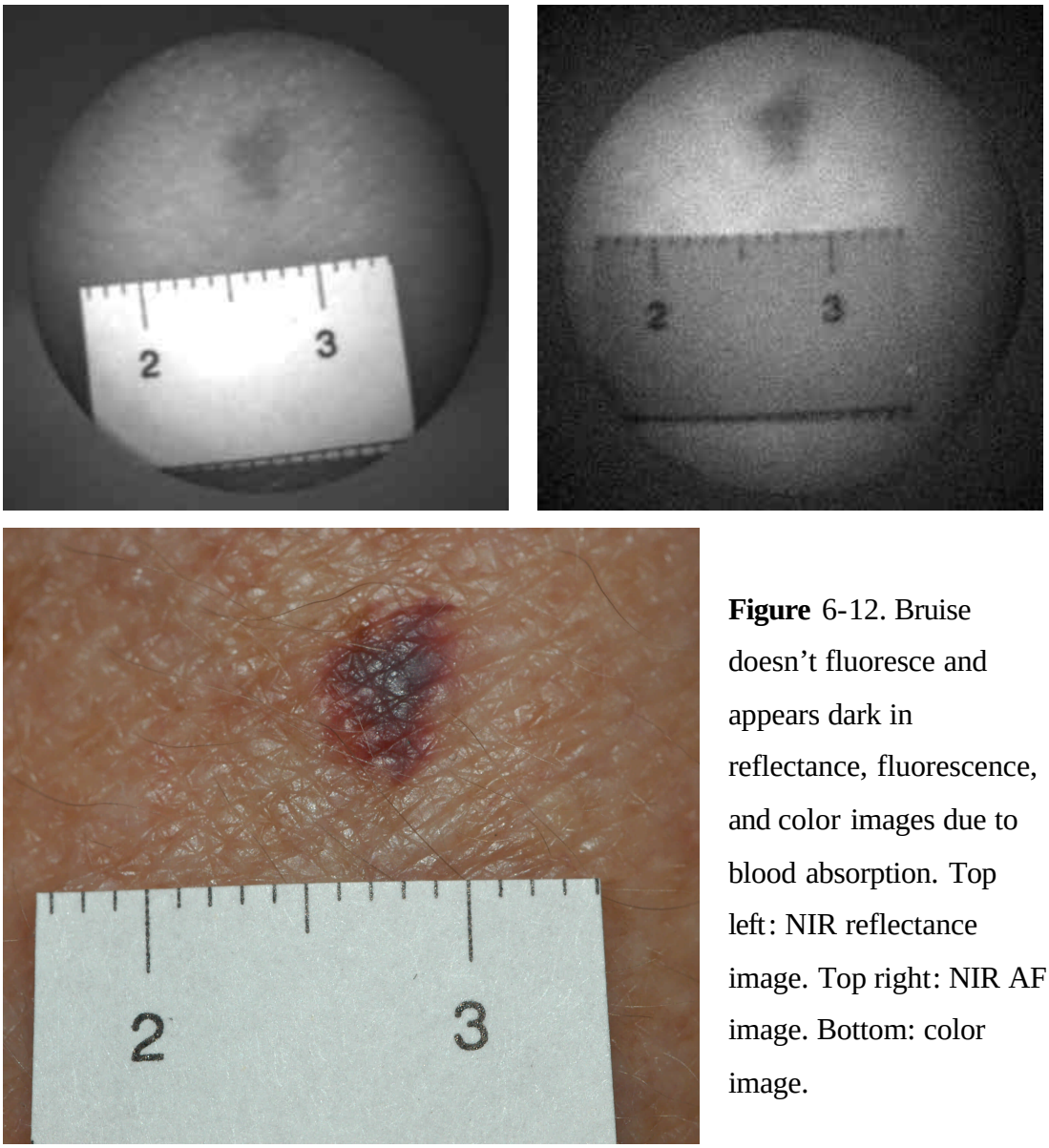

Figure 6-12. Bruise doesn't fluoresce and appears dark in reflectance, fluorescence, and color images due to blood absorption. Top left: NIR reflectance image. Top right: NIR AF image. Bottom: color image.

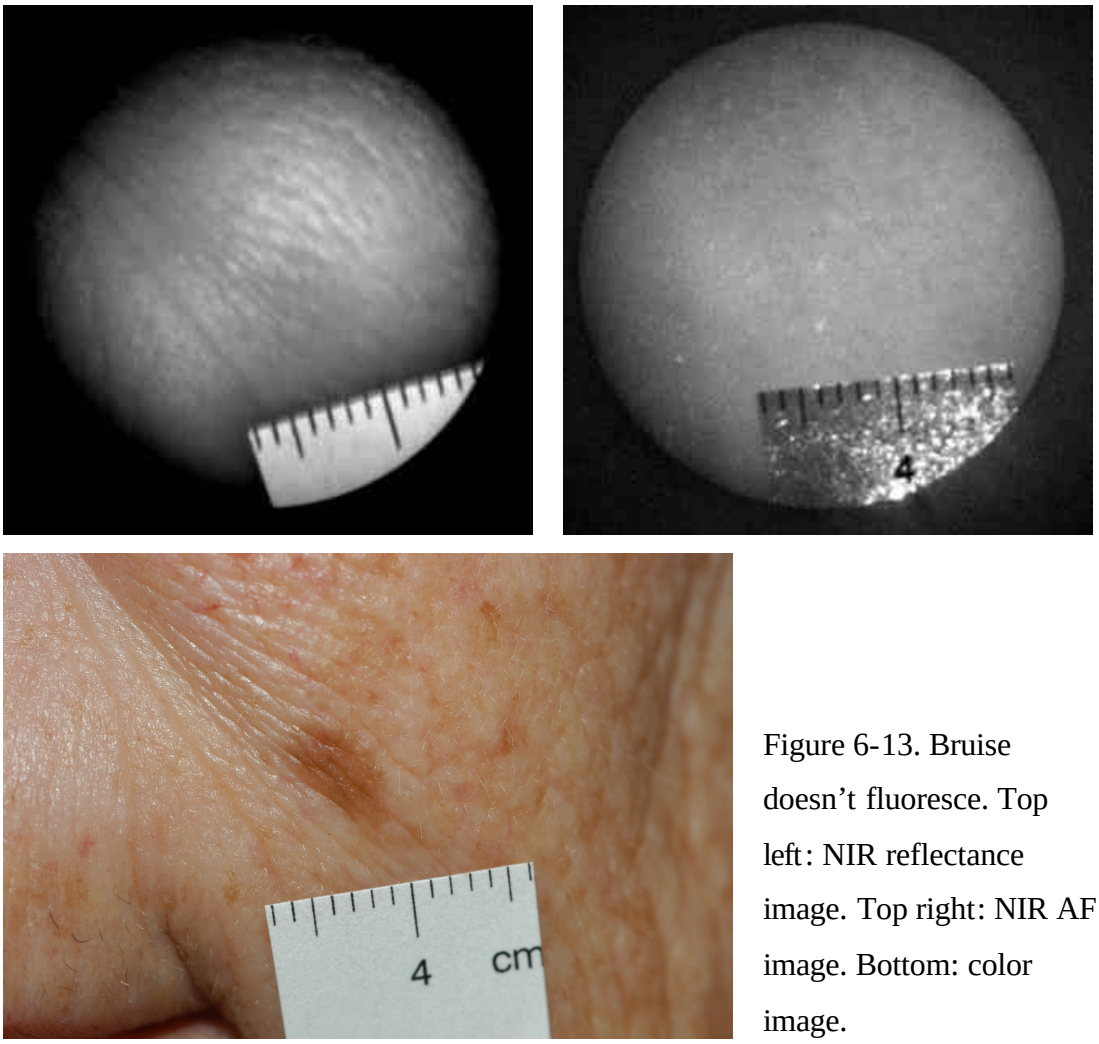

Figure 6-13. Bruise doesn’t fluoresce. Top left: NIR reflectance image. Top right: NIR AF image. Bottom: color image.

6.2.2. Melanoma

In figure 6-14., a superficial spreading melanoma looks very dark in reflectance and exhibits strong fluorescence. But the fluorescence distribution doesn't correspond to visual darkness level in color image and reflectance image.

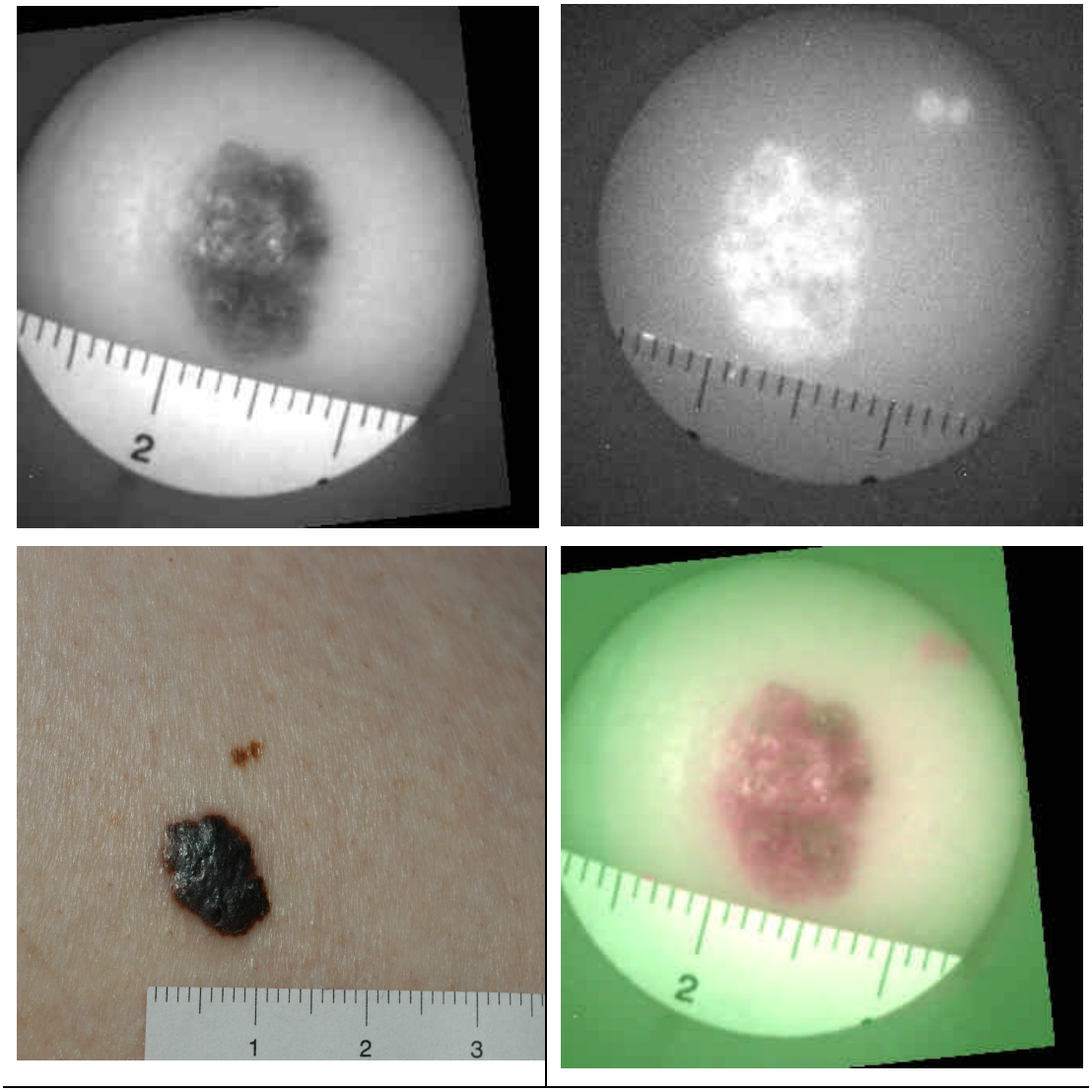

Figure 6-14. A superficial spreading melanoma. Top left: NIR reflectance image. Top right: NIR AF image. Bottom left: color image. Bottom right: hybrid image of NIR reflectance and autofluorescence images. (Green represents reflectance and red represents fluorescence).

6.2.3. Hair follicles

During our measurements, we noticed that there are very bright signals coming from hair follicles. In figure 6-15, a junctional nevus with two adjacent hair follicles are detected in the same NIR AF image. In the area plot, it is clear that the fluorescence from hair follicles is much higher than that from the nevus. The source of this strong fluorescence is most likely from the sebaceous gland attached to the hair follicle. However, this needs more experiment for confirmation.

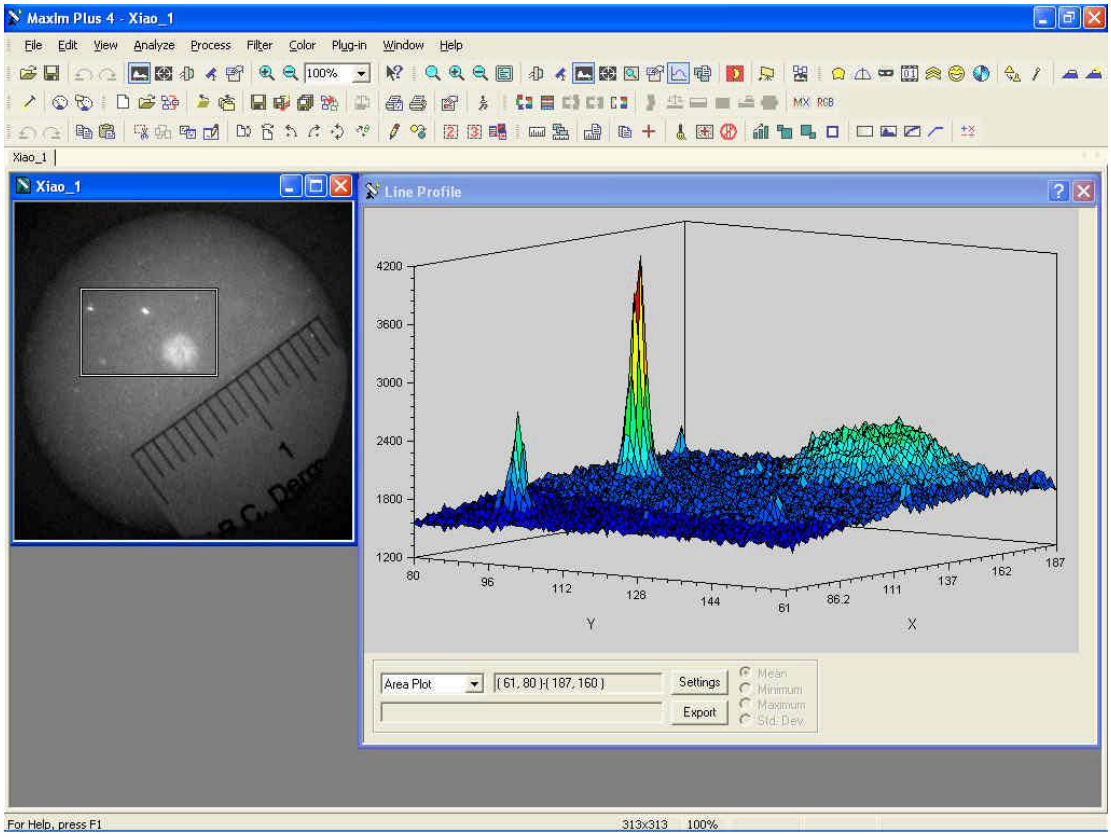

Figure 6-15. Hair follicles appear very bright in NIR AF images. Left: NIR AF image of a nevus and two hair follicles. Right: Area plot of the Region of Interest (ROI) outlined in the left-hand-side image.

6.2.4 Melanin particles

We used the same imaging system to try to detect fluorescence from synthetic melanin particles in both dry condition and in water suspension. However, it is interesting to see that the particles don't fluorescence under the NIR excitation (figure 6-16). It is therefore inferred that it is the micro-environment of *in vivo* cutaneous melanin that help change melanin's optical property and result in the fluorescence. However, this still needs further investigation for more convincing proof.

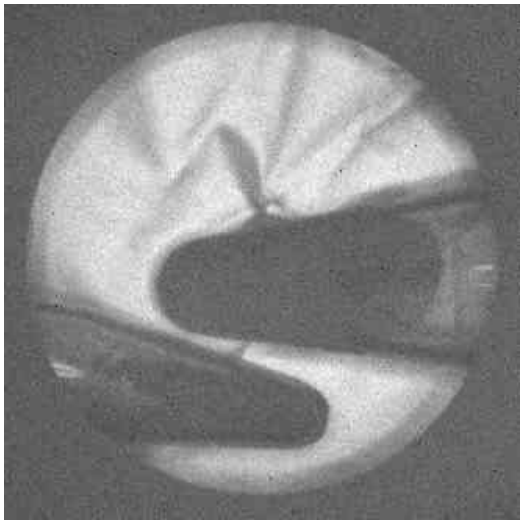

Figure 6-16. Synthetic melanin in vials. Left: dry melanin particles; Right: melanin in water suspension.

6.3. Discussions

6.3.1. Melanin causes NIR autofluorescence from skin pigmentation

From the results shown above, we can see that all measured skin disorders which are known to involve significant melanin concentration changes emit intensive fluorescence, which is in sharp contrast with the lower autofluorescence from its adjacent normal skin tissue. In the mean time, fluorescence was not detected from control lesions, which are known to have no or minimum involvement with melanin. Thus we can infer that it is the

cutaneous melanin which results in this strong fluorescence signal. With the current imaging system, however, relatively small difference of melanin concentration cannot be detected, such as in the case of vitiligo. This is due to the relatively low melanin concentration in normal skin, which gives little signal from a background (vitiligo area in this example) with noise. Thus the fluorescence between vitiligo and normal skin cannot be distinguished with the current sensitivity level.

6.3.2. Normal nevi compared with blue nevi

In theory the only difference between normal nevi and blue nevi is the depth distribution of melanocytes. Melanocytes in blue nevi reside deep in dermis, while melanocytes in normal nevi locate at epidermis, dermo-epidermal junction, or upper dermis layer. However, the NIR AF of blue nevi and normal nevi behave distinctly different. While autofluorescence intensity in a normal nevus is essentially proportional to their visual darkness level (in both the color images and reflectance images), surprisingly, the AF intensity of a blue nevus does not. The central area appears dark with no noticeable fluorescence, and the peripheral regions show strong AF emission. The cause of this irregular pattern is still unknown. A possible reason is the very densely-distributed melanin in the central region completely absorbs the fluorescence emitted from the melanin emission at deeper layer, while relatively less melanin on the lesion edge only absorbs part of the fluorescence emission from inside. This interesting phenomenon warranty further detailed investigations.

6.3.3. Nevi compared with Melanoma

Under the NIR AF camera, a melanoma behaves distinctively differently from a normal nevus or a blue nevus. The fluorescence emission from melanoma is irregular and is not proportional to the visual darkness distribution or the grey level in reflectance images. Since NIR autofluorescence emission is a direct measure of melanin concentration, this autofluorescence intensity distribution may be a better way to investigate melanin distribution and its biochemical activity within melanomas. The reason of this

inconsistence of fluorescence distribution with visual darkness is still not fully understood. Nevertheless it is probably associated with melanin's re-absorption of fluorescence emission within the tumor. Further study of this topic will help elucidate the internal structure of melanoma instead of just the surface inspection, in a non-invasive manner.

6.3.4. *In vivo* melanin compared with *in vitro* melanin

Cutaneous melanin exhibits strong NIR fluorescence in all the experiments on human subjects, however, synthetic melanin particles seem to lose the fluorescence property. Also black human hair don't seem to fluoresce in NIR, which contradicts the fact that melanin is rich in hair shaft. The most possible explanation is that the loss of NIR fluorescence is due to micro-scale biochemical environment changes when melanin is taken out from a live subject. Since tissue fluorescence is very sensitive to its close surrounding environment, melanin could behave drastically different outside of living tissue in terms of autofluorescence properties.

6.3.5. The unique advantage of NIR autofluorescence imaging

Currently, the most common method for characterization of cutaneous melanin is visual inspection and reflectance imaging. However, both methods are intrinsically indirect. The 'signal' one obtains using those methods is in effect based on melanin absorption of incident light, which results in some significant limitations:

1) Superficiality: only the surface of skin is observed. Deeper melanin is invisible under the 'black mask' on the very superficial layer. Also any useful signal from other UV or visible light fluorophores beneath the surface is attenuated or usually, completely blocked by the surface distributed melanin.

2) Low specificity: melanin is only one of many tissue chromophores which absorb incident light. All other chromophores, such as oxy-hemoglobin in blood, can result in

similar absorption effect as melanin, which obscures one another or even makes them indistinguishable. This is especially significant when those chromophores spatially overlap with melanin-rich area. An example is a blood vessel going beside a nevus, where both blood and nevus appear dark in color image or reflectance image (figure 6-17 top left).

Using NIR AF method, the above problems are easily avoided by its different signal-generating mechanism. Autofluorescence is the light signal directly from melanin and as such, allows us visualize its distribution in a direct manner. Other light-absorbing choromophores, no matter vertically or horizontally adjacent to melanin rich region, can be easily seen as dark, while melanin itself appears bright (figure 6-17 top right). In this way, melanin is no longer a signal mask or obscurer, but is a signal provider itself. Figure 6-17 shows an example of this significant advantage. The sebborheic keratosis overlaps with a blood vessel running beneath the pigmentation. In both color image and reflectance image, the blood vessel and the pigmentation cannot be easily distinguished, due to the fact that both blood and melanin absorb the diffuse reflectance light in the same way. However, in the fluorescence image, they are easily distinguishable because melanin appears bright while blood vessel appears dark.

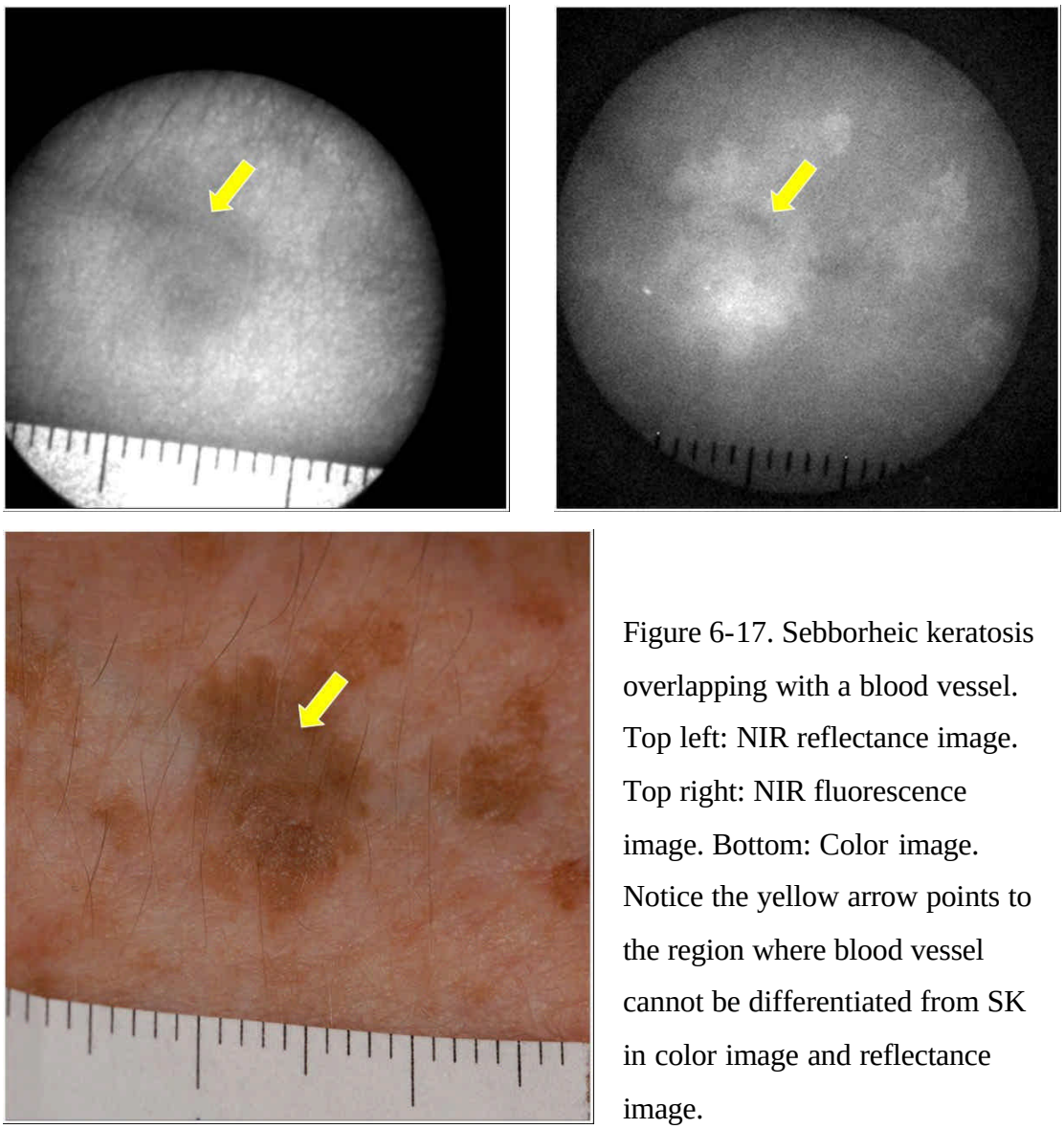

Figure 6-17. Sebborheic keratosis overlapping with a blood vessel. Top left: NIR reflectance image. Top right: NIR fluorescence image. Bottom: Color image. Notice the yellow arrow points to the region where blood vessel cannot be differentiated from SK in color image and reflectance image.

7. Conclusions and future directions

In this thesis we achieved the following three things:

- Built a prototype NIR imaging system for skin and its pigmentary system NIR AF measurements,

- Showed that melanin-involved skin disorders exhibit much stronger autofluorescence signal than surrounding normal skin,

- Further confirmed our earlier findings of melanin NIR AF emission in the spectroscopic study (Huang *et al*, 2006).

The prototype NIR imaging system that we built solved the low S/N problem that people have had in previous experiments on NIR tissue autofluorescence imaging. With the imaging system, the spatial distribution of melanin in those pigmentary skin disorders can be directly recorded by its NIR fluorescence emission, and offers a new way to directly characterize relative melanin concentration. Also it was discovered that benign nevi, blue nevi, and malignant melanomas have distinctly different NIR autofluorescence distribution patterns.

Since melanin has long been considered a poor tissue fluorophore (Nordlund, 2006), our results challenged the conventional understanding about this important molecule in human integument system. This discovery has impact on melanin photochemistry and photobiology, as well as on clinical dermatology. For further study on melanin fluorescence properties, a new path is pointed out and the tool is provided. For clinical dermatology, the first method for directly characterizing cutaneous melanin is offered, which has the potential in helping dermatologists improving diagnosing skin pigmentary disorders.

Based on this work, future studies can be performed in the following directions:

- Investigation of melanin fluorescence properties in different conditions. This study will try to answer the question of why *in vivo* cutaneous melanin fluoresces while synthetic melanin doesn't.

- Detailed classification of autofluorescence signal pattern for different skin diseases and skin cancers. More work on extracting and differentiating features in NIR autofluorescence images of benign and malignant skin tumors can be potentially used for early melanoma diagnosis.

- Study of other fluorophores contributing to skin NIR autofluorescence. More *in-vivo* and *in-vitro* studies can be done to clarify the source of the NIR fluorescence signal from hair follicles, thus potentially providing better ways to detect skin disorders related to hair follicles.

REFERENCES

Anderson, R. R. and J. A. Parrish (1981). "The optics of human skin." J Invest Dermatol 77(1): 13-9.

Benson, R. C. and H. A. Kues (1978). "Fluorescence properties of indocyanine green as related to angiography." Phys Med Biol 23(1): 159-63.

Demos, S. G., R. Gandour-Edwards, et al. (2004). "Near-infrared autofluorescence imaging for detection of cancer." J Biomed Opt 9(3): 587-92.

Gawkrodger, D. J., "Dermatology", 2nd Ed., 1997 Hong Kong: Churchill Livingstone

Han, X., Lui, H., McLean, D.I., Zeng, H. Lui, A technique for near-infrared autofluorescence imaging of skin: preliminary results SPIE 6078: 60780S (2006).

Hoet, P. H., I. Bruske-Hohlfeld, et al. (2004). "Nanoparticles - known and unknown health risks." J Nanobiotechnology 2(1): 12.

http://omlc.ogi.edu/index.html

http://www.cancer.org/docroot/SPC/content/SPC_1_ABCD_Mole_Check_Tips.asp

http://www.nlm.nih.gov/medlineplus/ency/article/000884.htm

Huang, Z., H. Zeng, et al. (2006). "Cutaneous melanin exhibiting fluorescence emission under near-infrared light excitation." J Biomed Opt 11(3): 34010.

Kim, S., Y. T. Lim, et al. (2004). "Near-infrared fluorescent type II quantum dots for sentinel lymph node mapping." Nat Biotechnol 22(1): 93-7.

Lakowicz, J. R., C. D. Geddes, et al. (2004). "Advances in surface-enhanced fluorescence." J Fluoresc 14(4): 425-41.

Levene, M. J., D. A. Dombeck, et al. (2004). "In vivo multiphoton microscopy of deep brain tissue." J Neurophysiol 91(4): 1908-12.

Licha, K., Contrast agents for optical imaging, Topics in Current Chemistry, (222), 2002

Malicka, J., I. Gryczynski, et al. (2003). "Metal-enhanced emission from indocyanine green: a new approach to in vivo imaging." J Biomed Opt 8(3): 472-8.

Nordlund, J. J., Boissey, R. E., et al. (2006). "The pigmentary system" 2nd Ed., Chap. 16. Blackwell Publishing

Ntziachristos, V., A. G. Yodh, et al. (2000). "Concurrent MRI and diffuse optical tomography of breast after indocyanine green enhancement." Proc Natl Acad Sci U S A 97(6): 2767-72.

Ntziachristos, V., C. Bremer, et al. (2003). "Fluorescence imaging with near-infrared light: new technological advances that enable in vivo molecular imaging." Eur Radiol 13(1): 195-208.

Pinaud, F., X. Michalet, et al. (2006). "Advances in fluorescence imaging with quantum dot bio-probes." Biomaterials 27(9): 1679-87.

Sevick-Muraca, E. M., J. P. Houston, et al. (2002). "Fluorescence-enhanced, near infrared diagnostic imaging with contrast agents." Curr Opin Chem Biol 6(5): 642-50.

Vo-Dinh, T., Biomedical Photonics Handbook. Boca Raton, FL: CRC Press LLC; 2003.

www.cancer.org/docroot/SPC/content/SPC_1_ABCD_Mole_Check_Tips.asp

APPENDIX: NIR imaging of skin: preliminary result of clinical pilot study

This section lists all the data of the NIR imaging pilot study conducted at the Skin Care Center of the Vancouver General Hospital during March to July, 2006. For each lesion, three images are listed in the order of clinical picture (color image), NIR reflectance image, and NIR fluorescence image (from left to right).

A1. Skin disorders with involvement of cutaneous melanin

A1.1 Blue nevi

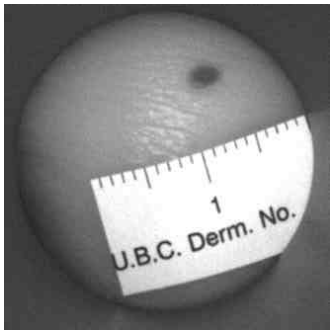

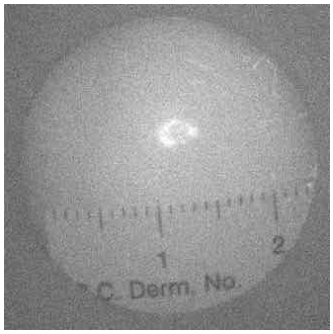

Missing data

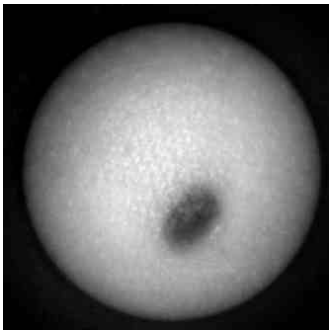

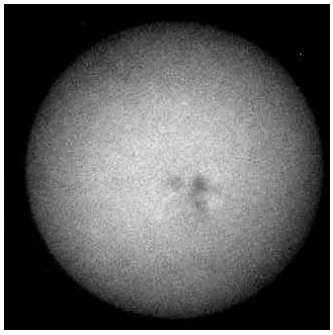

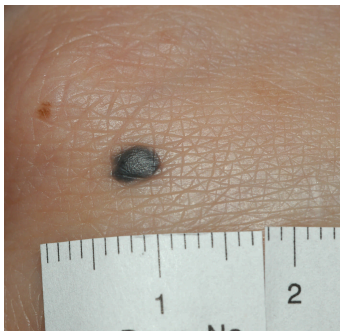

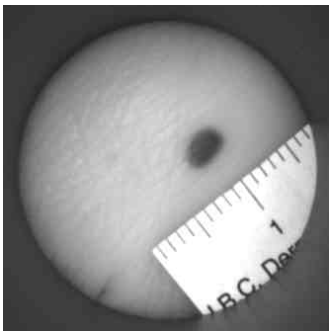

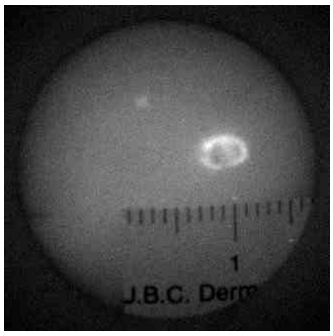

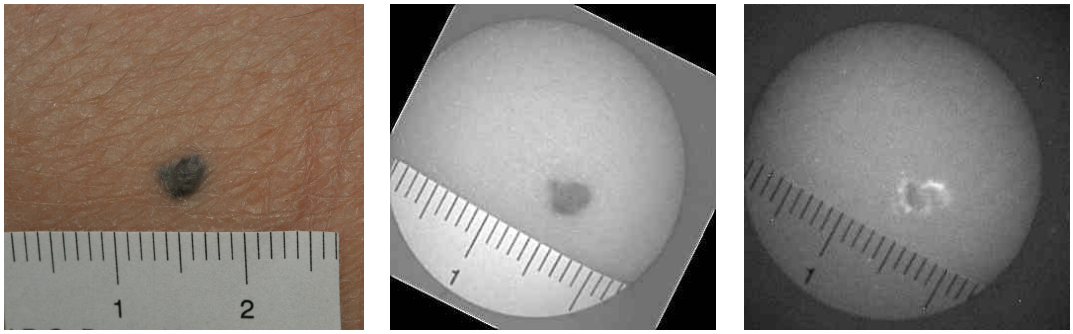

A1.2 Sebohrreic Keratosis

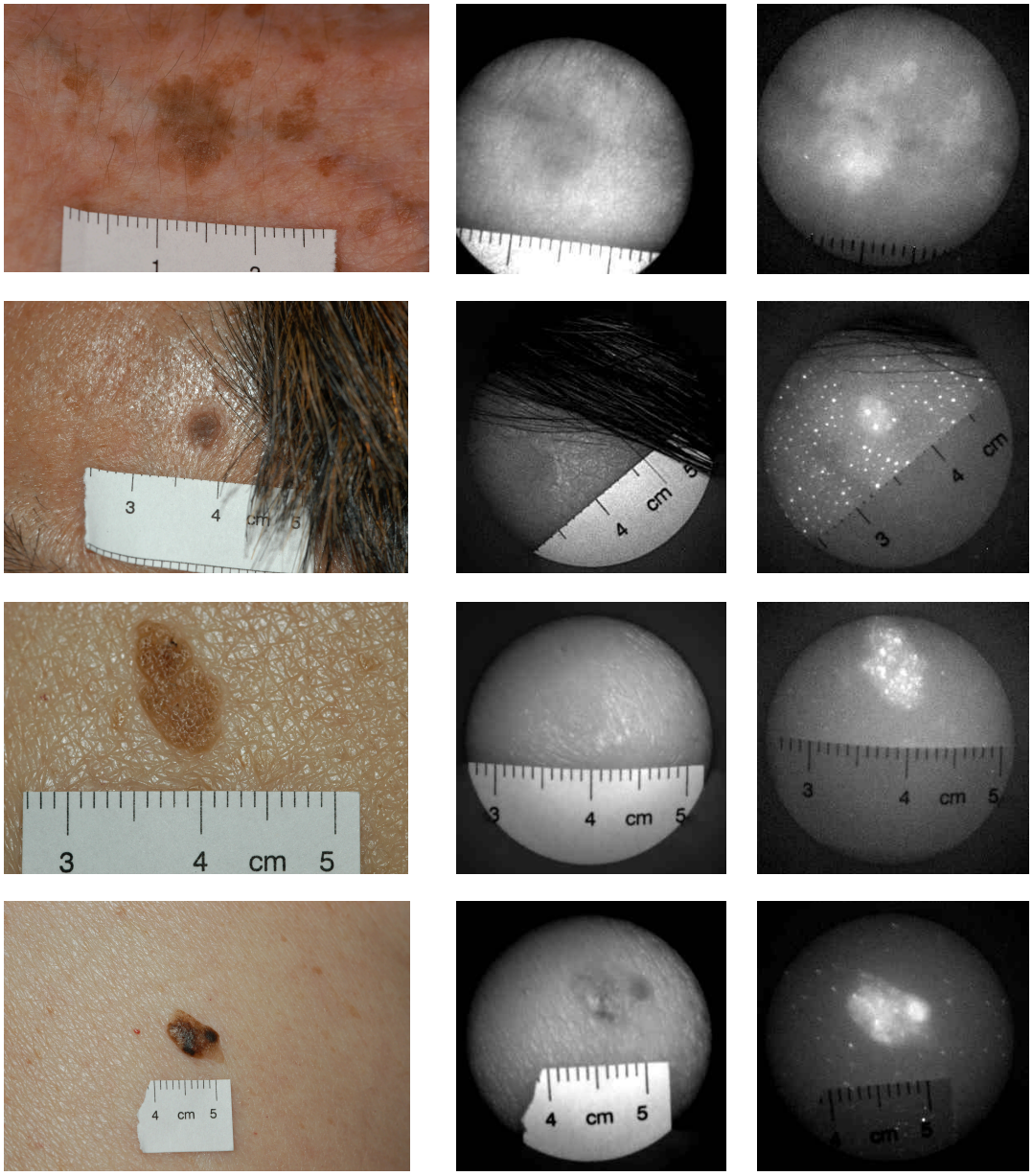

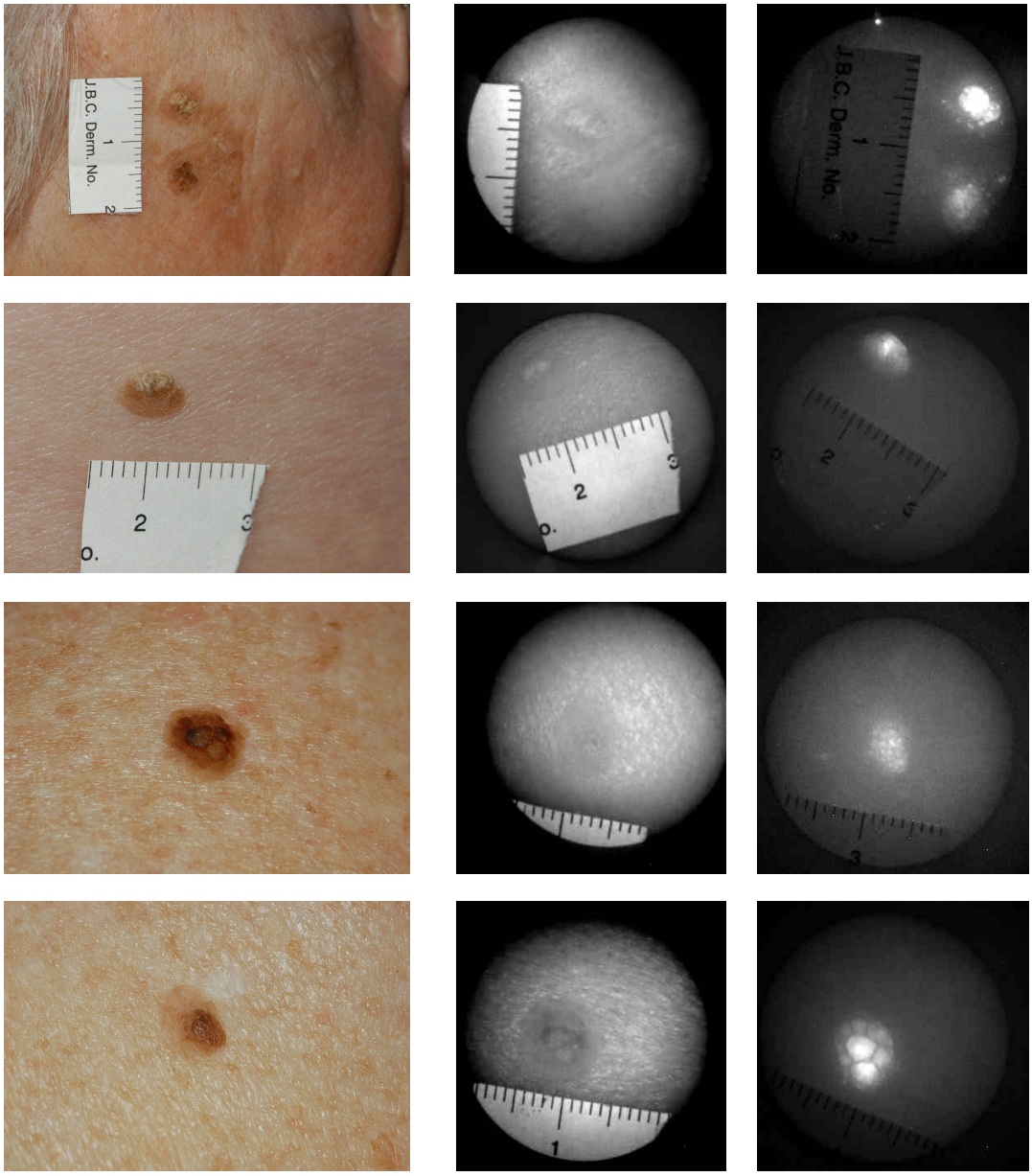

A1.3 Nevus of Ota

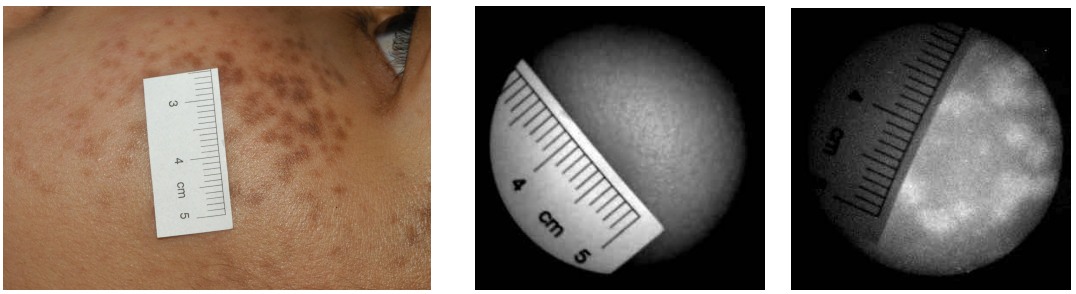

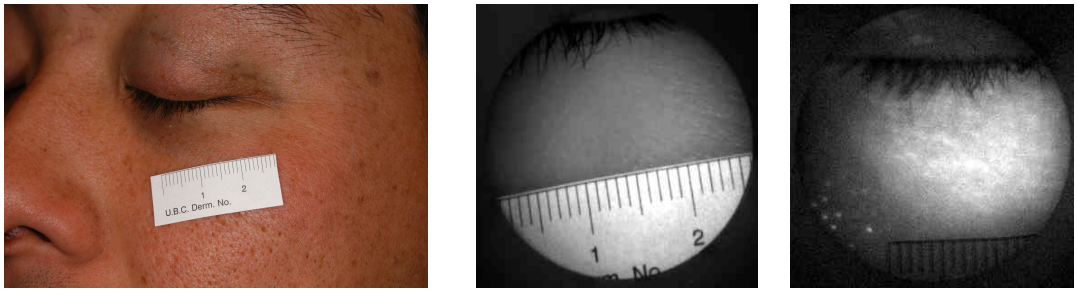

A1.4 Nevus of Ito

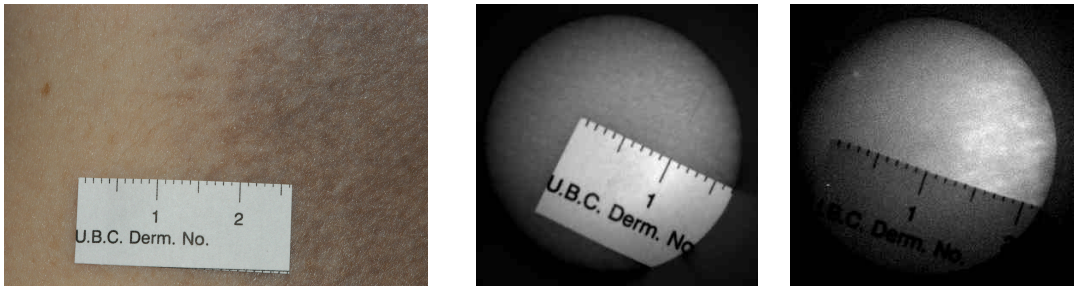

A1.5 Junctional Nevus

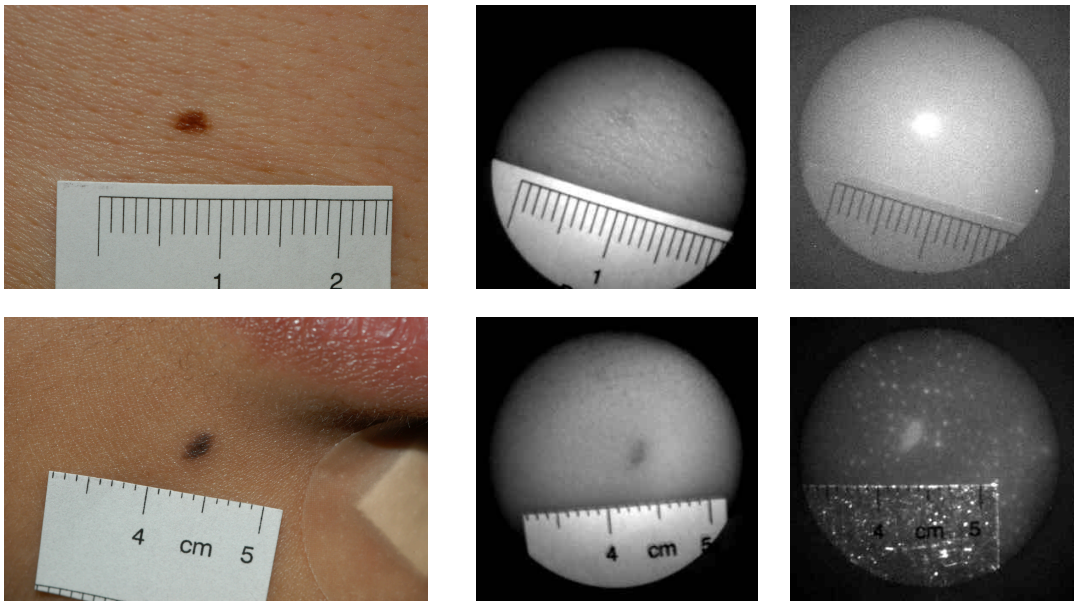

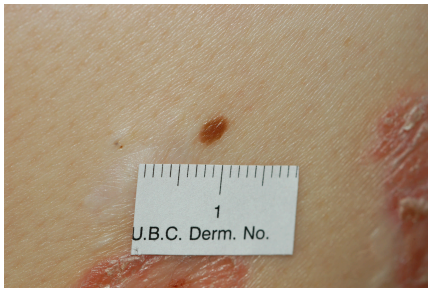
1
U.B.C. Derm. No.
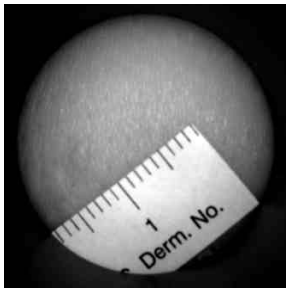
1
Derm. No.
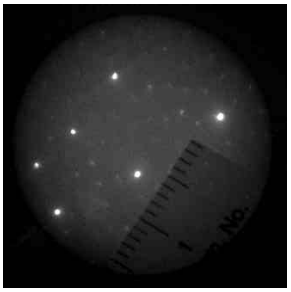

1
2
U.B.C. Derm. No.
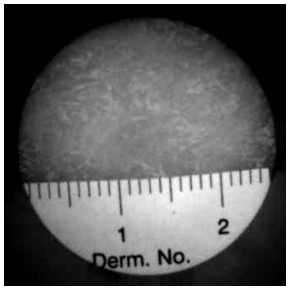
1
2
Derm. No.
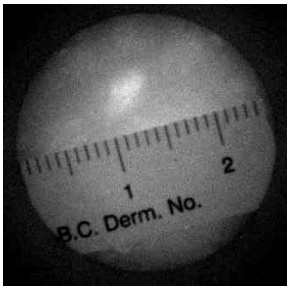
1
2
B.C. Derm. No.
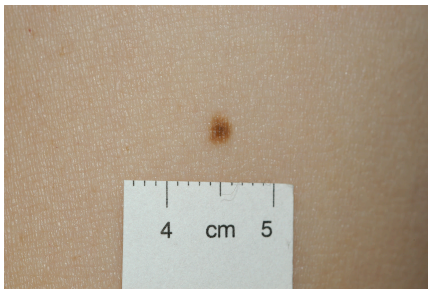
4 cm 5
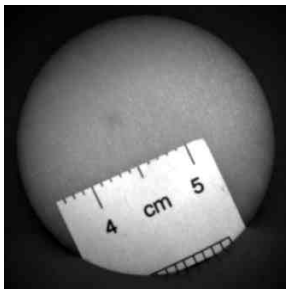
4 cm 5
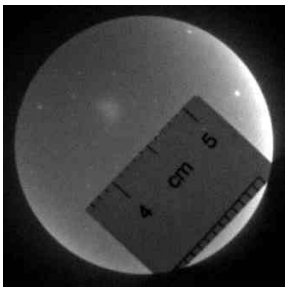
4 cm 5

1
2
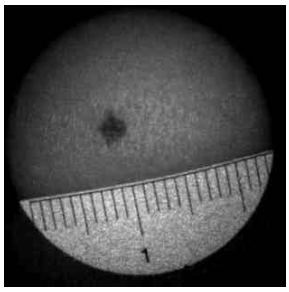
1
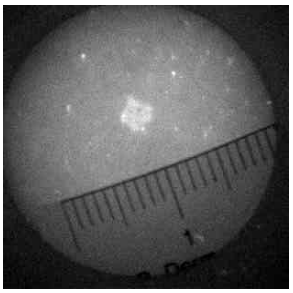
1
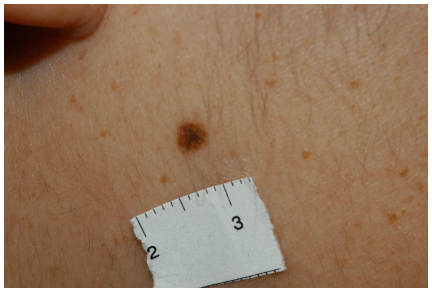
2
3
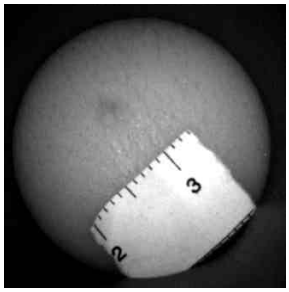
2
3
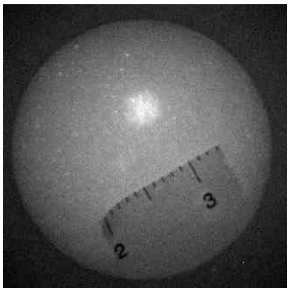
2
3

A1.6 Epidermal nevus


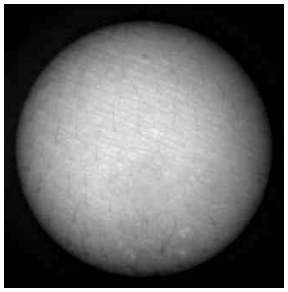


A1.7 Compound nevus

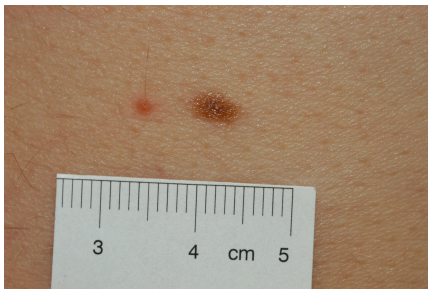

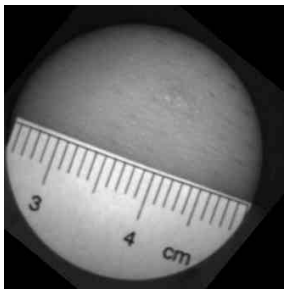

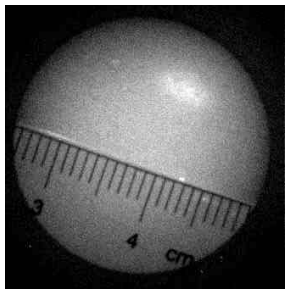

Missing data

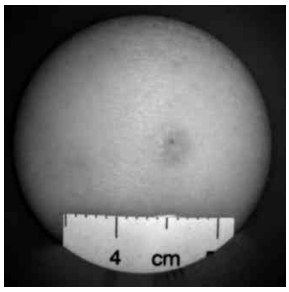

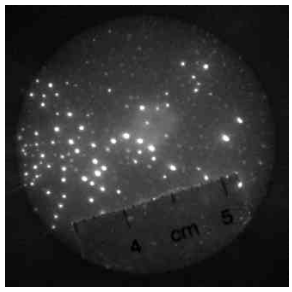

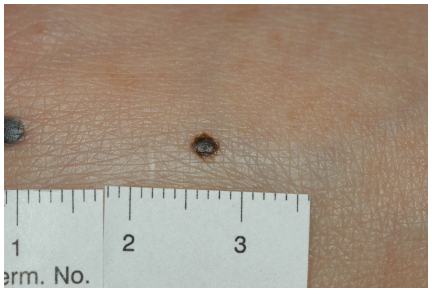

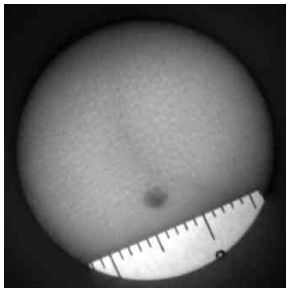
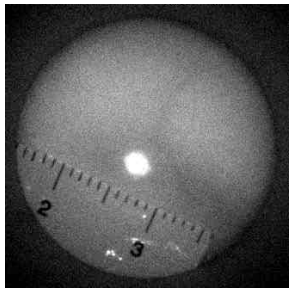

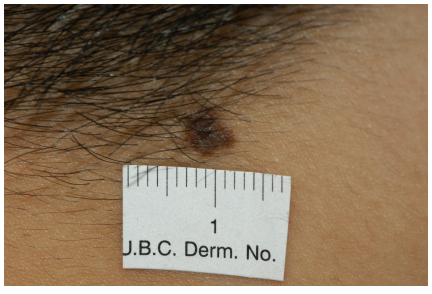

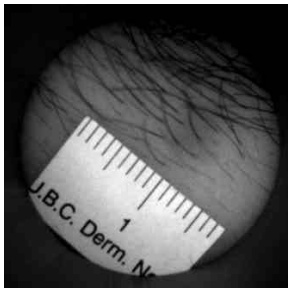

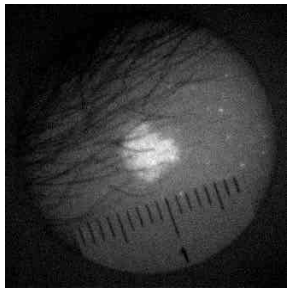

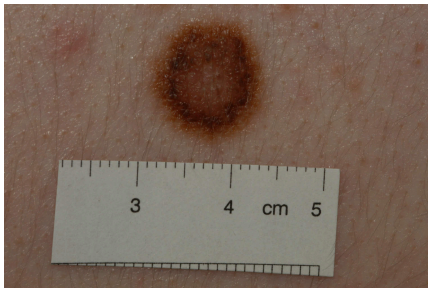

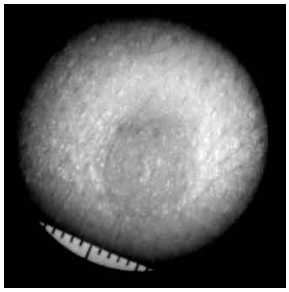
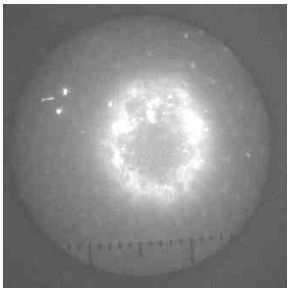

A1.8 Intradermal nevus

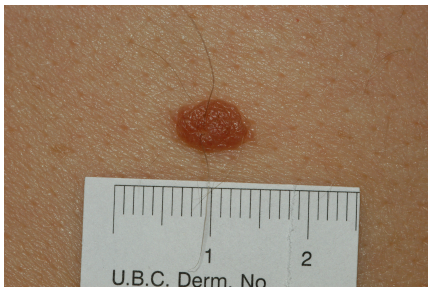

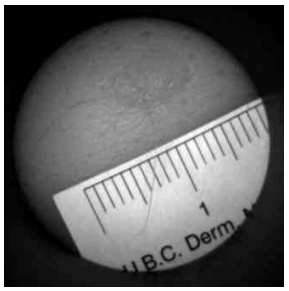

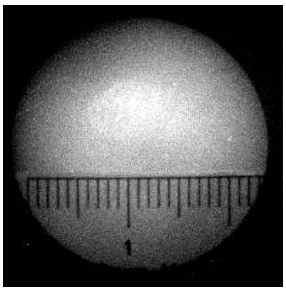

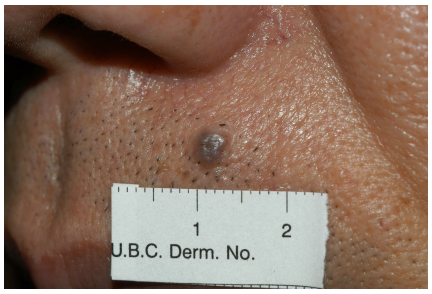

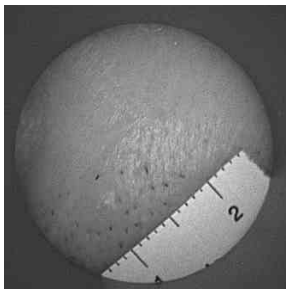

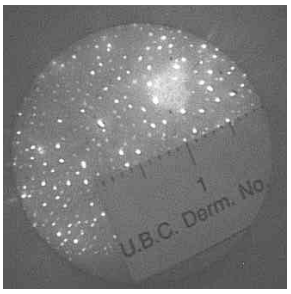

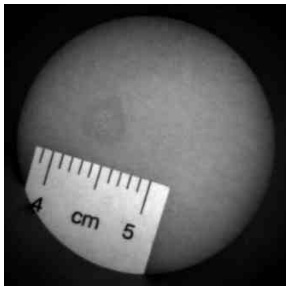

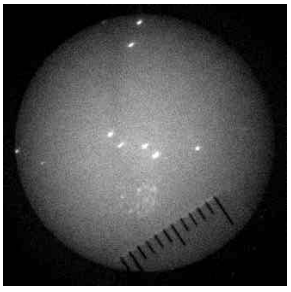

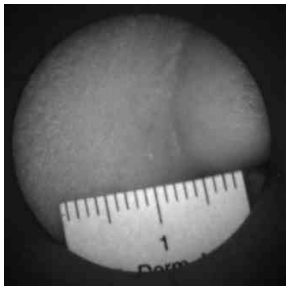

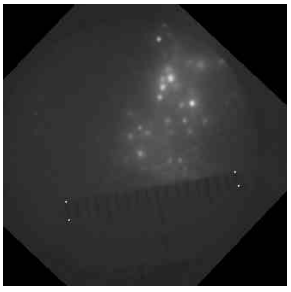


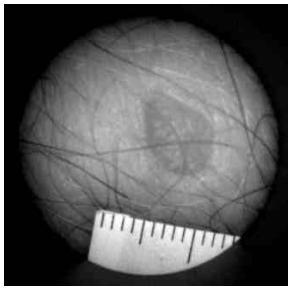
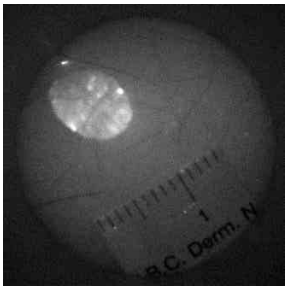

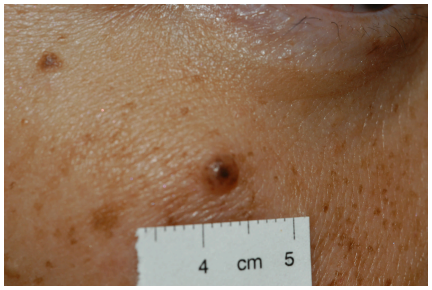

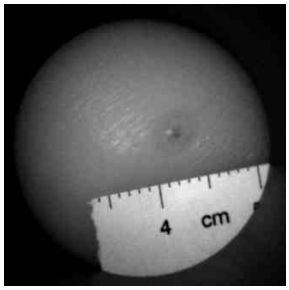

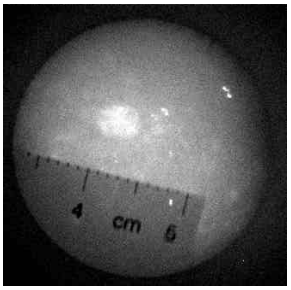

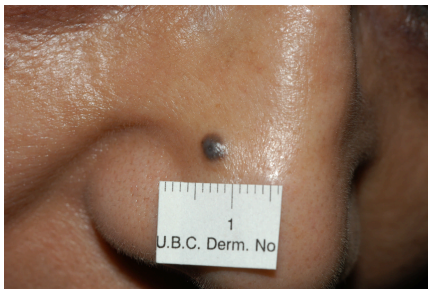

Missing data

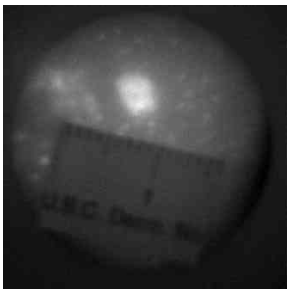

A1.9 Hypopigmentation

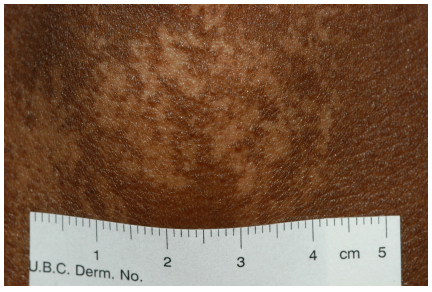

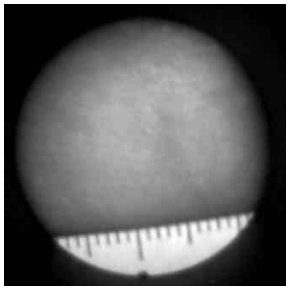
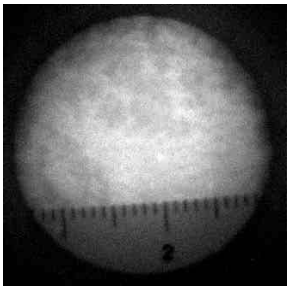

A1.10 Atypical nevus

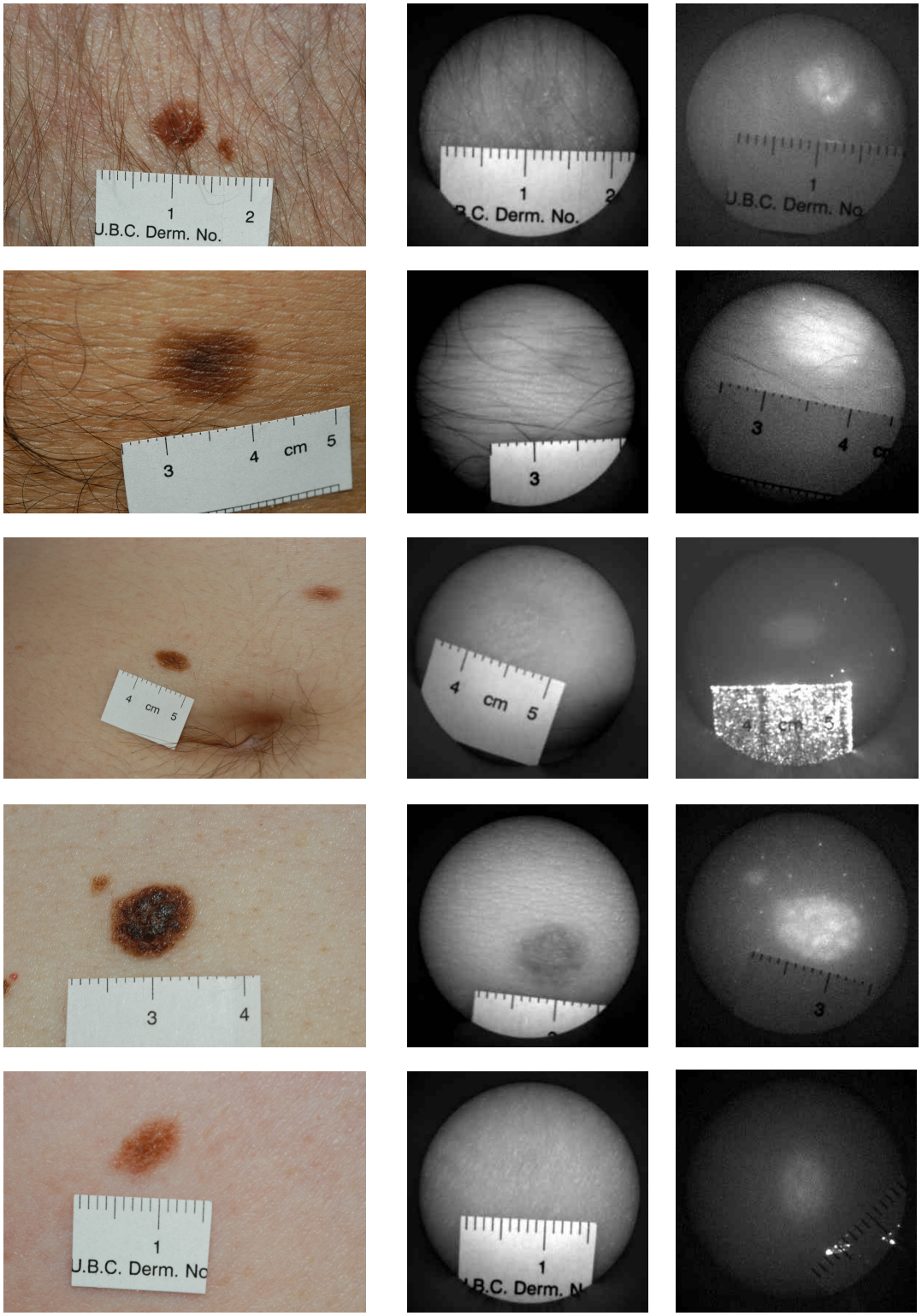

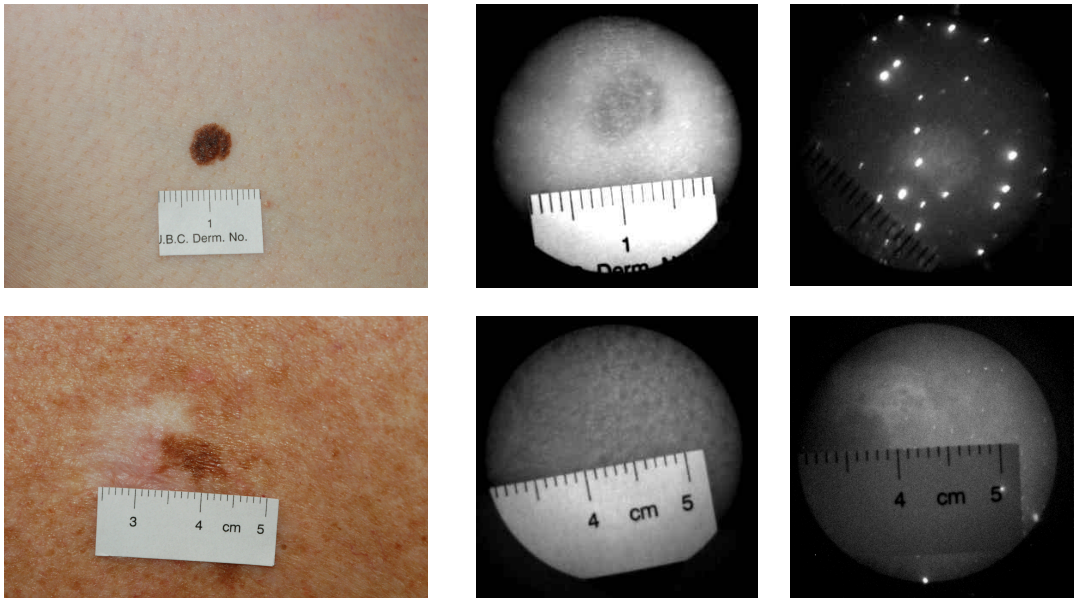

A1.11 Vitiligo

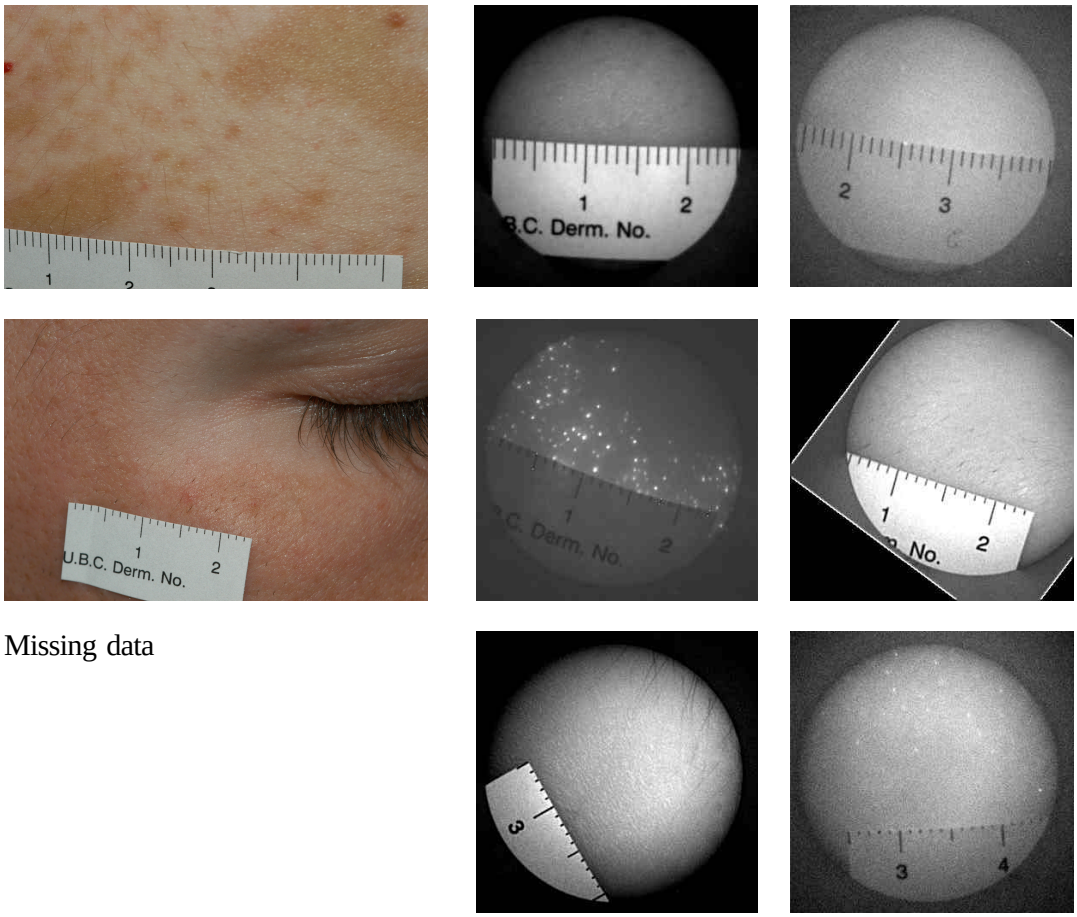

Missing data

A1.12 Freckle

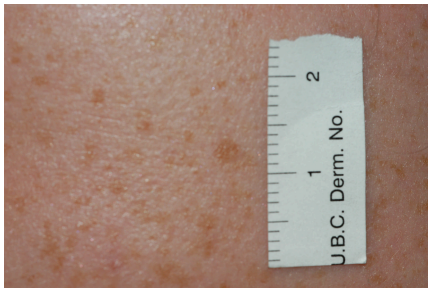

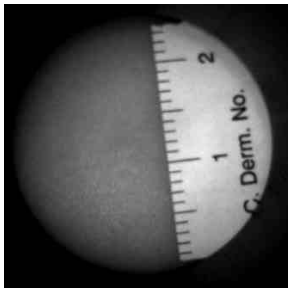

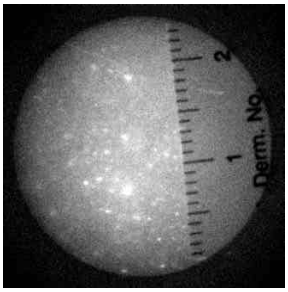

A1.13 Melasma

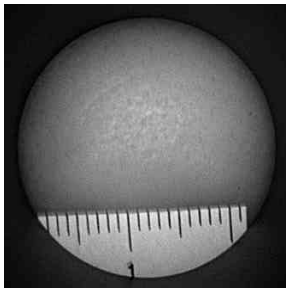
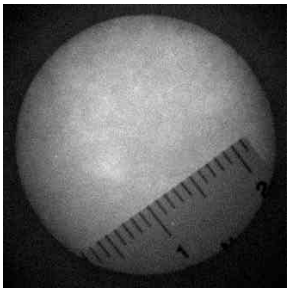

A2. Skin disorders without involvement of cutaneous melanin

A2.1 Mastocytosis

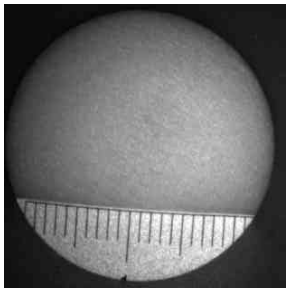
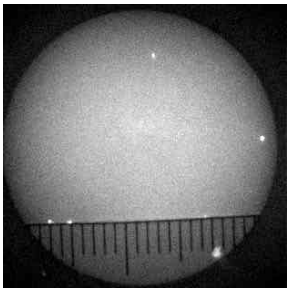

A2.2 Viral warts

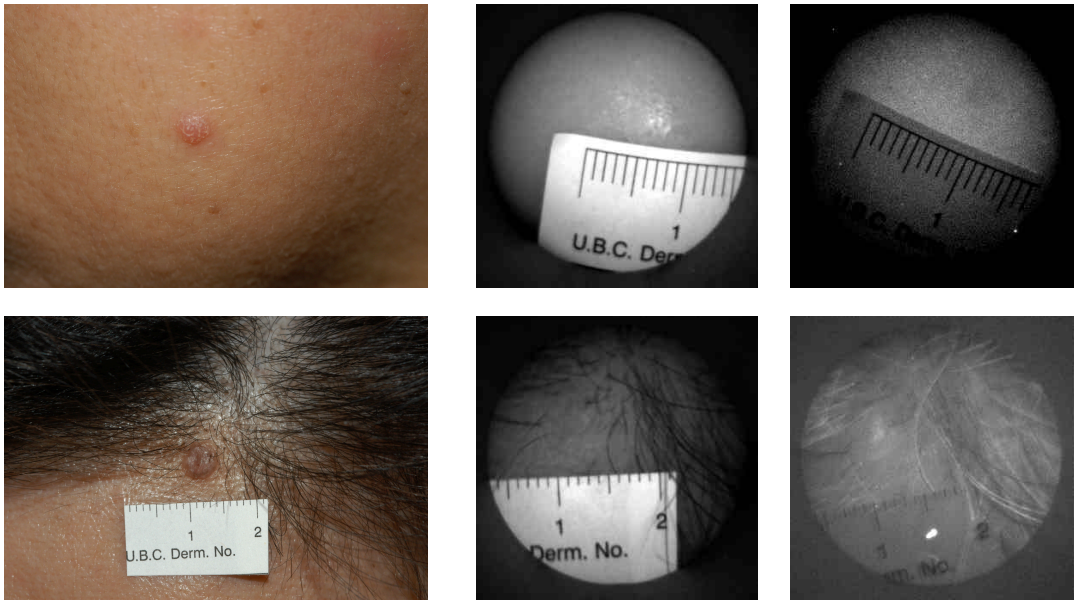

A2.3 Psoriasis

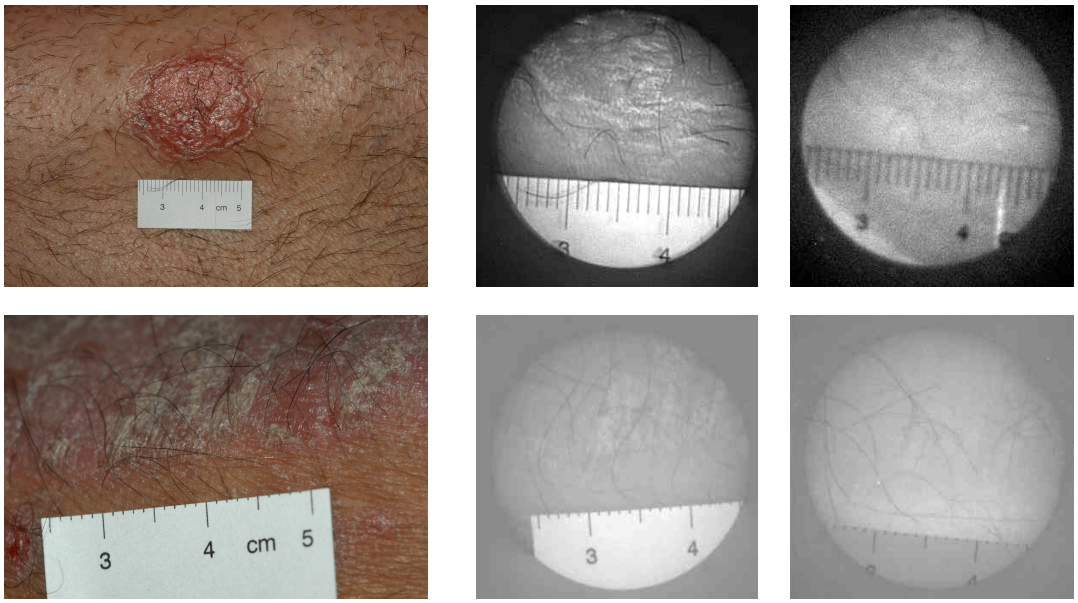

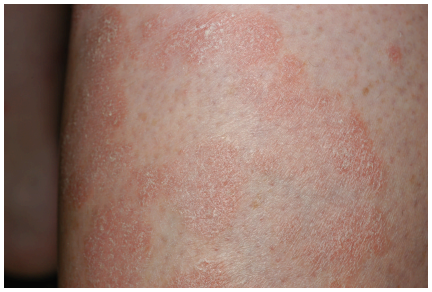
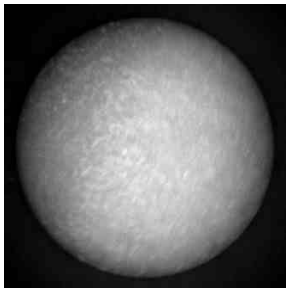
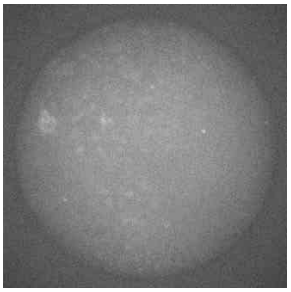

A2.4 Port Wine Stain

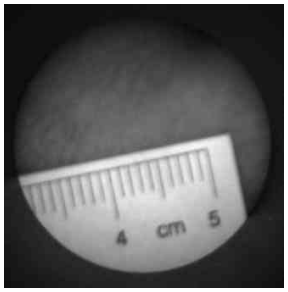

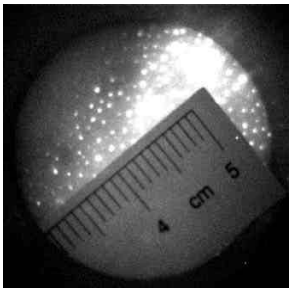

Missing data

Missing data

A2.5 Tattoo

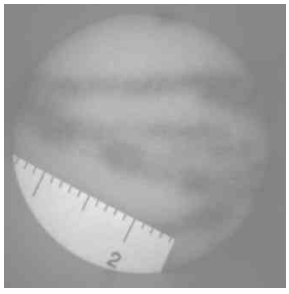

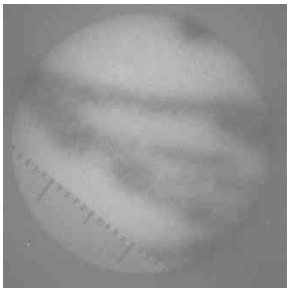

A2.6 Cherry Angioma

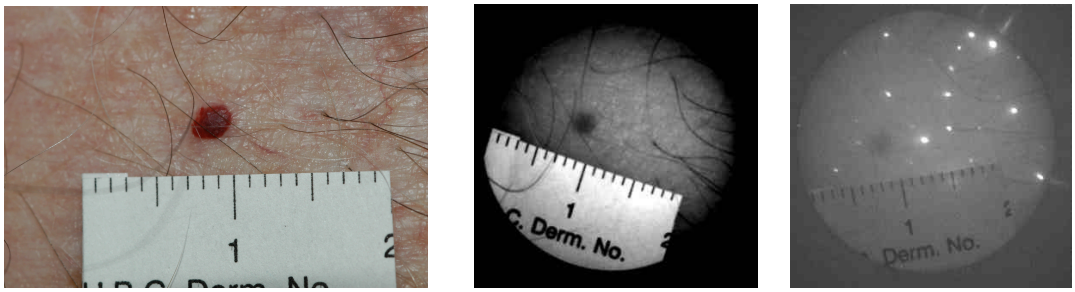


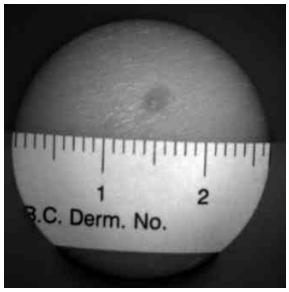
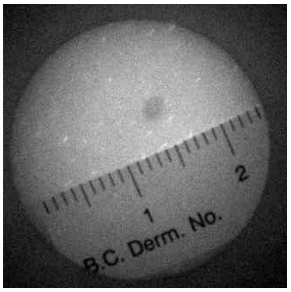

A2.7 Bruise

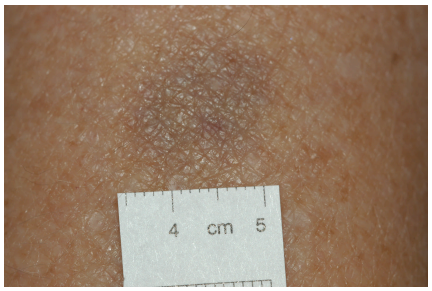
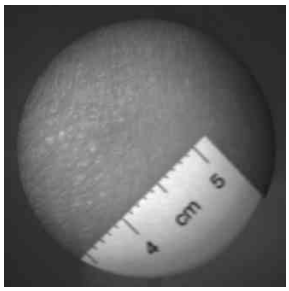
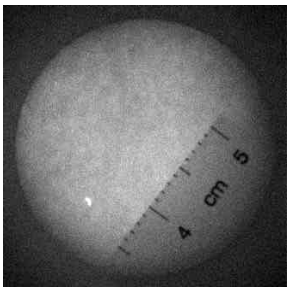
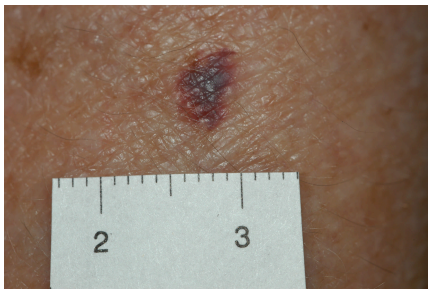
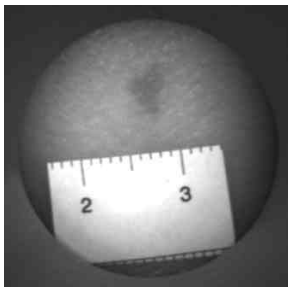
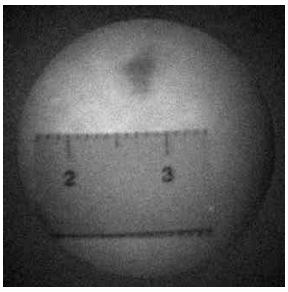

A2.8 Lentigo


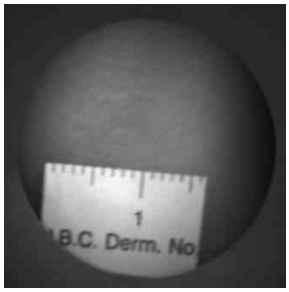
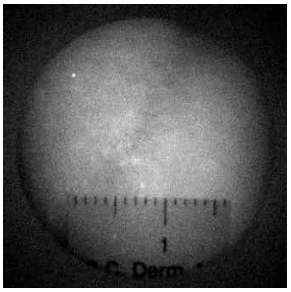
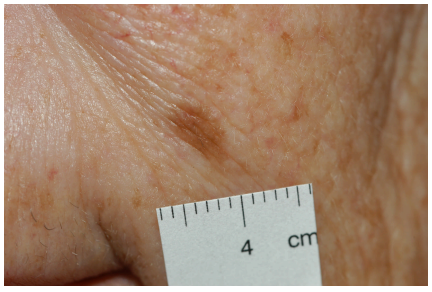
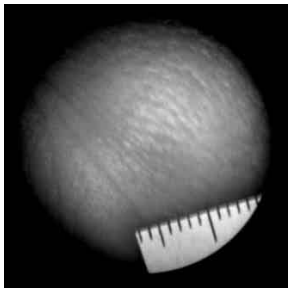
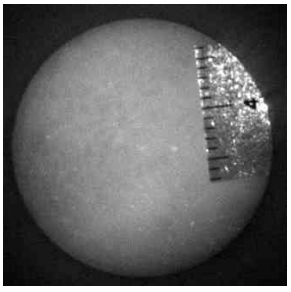

A2.9 Dermatofibroma

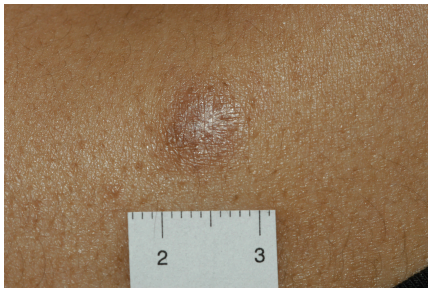
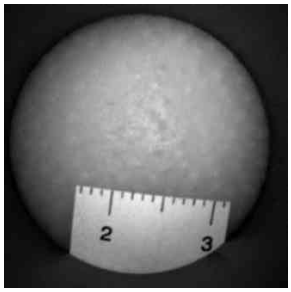
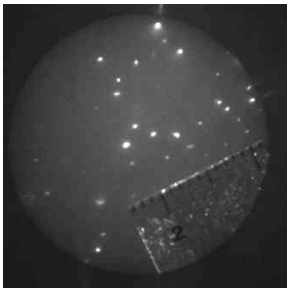

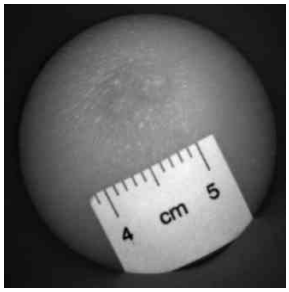
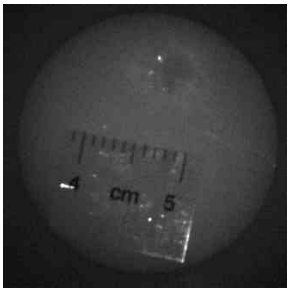

Missing data

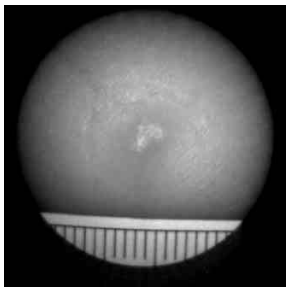
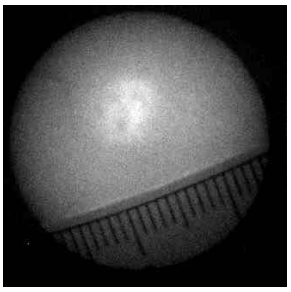

A2.10 Vasculitis


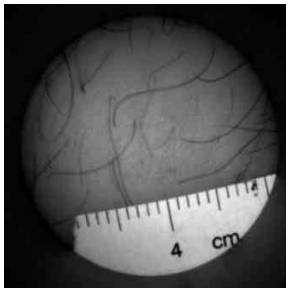
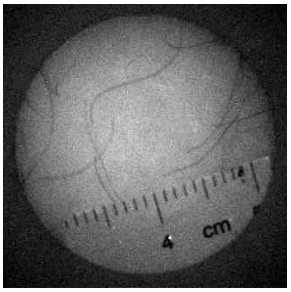

A2.11 Pityriasis

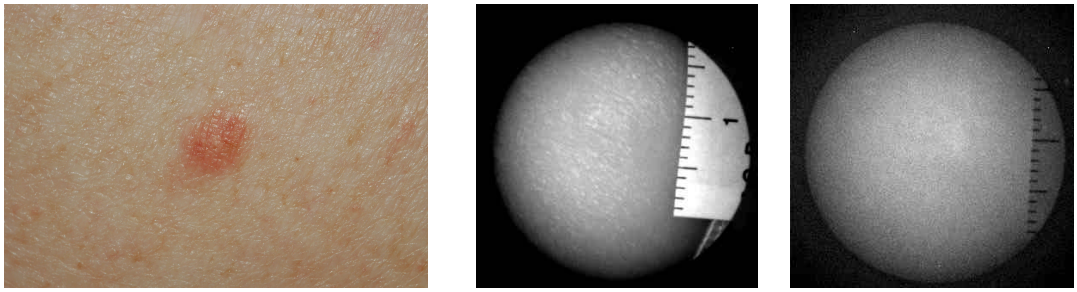

A3. Melanoma